Dissertation

submitted to the

Combined Faculties for the Natural Sciences and for Mathematics

of the Ruperto-Carola University of Heidelberg, Germany

for the degree of

Doctor of Natural Sciences

presented by

Barbara Vodicska, Biochemical engineer, M.Sc.

born in: Esztergom, Hungary

Oral examination: 19.03.2018

Deciphering the function of MISP in mitotic spindle orientation

Referees: *Prof. Dr. Ingrid Hoffmann*

Prof. Dr. Elmar Schiebel

I hereby declare that I have prepared the dissertation submitted independently and without any unauthorised assistance.

Hiermit erkläre ich an Eides statt, dass ich die vorliegende Dissertation selbstständig und ohne unerlaubte Hilfsmittel durchgeführt habe.

Heidelberg, den 12. Januar 2018

…….....

Barbara Vodicska

Table of Contents

Abbreviations

APC/C – anaphase-promoting complex / cyclosome
CA – constitutively active
Cdc42 – cell division cycle 42
Cdk1 – Cyclin-dependent kinase 1
CIN – chromosomal instability
DMEM – Dulbecco's Modified Eagle Medium
DN – dominant negative
GAP – GTPase activating protein
GEF – guanine nucleotide exchange factor
GFP – green fluorescent protein
GRD – GAP-related domain
GST – glutathione S-transferase
GTP – guanosine-5'-triphosphate
GTPase – guanosine-triphosphatase (GTP hydrolyzing enzyme)
IP – immunoprecipitation
IQGAP1 – IQ-motif containing GTPase activating protein 1
KD – knock-down
KO – knock-out
LGN – Leu-Gly-Asn repeat-enriched protein
MBP – maltose-binding protein
MISP – mitotic interactor and substrate of Polo-like kinase 1
MT – microtubule
NuMA – Nuclear Mitotic Apparatus protein 1
OE – overexpression
PBS – phosphate buffered saline
PD – pulldown
PEI - polyethylenimine
PIP_2 – phosphatidylinositol-4,5-bisphosphate
Plk1 – Polo-like kinase 1
RGCT – RasGAP C-terminus
RT – room temperature
SAC – spindle assembly checkpoint
siRNA – small interfering ribonucleic acid
WT – wild-type

Abstract

Precise spindle orientation during mitosis is essential for determining both cell fate and tissue organization. Proper alignment of chromosomes is a result of many processes that have to be orchestrated in a precise manner. Although some of the molecular mechanisms that underlie spindle orientation have been described recently, many aspects of this fundamental process remain unknown. Our protein of interest, MISP (mitotic interactor and substrate of Plk1, C19orf21), which was first characterized by our group as a substrate of Polo-like kinase 1 (Plk1), also seems to play a role in spindle orientation and positioning and in metaphase-to-anaphase transition (Zhu et al. 2013).

In a mass spectrometrical screen aiming at identifying MISP-interacting proteins I identified IQGAP1, a multidomain scaffolding protein that is believed to link the microtubule network with the actin cytoskeleton, as a potential binding partner. By using co-immunoprecipitation experiments the interaction between MISP and IQGAP1 was confirmed both after their overexpression and endogenously. Functionally, I discovered that depletion of MISP leads to increased accumulation of IQGAP1 at the cell cortex in mitosis. The cortical accumulation of IQGAP1 seems to be dependent on Cdc42, since overexpression of Cdc42 can revert the cortical accumulation of IQGAP1. Cdc42 is a small signaling molecule belonging to the Rho family of GTPases and it is a well-characterized binding partner of IQGAP1. The altered localization of IQGAP1 also coincides with a decrease in its Cdc42 binding capacity and thereby reduced active Cdc42 levels upon MISP knock-down. Furthermore, I found that MISP shows a preferential binding to active Cdc42 similar to IQGAP1. Not surprisingly, I could show that this interaction is not direct and is indeed mediated by IQGAP1.

Interestingly, overexpression of IQGAP1 can rescue the mitotic defects caused by MISP downregulation including spindle misorientation, loss of astral microtubules, prolonged mitosis and cortical accumulation of the dynactin subunit $p150^{glued}$. In addition, it also restores active Cdc42 levels. Importantly, MISP-depletion leads to a reduction in active Cdc42 levels in wild-type but not in IQGAP1 knock-out cells pointing to the effector role of IQGAP1 in regulating active Cdc42 levels upon MISP

depletion. Altogether, stabilization of active Cdc42 by IQGAP1 can restore mitotic defects upon MISP silencing.

In conclusion, I found that IQGAP1 acts downstream of MISP in regulating active Cdc42 levels, astral microtubule dynamics and the localization of $p150^{glued}$. Collectively, these results identify a novel pathway, namely that MISP regulates IQGAP1 and Cdc42 to ensure proper mitotic progression and correct spindle orientation.

Zusammenfassung

Eine präzise Orientierung der Mitosespindel ist entscheidend für die Bestimmung von Zellschicksal und Gewebeorganisation. Die korrekte Ausrichtung der Chromosomen während der Zellteilung ist ein Ergebnis vieler Prozesse, die genau reguliert werden müssen. Obwohl einige der molekularen Mechanismen, die der Spindelorientierung zugrunde liegen, kürzlich beschrieben wurden, sind noch viele Aspekte dieses grundlegenden Prozesses unbekannt. MISP (mitotic interactor and substrate of Plk1, C19orf21), das erstmals von unserer Gruppe als Substrat der Polo-like Kinase 1 (Plk1) charakterisiert wurde, spielt eine Rolle in der Spindelorientierung und -positionierung sowie im Metaphase-zu-Anaphase-Übergang (Zhu et al. 2013).

Auf der Suche nach MISP-interagierenden Proteinen identifizierte ich in einem Screen mit Hilfe der Massenspektrometrie IQGAP1 als potentiellen Bindungspartner. IQGAP1 ist ein sogenanntes Gerüstprotein mit verschiedenen Domänen, von dem angenommen wird, dass es das Mikrotubulinetzwerk mit dem Actin-Zytoskelett verbindet. Mit Hilfe von Co-Immunpräzipitationsexperimenten wurde die Interaktion sowohl nach Überexpression beider Proteine als auch endogen bestätigt. Funktionell habe ich entdeckt, dass die Herunterregulation von MISP zu einer erhöhten Akkumulation von IQGAP1 am Zellkortex in der Mitose führt. Die kortikale Akkumulation von IQGAP1 scheint von Cdc42 (ein kleines Signalmolekül, das zur Rho-Familie der GTPasen gehört und das ein gut charakterisierter Bindungspartner von IQGAP1 ist) abhängig zu sein, da die Überexpression von Cdc42 die kortikale Akkumulation von IQGAP1 verhindern kann. Die veränderte Lokalisierung von IQGAP1 wird auch von einer Abnahme der Cdc42-Bindungskapazität begleitet und reduziert dadurch die aktiven Cdc42-Levels nach der Herunterregulation von MISP. Außerdem stellte ich fest, dass MISP ähnlich wie IQGAP1 eine bevorzugte Bindung an aktives Cdc42 zeigt. Erwartungsgemäß gelang es nachzuweisen, dass diese Interaktion nicht direkt ist und tatsächlich von IQGAP1 vermittelt wird.

Interessanterweise kann die Überexpression von IQGAP1 den mitotischen Defekten, die durch MISP-Runterregulation verursacht werden, einschließlich Spindel-Fehlorientierung, Verlust von astralen Mikrotubuli, verlängerter Mitose und kortikaler Akkumulation von $p150^{glued}$ (einer Untereinheit von Dynaktin) entgegenwirken. Außerdem werden auch die physiologischen Mengen von aktivem

Cdc42 wiederhergestellt. Hervorzuheben ist, dass die Herunterregulation von MISP zu einer Verringerung der Mengen an aktivem Cdc42 im Wildtyp aber nicht in IQGAP1-Knock-out-Zellen führt. Diese Ergebnisse lassen auf eine Effektorrolle von IQGAP1 bei der Regulierung der Mengen an aktivem Cdc42 nach MISP-Runterregulation schließen. IQGAP1 kann also durch die Stabilisierung von aktivem Cdc42 mitotische Defekte verhindern, die durch die Herunterregulation von MISP ausgelöst werden.

Zusammenfassend habe ich festgestellt, dass IQGAP1 unterhalb von MISP in der Kaskade der Regulierung der aktiven Cdc42-Levels, der Dynamik von astralen Mikrotubuli und der Lokalisation von $p150^{glued}$ wirkt. Meine Ergebnisse deuten darauf hin, dass MISP, IQGAP1 und Cdc42 zusammenarbeiten, um einen ordnungsgemäßen Verlauf der Mitose und eine korrekte Spindelorientierung zu gewährleisten.

1 Introduction

1.1 The eukaryotic cell cycle

(Bruce *et al.*, 2008)

Since the famous dictum of Rudolph Virchow: “All cells only arise from pre-existing cells” (meaning that spontaneous cell generation does not occur) has not been disproven so far, cells have to reproduce themselves. In order to duplicate, resting cells enter the eukaryotic cell cycle, which results in the production of two genetically identical daughter cells. The cell cycle consists of four phases and three checkpoints in between which ensure proper duplication and segregation of the genetic material and other essential organelles.

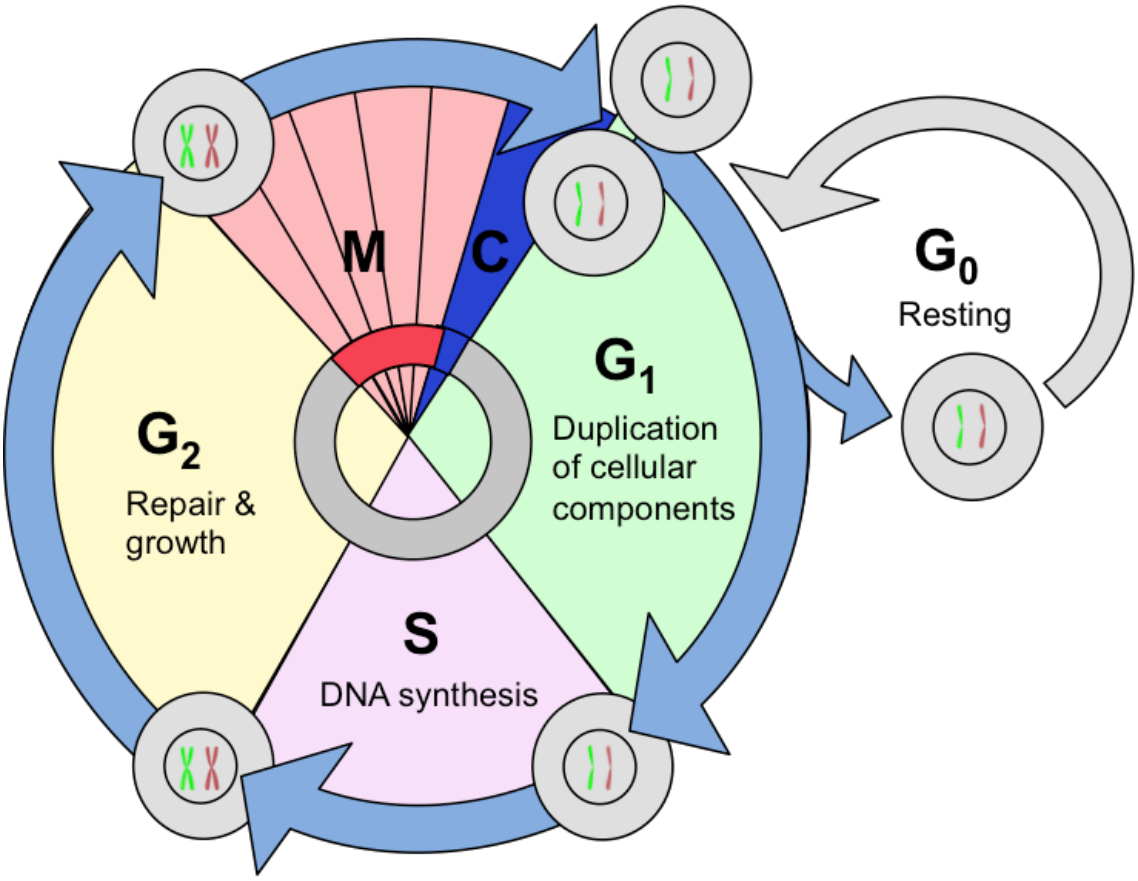

Figure 1. The cell cycle clock.

Gap phases (G_1 and G_2) separate the major events of duplication (S-phase, synthesis (S)) and segregation (M-phase, with mitosis (M) and cytokinesis (C)) and allow the cells to prepare for the next phase. Cells exiting the cell cycle enter the G_0 resting phase.

1.1.1 Phases of the cell cycle

The phases of the cell cycle are called the G_1-, S-, G_2 and M-phases (Figure 1). The umbrella term for the G_1-, S- and G_2-phases is interphase; during this time the cells prepare for the division. The M-phase is where the partitioning of the genetic material and the actual cell division happens. Cells can reversibly or irreversibly exit the cell cycle and so the constant process of reproduction by entering the G_0, or resting phase.

1.1.1.1 Interphase

The G_1- and G_2- phases are so-called gap phases, which are important for cell growth and for the duplication of specific cellular compartments. In the G_1-phase, where major metabolic changes take place in order to ensure the duplication of the cellular content, decision can be made about entering the G_0-phase in case the growth conditions are not favorable. For some cell types, entering the G_0-phase is unidirectional meaning that they never divide again. If a G_1 cell reaches the so-called restriction point, it is committed to division and moves on to S-phase.

During S- or synthesis phase, the cell duplicates its genetic material, so that each chromosome will consist of two sister chromatids and also duplicates the centrosomes, the main microtubule organizing centers, which are important for the segregation of sister chromatids in M-phase.

In G_2-phase the cells prepare for mitosis and try to detect and correct errors, which occurred during DNA duplication.

1.1.1.2 M-phase

The nuclear division (mitosis) and cell division (cytokinesis) are collectively called M-phase. In M-phase, sister chromatids produced in S-phase are divided equally between the two newly forming daughter cells. M-phase can be divided into several phases, from prophase to cytokinesis (Figure 2). In actively dividing human cells, the mitotic process is completed in about one hour.

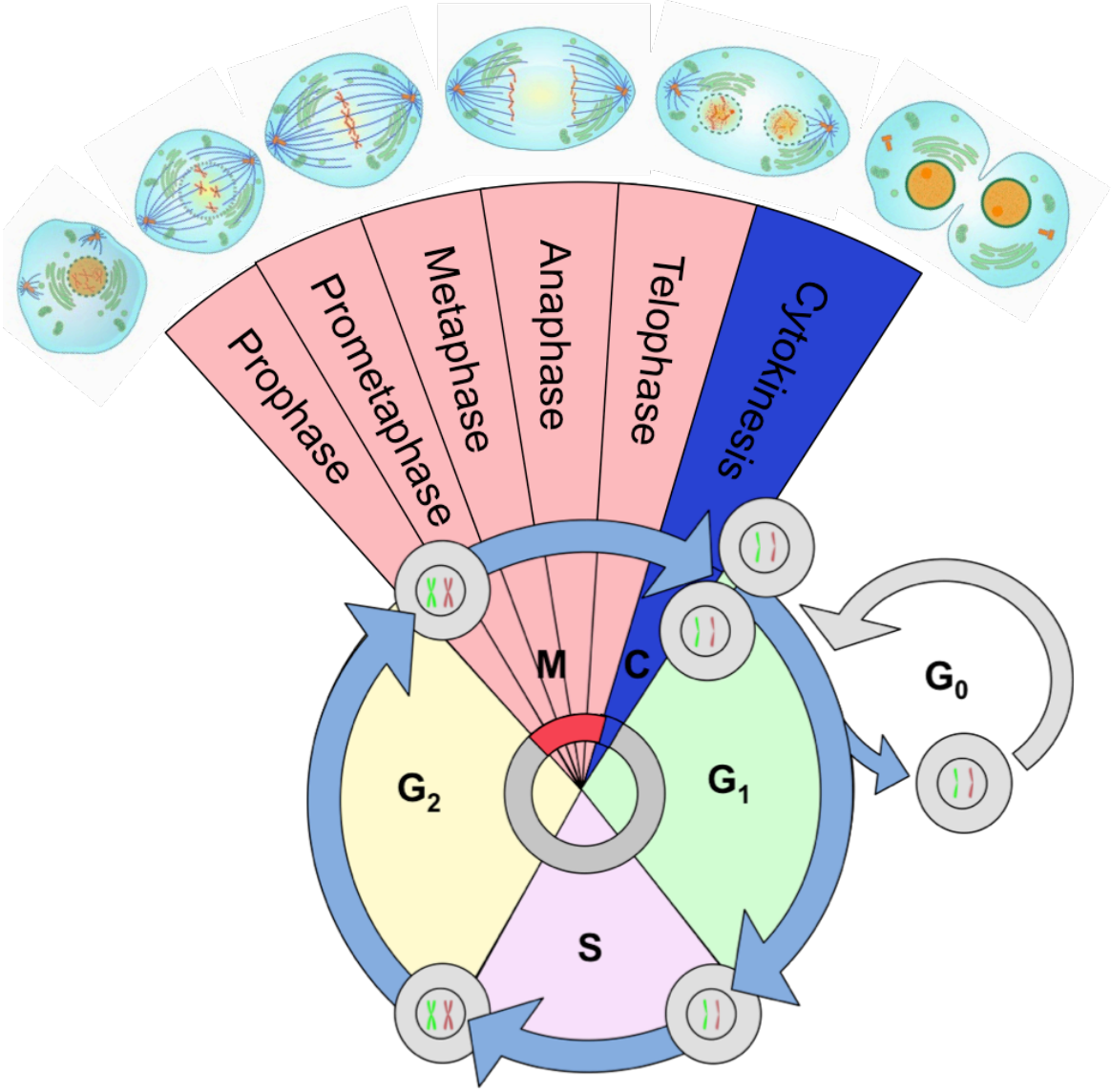

Figure 2. The stages of M-phase from prophase to cytokinesis.

The temporal order and the main events of the five stages of mitosis (prophase – telophase) and the final step of cytokinesis are shown.

1.1.1.2.1 The six stages of M-phase

The initiating stage of mitosis is called prophase. During this phase, the chromosomes condense and become visible in their characteristic X- (or Y) shape. At the same time, the centrosomes move apart to the opposite sides of the cell and their microtubule nucleation capacity increases.

In the following prometaphase, the nuclear membrane breaks down and the nucleolus disintegrates. Additionally, microtubules emanating from the spindle poles

capture the chromosomes at the kinetochores (middle and connective parts of the sister-chromatids) and drive their alignment at the metaphase plate, the equatorial plane of the cell's pole-to-pole axis.

Metaphase is defined by the alignment of chromosomes at the metaphase plate and is directly followed by anaphase, when the separation of sister chromatids happens. The M-phase checkpoint, also called spindle assembly checkpoint (SAC) is a protein complex that monitors the bipolar attachment and correct tension on the sister chromatids at the kinetochores and arrests the cells in a prometaphase/metaphase-like state until the completion of these requirements. The metaphase-to-anaphase transition happens through the destruction of sister-chromatid cohesion allowing the sister chromatids to be pulled to the opposite poles of the mitotic spindle.

After the separation of the sister chromatids is completed, the mitotic spindle disassembles, the chromosomes decondense and the nuclear envelope reappears around the two newly formed nuclei at telophase.

Finally, during cytokinesis the cleavage furrow, which forms at the former place of the metaphase plate, pinches off the two nuclei, establishing the two separate daughter cells. With this final act, cell division is completed.

1.1.1.2.2 The spindle assembly checkpoint (SAC)

After having been duplicated in S-phase, sister-chromatids are held together at many points via a ring-like structure consisting of the protein complex cohesin. In order to allow sister chromatid separation in M-phase, these rings have to be cleaved at the metaphase-to-anaphase transition by a protease called separase. Separase has an inhibitory protein named securin, which prevents the activation of separase.

The key regulator of the metaphase-to-anaphase transition is the ubiquitin ligase anaphase-promoting complex, or cyclosome (APC/C). One of its targets is securin. But before the SAC requirements are completed, the activity of the APC/C is blocked to prevent premature sister-chromatid separation. Spindle assembly checkpoint proteins (Mad2 and BubR1) at unattached kinetochores associate with Cdc20 – the mitotic cofactor of the APC/C. Without the Cdc20 cofactor, the APC/C remains

inactive. Once the kinetochores of all the sister chromatids have proper bipolar attachment, Cdc20 gets released and can assoicate with the APC/C allowing it to target securin for degradation. As a result, separase can reach its full activity and cleave securin, eliminating the cohesion between the sister chromatids and allowing the pulling forces to separate the two sets of genetic material.

1.1.2 Cell cycle errors and chromosomal instability (CIN)

A cell can collect mutations in its genetic material throughout its lifetime due to environmental factors or cell cycle errors. Cell cycle errors can arise from failures in the duplication process during S-phase or from missegregation of chromosomes during M-phase. The cell cycle checkpoints can recognize some of these alterations and may either repair them or drive the cell into a process called apoptosis leading to cell death. However, some of these errors stay undiscovered and might accumulate over time. As a result, the cell's genome changes, which might give rise to cancer formation.

DNA segregation failures during mitosis can lead to aneuploidy (incorrect number of chromosomes). A number of solid tumors were found to be aneuploid through missegregating their chromosomes in a phenomenon termed chromosomal instability (CIN) (Thompson *et al.*, 2010). CIN, by definition, is a persistently high rate of loss and gain of whole chromosomes. There are multiple possible causes for chromosome missegregation including cohesion defects, SAC defects, supernumerary centrosomes, kinetochore-microtubule attachment defects or cell cycle regulation failures (Thompson *et al.*, 2010). CIN can be fatal but it can also make tumor cells capable to adapt better to the changing environment and to acquire new phenotypes, such as drug resistance. Eliminating or over-activating CIN might therefore be a promising therapeutical strategy to suppress the high adaptability of tumor cells.

1.2 Regulation of mitotic spindle orientation

During mitosis, the dynamic structure of the mitotic spindle ensures faithful separation of the duplicated genetic material. The mitotic spindle connects (1) the cell cortex with the microtubule (MT) organizing centers, the two centrosomes via astral

MTs, (2) the centrosomes with the chromosomes via kinetochore MTs and (3) the two spindle poles via interpolar MTs, which push the spindle poles apart and position the cleavage furrow during cytokinesis (Tanaka, 2010). It is mainly the dynamic anchoring mechanism of the astral MTs at the cell cortex, which defines the orientation of cell division according to cell-intrinsic or cell-extrinsic signals (Théry and Bornens, 2006).

1.2.1 Importance of the plane of division

Spindle positioning and orientation during mitosis play a crucial role in determining both daughter cell fate and tissue organization (Figure 3) (Nestor-Bergmann *et al.*, 2014). In polarized cells, the plane of division controls the distribution of polarized constituents. If a polarized cell divides parallel to the polarity axis, the emerging daughter cells will have identical contents that destine them for the same fate (symmetric division). By contrast, if the division happens in a perpendicular plane to the polarity axis, the two daughter cells will inherit different constituents and thereby will later fulfil different functions (asymmetric division) (Morin and Bellaïche, 2011). In order to control the shape of a tissue, cells need to undergo oriented divisions. However, if there is an error in the spindle orientation machinery, the spindles orient randomly, giving rise to growth in unwanted directions. Moreover, converging evidence suggests that spindle misorientation can be linked to tumor formation and certain developmental diseases (Baena-López *et al.*, 2005; Quesada-Hernández *et al.*, 2010). It is therefore of vital importance to get a better understanding of the processes of spindle orientation.

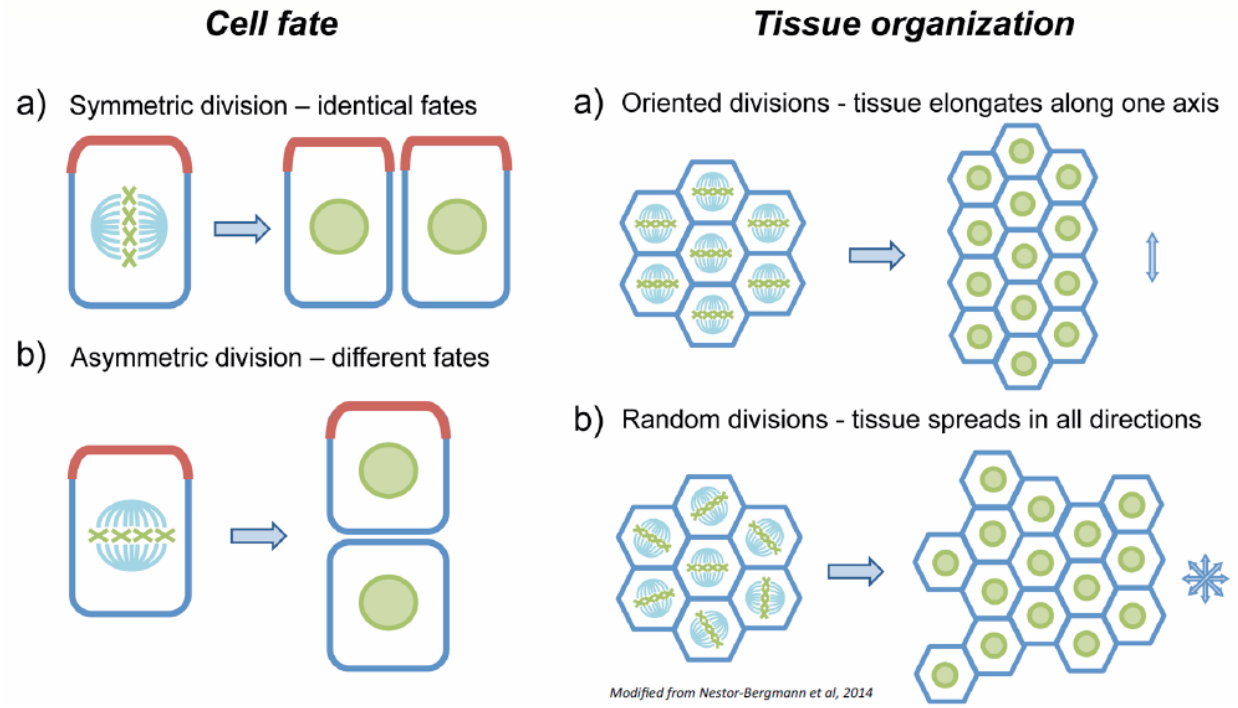

Figure 3. Spindle orientation determines cell fate and tissue organization.

In polarized epithelial cells, the orientation of the mitotic spindle can decide between symmetric or asymmetric divisions. Another level of spindle orientation control can determine how a tissue expands – if spindles align in the same direction the tissue will elongate along that axis. Adapted from Nestor-Bergmann et al., 2014.

1.2.2 Mechanism and influencing factors of spindle orientation

Proper alignment of chromosomes in mitosis is a result of many processes that have to be orchestrated in a precise manner. The number of proteins that regulate spindle orientation is increasing rapidly but the key players of how cells couple cortical polarity with spindle positioning are some molecular links that anchor the astral microtubules to the cortical actin cytoskeleton. Astral microtubules (which emanate from spindle poles but do not contribute to the mitotic spindle) reach the actin-rich cell cortex, where pulling forces can be applied on their plus-ends to control the placement of the mitotic spindle in respect of intrinsic and extrinsic signals. These signals include cell shape (Minc *et al.*, 2011) or the spindle poles and chromosomes (Kiyomitsu and Cheeseman, 2012) as intrinsic factors, and growth factors (Wu and Mlodzik, 2008), the extracellular matrix (Théry *et al.*, 2005), and cell–cell contacts (Gloerich *et al.*, 2017) as extrinsic factors. Mitotic cells probably integrate several of these signals in deciding about the spindle orientation axis.

1.2.3 The ternary and the dynein-dynactin complex

Microtubule plus-end binding proteins together with the dynein-dynactin motor complex are captured by cortical landmarks, namely the ternary complex proteins: Gαi, LGN (Leu-Gly-Asn repeat-enriched protein) and NuMA (Nuclear Mitotic Apparatus protein 1) (Gillies and Cabernard, 2011). According to the current model, this complex is localized to particular subcortical domains during mitosis and directs the recruitment of the minus-end-directed microtubule motor dynein. The directed movement of cortically anchored dynein along astral microtubules generates pulling forces on the spindle poles in order to orient or position the spindle. Therefore, the specific localization of the ternary complex determines the axis of spindle orientation (di Pietro *et al.*, 2016).

The lipid-anchored Gαi subunits cover the whole inner cell surface (Figure 4). Polarity factors contribute to the cortical recruitment of the adaptor protein LGN at polarized Gαi sites (Du and Macara, 2004), which localizes the dynein- and MT-binding protein NuMA. Through these interactions, NuMA orients the mitotic spindle by anchoring astral MTs to the cell cortex and applying pulling forces on the spindle through associated dynein (Laan *et al.*, 2012; Seldin *et al.*, 2016).

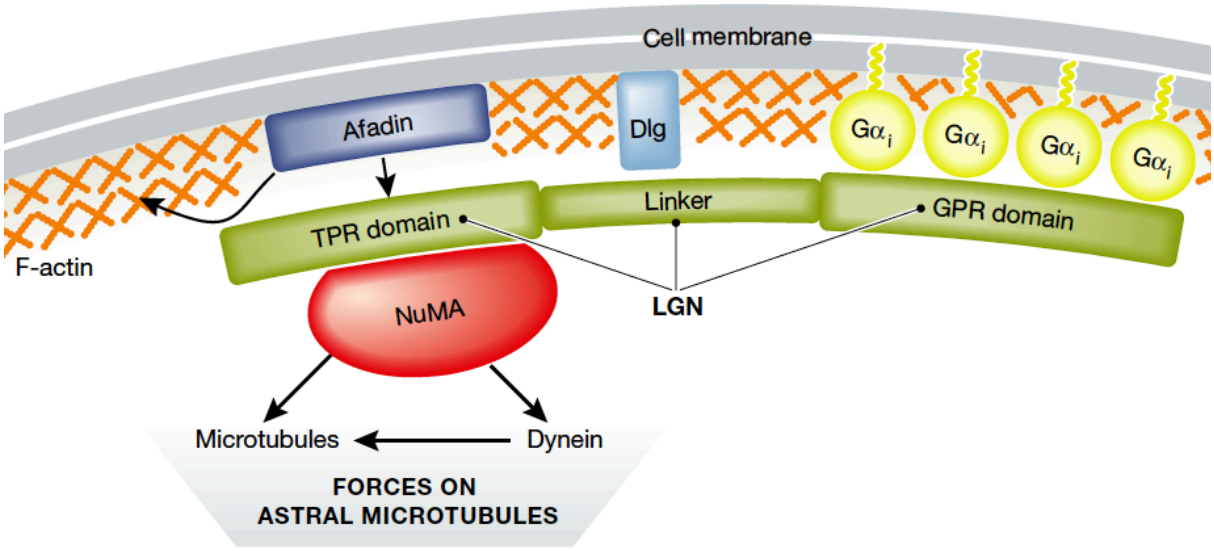

Figure 4. The ternary complex components.

Different LGN domains interact with Gαi and with NuMA. The interaction with other cortical proteins (Dlg, Afadin) can also regulate LGN's cortical localization. Adapted from di Pietro et al., 2016.

1.2.4 Dynamic regulation of the ternary and the dynein-dynactin complex

Recent studies have revealed different mechanisms for regulation of LGN, NuMA and dynein localization during mitosis by molecules located on chromosomes, centrosomes and at the cell cortex (Kiyomitsu and Cheeseman, 2012, 2013, Kotak *et al.*, 2013, 2014; Tame *et al.*, 2014). At metaphase, LGN and NuMA localize at the cortex in a crescent-shape overlying the spindle poles. However, the subcellular localization of these three proteins is highly dynamic throughout mitosis and the regulation of their localization happens through diverse pathways (Figure 5).

NuMA and LGN localization was shown to be influenced by the chromosome-derived Ran-GTP gradient (Kiyomitsu and Cheeseman, 2012). If the chromosomes get in close proximity with the cortex, the Ran-GTP gradient negatively regulates NuMA–LGN distribution at that cortical region.

The dynamics of the dynein/dynactin force-generator complex is controlled by Plk1, which can be found at the centrosomes in mitosis (Kiyomitsu and Cheeseman, 2012). The proximity of a spindle pole to the cortex excludes dynein, which is targeted to the cortex by astral MTs, from the neighboring cortical regions. Therefore, dynein/dynactin accumulates at the opposite side of the cell and generates pulling forces, which in turn reposition the spindle.

Cortical localization of NuMA, which is related to its phosphorylation status on T2055, becomes more pronounced with anaphase onset (Kotak *et al.*, 2013). NuMA is phosphorylated by Cdk1 (Cyclin-dependent kinase 1) in mitosis and this phosphorylated pool localizes to spindle poles. Upon Cdk1 inactivation in anaphase, the dephosphorylated pool of NuMA can increase due to the phosphatase PP2A, allowing the enrichment of NuMA at the cortex. This in turn leads to cortical dynein enrichment, and thereby spindle elongation.

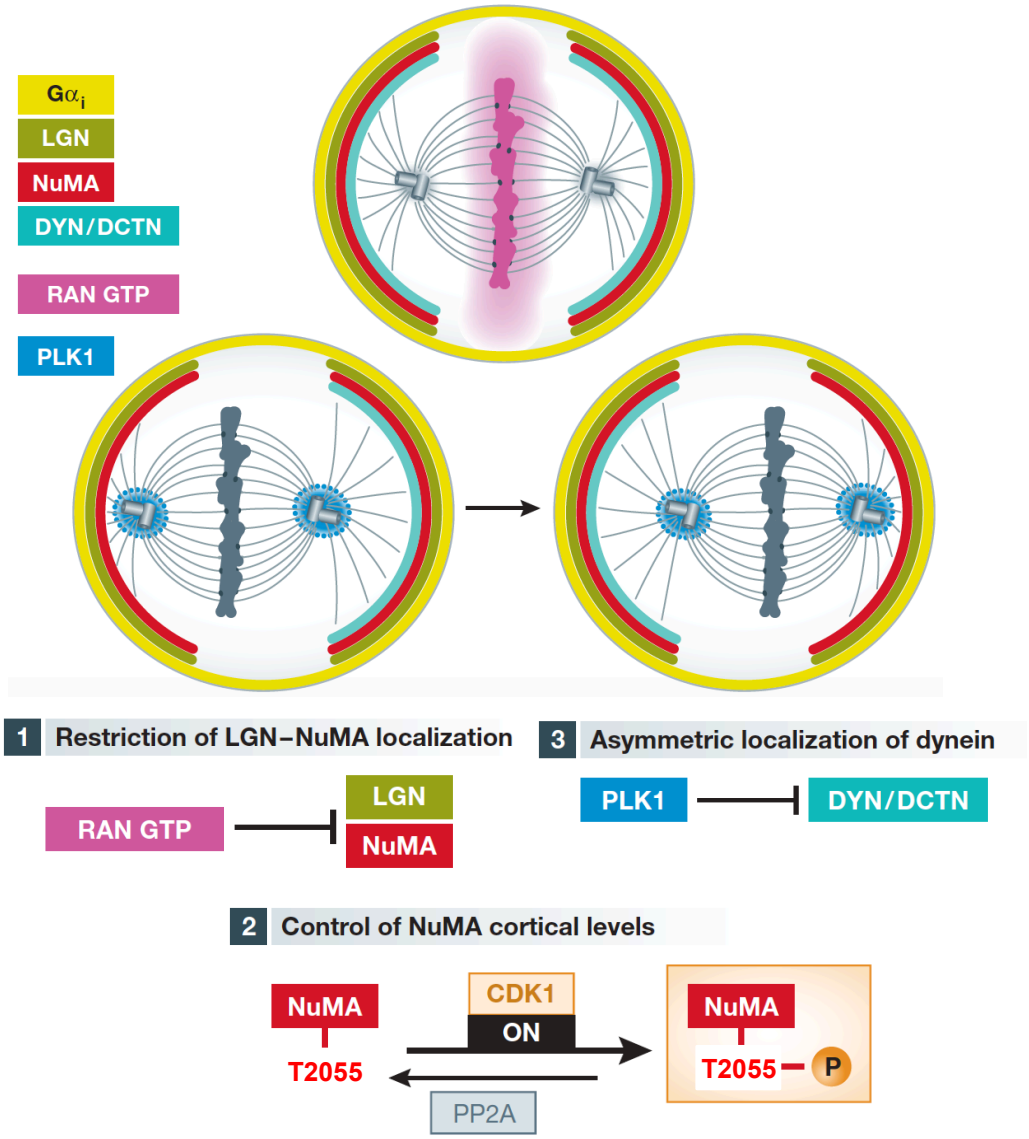

Figure 5. Mechanisms for regulating the distribution of the ternary complex.

Spindle-pole- and chromosome-derived signals regulate the localization of the ternary complex and the force-generator dynein. The phosphorylation of NuMA by Cdk1 happens on T2055. Adapted from di Pietro *et al.*, 2016.

1.2.5 Measuring spindle orientation of adherent cells

In order to measure spindle orientation, cells have to experience polarity-generating forces guided by external cues. This polarization can happen in 2 or 3 dimensions (2/3D). 2D methods include measurement of spindle orientation relative to substratum, using fibronectin-coated coverslips; or relative to specific patterns, using micropatterned coverslips (Figure 6a-b). Almost all adherent cells can be used for the 2D studies. When using fibronectin-coated coverslips, HeLa cells orient the

mitotic spindle parallel to the substratum, which depends on astral microtubules (Figure 6a) (Toyoshima *et al.*, 2007).

Micropatterned coverslips are not so easy to generate. In this model, single cells are cultured on defined geometrical-shaped adhesive (fibronectin) surfaces, dictating a specific adhesion pattern to the cells, which can induce specific spindle orientation in the xy-plane (Figure 6b). The orientation according to cortical cues is dependent on actin retraction fibers and astral microtubules (Théry *et al.*, 2005, 2007; Fink *et al.*, 2011; Machicoane *et al.*, 2014).

3D measurements, however, require cell lines that can form cysts (MDCK, CaCo-2), or can be conducted in vivo. In cyst formation assays, spindle orientation occurs in the plane of the epithelium and defective spindle orientation commonly results in multiple lumen formation (Figure 6c) (Jaffe *et al.*, 2008; Zheng *et al.*, 2010).

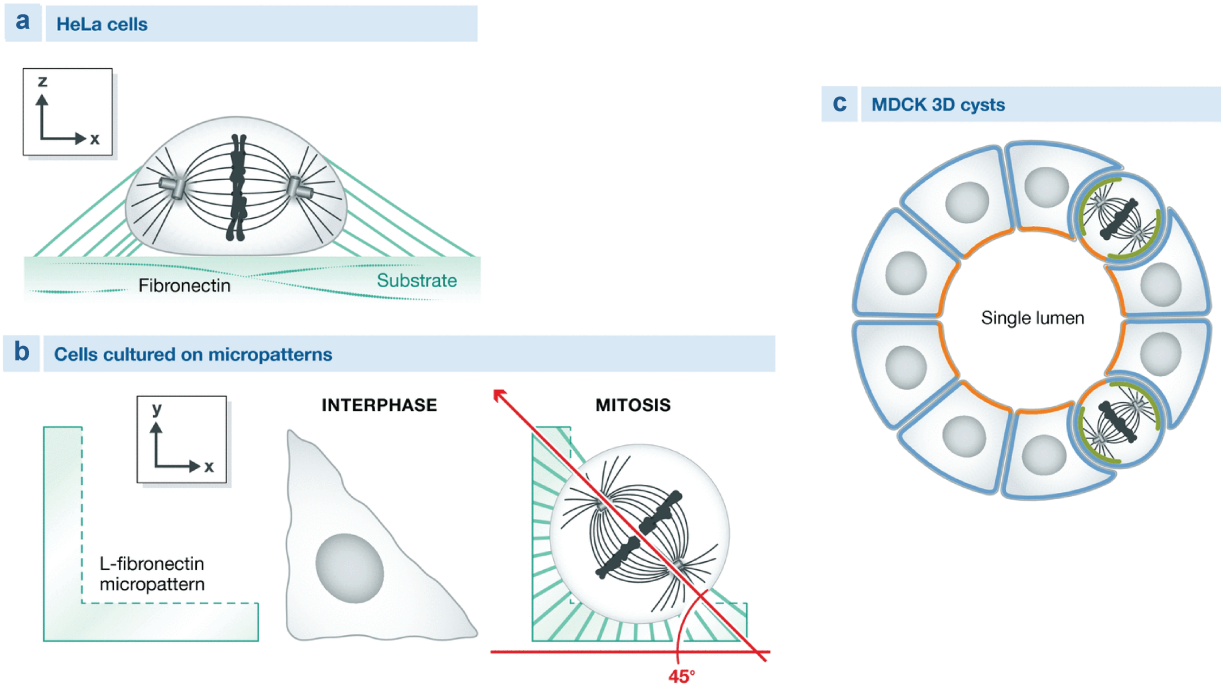

Figure 6. Ways of measuring spindle orientation.

Spindle orientation in cultured cells can be measured relative to the substratum using fibronectin-coated coverslips (a), micropatterned coverslips (b) or three-dimensionally using cysts (c). Adapted from di Pietro *et al.*, 2016.

The most cost- and time-effective method is the usage of fibronectin-coated coverslips, which can also be applied on HeLa cells, therefore I chose this method for my experiments.

1.3 MISP (mitotic interactor and substrate of Plk1, C19orf21)

My protein of interest, MISP (mitotic interactor and substrate of Plk1, C19orf21), which was first characterized by our group as a substrate of Polo-like kinase 1 (Plk1) (Zhu *et al.*, 2013), is mostly found in epithelial cells. MISP is a mainly cortically localized protein strongly co-localizing with (and binding to) actin but not with the mitotic spindle, although MISP was found in the mitotic spindle phosphoproteome (Nousiainen *et al.*, 2006; Santamaria *et al.*, 2011).

MISP is phosphorylated by Cdk1 and Plk1 in mitosis, with Cdk1 being the priming kinase for Plk1 phosphorylation. Upon siRNA-mediated down-regulation of MISP, cells suffer from spindle orientation and positioning disorders and loss of astral microtubules leading to prolonged metaphases and thereby SAC activation, chromosome misalignment, disrupted poles, multipolar spindles and increased mitotic index (Zhu *et al.*, 2013). Notably, MISP depletion also compromises the migratory ability of cultured cells (Maier *et al.*, 2013). The observed mitotic phenotypes can be rescued by overexpression of wild-type MISP or the phospho-mimicking mutant but not with the non-phosphorylatable variant, suggesting that phosphorylation has an important role in the function of the protein (Zhu *et al.*, 2013). MISP was also proven to interact with $p150^{glued}$, a dynactin subunit (Zhu *et al.*, 2013), End-binding protein 1 (EB1), a microtubule plus-end-binding protein, and focal adhesion kinase (FAK) (Maier *et al.*, 2013). Through its interactions with EB1, $p150^{glued}$ and actin, MISP is thought to link the astral microtubules to cell cortex and provide cortical cues to orient the mitotic spindle.

In another study, under the name Caprice (C19orf21 actin-bundling protein in characteristic epithelial cells), MISP was characterized as an effector for actin reorganization with its direct actin-binding and -bundling properties in interphase epithelial cells (Kumeta *et al.*, 2014). While MISP overexpression led to stress fiber-like thick filamentous structures, its knock-down induced filopodia formation, making MISP a suppressor of filopodial protrusions.

1.4 The family of Rho GTPases

Through regulating the actin cytoskeleton, the Rho family of GTPases (with key members RhoA, Rac1 and Cdc42) control many cellular processes including adhesion, cell motility and mitotic progression (Figure 7) (Iden and Collard, 2008).

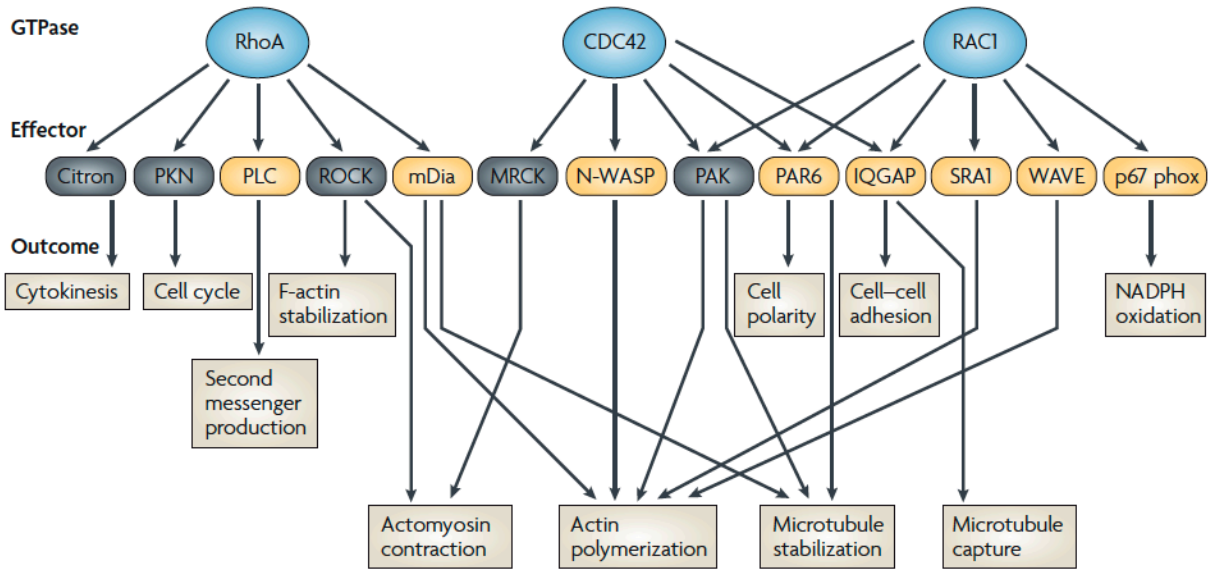

Figure 7. Effectors and functions of Rho GTPases.

Rho GTPases regulate many cellular events, including cytoskeletal organization, gene expression and proliferation and (Iden and Collard, 2008).

These small signalling molecules act as molecular switches, with an active, GTP-bound and an inactive, GDP-bound state (Figure 8). The transition into the active, GTP-bound state is catalyzed by guanine nucleotide-exchange factors (GEFs) while their counteractors, the GTPase-accelerating (or activating) proteins (GAPs) accelerate the hydrolysis of GTP thereby leading to the inactivation of the GTPase (Cherfils and Zeghouf, 2013). There is also a third class of regulatory proteins that coordinate the GTPase cycle, the guanine nucleotide-dissociation inhibitors (GDIs), which bind to the inactive GTPase and localize a pool of the quickly activatable protein. The GTPases interact with their effectors in the GTP-bound state. This interaction facilitates the effectors to exert their functions downstream of the signalling molecules (Cherfils and Zeghouf, 2013).

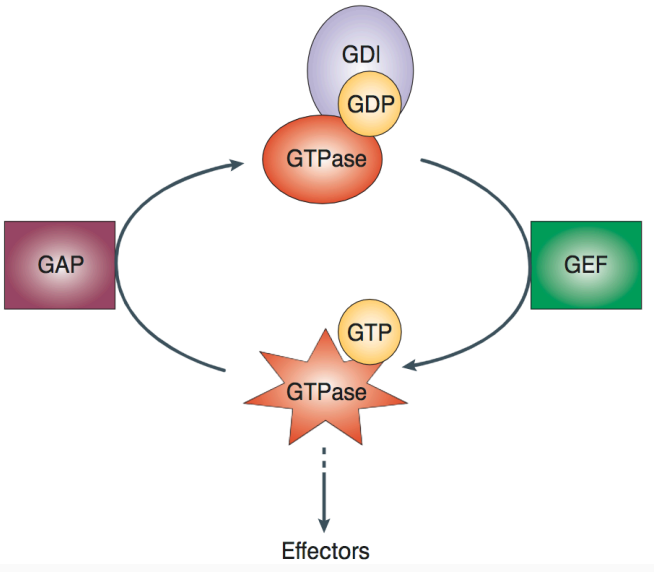

Figure 8. The GTPase cycle.

The cycle of Rho GTPases (Coleman et al., 2004). GEFs activate, while GAPs deactivate the GTPases. GAP - GTPase-accelerating protein, GEF - guanine nucleotide exchange factors, GDI - GDP-dissociation inhibitors.

Not only other proteins but also the localization of the Rho GTPases itself can influence their function and activity. At their C-terminus, the Rho GTPases harbor a stretch of basic amino acids, which facilitates their association with acidic membrane lipids, and the post-translational modification signal CAAX motif (C - cysteine, A - any aliphatic amino acid, X - any amino acid), which targets them for isoprenylation (Roberts et al., 2008). This means, for example in the case of Cdc42 and Rac1, that prenyltransferases add a geranylgeranyl lipid tail to the cysteine residue of the CAAX motif, and with this lipid modification, Cdc42 and Rac1 are able to insert into the plasma membrane or into intracellular membranes.

1.4.1 Cdc42 (Cell division cycle 42)

Cdc42 (Cell division cycle 42), a member of the Rho family of GTPases, is often referred to as a master regulator of cell polarity and cytoskeletal rearrangements. GTP-bound Cdc42 activates a large number of effector proteins and promotes different signaling pathways. For example, Cdc42 induces actin cytoskeleton changes by activating the Wiscott-Aldrich syndrome proteins (WASPs), which in turn bind to the Actin-related protein 2/3 complex (Arp2/3) leading to actin polymerization and filopodia formation (Carlier *et al.*, 1999). Another important function of Cdc42 is

polarity establishment in developing organisms. The polarity proteins PAR3 and PAR6 form a complex with Cdc42 and atypical protein kinase Cζ (PKCζ) to define the anterior/posterior axis (Erickson and Cerione, 2001).

Since Cdc42 promotes cell motility, it is not surprising that Cdc42 has been shown to actively assist in cancer progression. Cdc42 was shown to be overexpressed in many cancer types including non-small cell lung cancer, colorectal adenocarcinoma, melanoma, breast cancer, and testicular cancer and elevated levels of Cdc42 have been correlated with negative patient survival (Stengel and Zheng, 2011).

1.4.1.1 Role of Cdc42 in mitotic progression

Regarding that Cdc42 localizes to the mitotic spindle and centrosomes during metaphase (Ban *et al.*, 2004), it is conceivable that Cdc42 has a function in mitotic progression. Cdc42 was shown to regulate the bi-orient attachment of spindle microtubules to kinetochores together with mDia3 (Yasuda *et al.*, 2004). Moreover, GTP-Cdc42 level elevates in metaphase, whereas the level of GTP-Rac1 does not change significantly in mitosis (Figure 9) (Oceguera-Yanez *et al.*, 2005), pointing to a specific role of Cdc42 in this process. Cdc42 was also shown to regulate cytokinesis in mouse oocytes and embryos and to act upstream of IQGAP1 (Bielak-Zmijewska *et al.*, 2008).

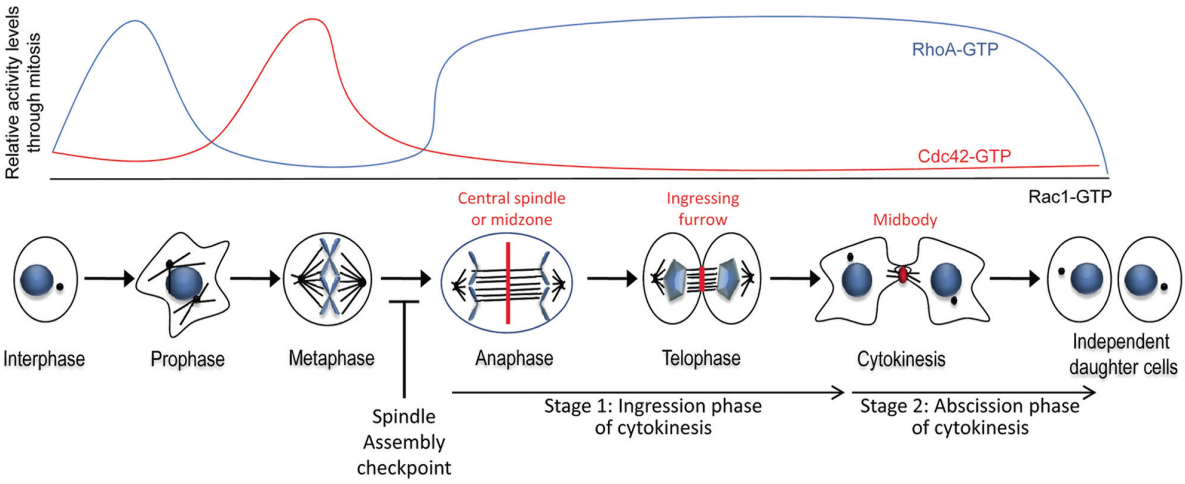

Figure 9. Active Cdc42 and RhoA levels during mitosis.

Active, GTP-bound Cdc42 and RhoA levels were measured relative to the total amount of the GTPases in interphase and in different phases of mitosis. Active Cdc42 levels peak in metaphase. Adapted from Chircop, 2014.

1.4.1.2 Role of Cdc42 in spindle orientation

The metaphase function of Cdc42 has been linked to the regulation of spindle orientation and thereby the formation of the central lumen in 3D MDCK and CaCo-2 cell models (Jaffe *et al.*, 2008; Rodriguez-Fraticelli *et al.*, 2010). The Cdc42 specific GEF, intersectin 2 (ITSN2) is indispensable for the centrosomal localization of Cdc42. Cells depleted of either Cdc42 or ITSN2 display incorrect spindle orientation (Rodriguez-Fraticelli *et al.*, 2010). Interference with LGN function causes a similar spindle misorientation phenotype, thus, the role of ITSN2/Cdc42 in spindle orientation might be mediated through an LGN-dependent pathway.

Mitsushima and colleagues showed that Cdc42 has an essential role in spindle orientation by regulating both the actin cytoskeleton and PtdIns(3,4,5)P_3. Knock-down of Cdc42 suppresses PI(3)K activity in mitosis, disrupts the cortical actin structures and induces spindle misorientation (Mitsushima *et al.*, 2009).

Regarding the regulation of Cdc42 activity in mitosis, the junctional adhesion molecule-A (JAM-A) was shown to trigger activation of Cdc42 and PI(3)K and to generate a PtdIns(3,4,5)P_3 gradient at the cortex. This in turn contributes to the correct formation of the cortical actin cytoskeleton and proper spindle orientation (Tuncay *et al.*, 2015).

1.5 IQGAP1 (IQ-motif containing GTPase activating protein 1)

IQGAP1, 2 and 3 (IQ-motif containing GTPase activating proteins) are multidomain scaffolding proteins expressed in eukaryotes, from *Saccharomyces cerevisiae* to humans. All the three family members were shown to bind active Cdc42 and Rac1 and can regulate diverse cellular mechanisms including crosslinking of actin filaments, microtubule dynamics, migration and E-cadherin-mediated cell–cell adhesion (Mataraza *et al.*, 2003; Noritake *et al.*, 2005; Smith *et al.*, 2015). The best-characterized member is the ubiquitously expressed 190-kDa IQGAP1. Interestingly, in spite of their sequence similarity, IQGAP1 and IQGAP3 are oncogenes, while IQGAP2 is a tumor suppressor (Johnson *et al.*, 2009; White *et al.*, 2009).

1.5.1 The functional domains of IQGAP1

Due to its 6 distinguishable domains IQGAP1 has a wide range of binding partners and therefore contributes to many cellular processes (Figure 10). F-actin binds to its N-terminal calponin-homology (CH) domain followed by a sixtuple coiled-coil (CC) domain serving a binding site for ezrin. Right after CC domain come the short tryptophan (WW) domain and the isoleucine-glutamine (IQ) domain. To the latter one many partners can bind, including calmodulin (Mateer *et al.*, 2002) and the epidermal growth factor receptor (EGFR) (Bañón-Rodríguez *et al.*, 2014) but this part also seems to be responsible for the self-association and dimerization of IQGAP1 (Ren *et al.*, 2005; LeCour *et al.*, 2016).

The following GAP-related domain (GRD) is responsible for the interaction with Cdc42 and Rac1 (Hart *et al.*, 1996; Kuroda *et al.*, 1996). Despite its name and the domain homology, IQGAP1 is not a GAP. Due to a point mutation in the active site of the GAP domain, IQGAP1 cannot hydrolyze GTP-bound Cdc42 or Rac1. Instead, it has been reported to stabilize them in their active form. Therefore overexpression of IQGAP1 leads to an increase in the levels of GTP-bound Cdc42 and Rac1 (Hart *et al.*, 1996; Swart-Mataraza *et al.*, 2002).

Finally, the RasGAP C-terminus (RGCT) mediates the binding to E-cadherin, β-catenin (Kuroda *et al.*, 1998), CLIP-170 (Fukata *et al.*, 2002), APC (Watanabe *et al.*, 2004), and PIP_2 (Choi *et al.*, 2013) thereby anchoring IQGAP1 to the cell cortex and the microtubule plus ends. This C-terminal domain also contains a phosphorylation site (Ser1443), which site is an in vitro PKCε substrate and thought to be responsible for conformational changes of IQGAP1 (Grohmanova *et al.*, 2004).

1.5.2 IQGAP1 functions and interactions

As seen above, IQGAP1 has a myriad of interaction partners. (For the newest list see review: Hedman *et al.*, 2015, with around 140 proteins). Since it cannot bind all of them at the same time, these interactions have to be regulated by other proteins, or by IQGAP1 itself through conformational changes. In this chapter, I am going to present the most relevant interaction partners of IQGAP1 and shed some light on how these interactions are regulated. The list is by no means exhaustive.

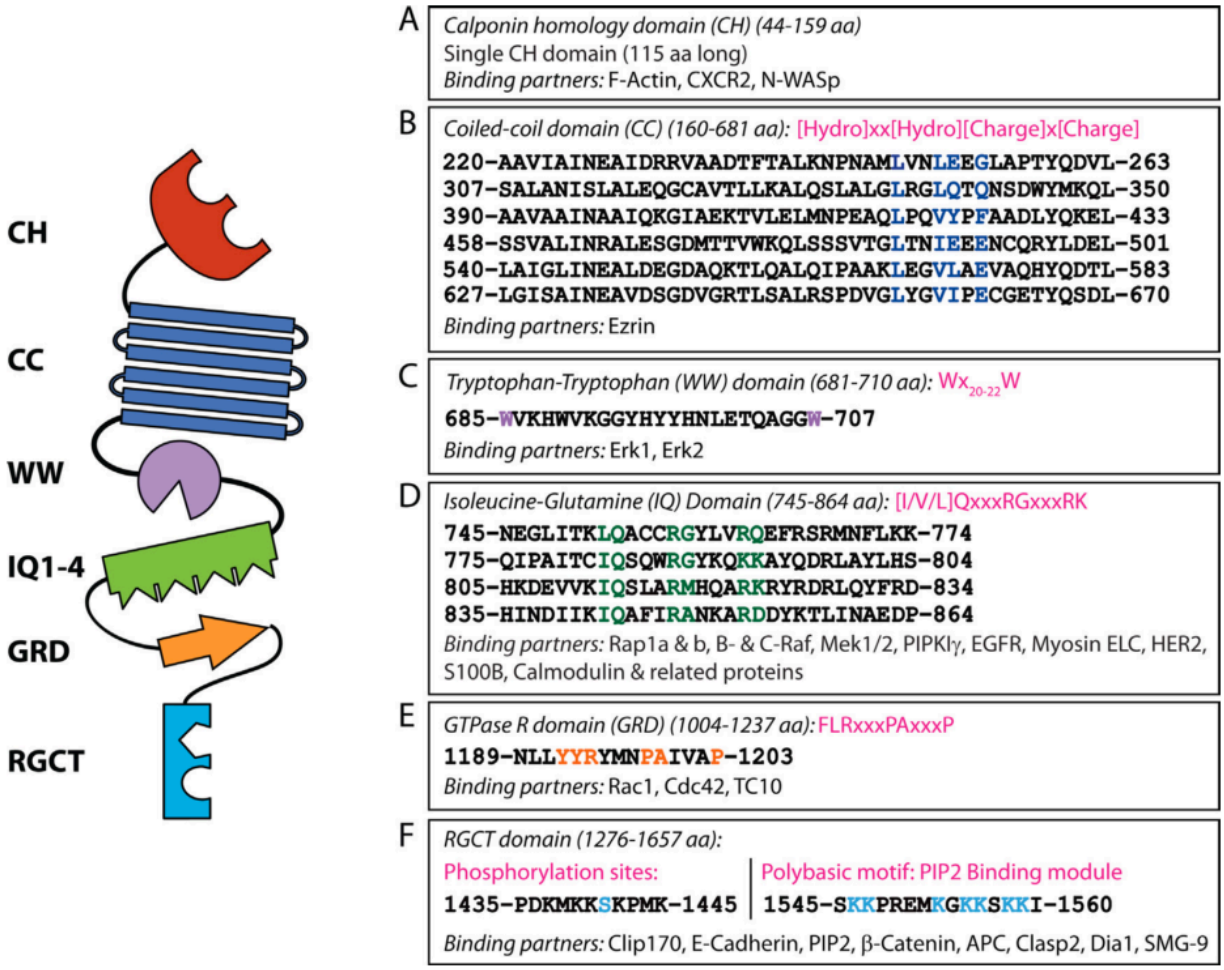

Figure 10. Protein structure of and specific domain-interacting partners of IQGAP1.

The 6 main domains of IQGAP1: CH – calponin homology domain, CC – coiled-coil domain, WW – Tryptophan-Tryptophan domain, IQ – Isoleucine-Glutamine domain with 4 repeats, GRD – RasGAP-related domain, RGCT – RasGAP C-terminus. Figure from Abel et al., 2015.

Cdc42 is one of the best-characterized interaction partners of IQGAP1. Overexpression of IQGAP1 increases the pool of active Cdc42 (and Rac1), while knock-down of endogenous IQGAP1 significantly decreases it in mammalian cells (Swart-Mataraza *et al.*, 2002; Jadeski *et al.*, 2008). In agreement with this, a dominant-negative IQGAP1 construct, where the GRD domain was deleted (IQGAP1ΔGRD), making it unable to bind Cdc42, also decreases the amount of GTP-Cdc42 in cell lysates (Swart-Mataraza *et al.*, 2002). Notably, IQGAP1 is not only able to bind the active form of Cdc42 but it also has less affinity to the nucleotide-depleted (ND) form of Cdc42 (Grohmanova *et al.*, 2004). It harbours two binding domains for Cdc42-ND, whose interaction favours the binding of GTP-Cdc42. Additionally it was shown that the GRD domain alone is not sufficient for the binding

of GTP-Cdc42, but this interaction depends on the tertiary structure of the whole C-terminus (Grohmanova *et al.*, 2004).

The conformation of IQGAP1 seems to play a role in its affinity towards its interaction partners. IQGAP1 is believed to be kept inactive through an autoinhibitory interaction between the GRD domain and RGCT domain (Figure 11) (Brandt and Grosse, 2007). This autoinhibited state can be relieved by Cdc42/Rac1 binding to the GRD domain or phosphorylation of IQGAP1 on Ser1443 (Grohmanova *et al.*, 2004). In agreement with this model, a mutant IQGAP1, defective in Rac1/Cdc42 binding in the GRD domain, induces multiple leading edges (Fukata *et al.*, 2002) and a phosphomimetic variant of IQGAP1 on Ser1443, resembling the active, Cdc42-bound state of IQGAP1, stimulates neurite outgrowth (Li *et al.*, 2005).

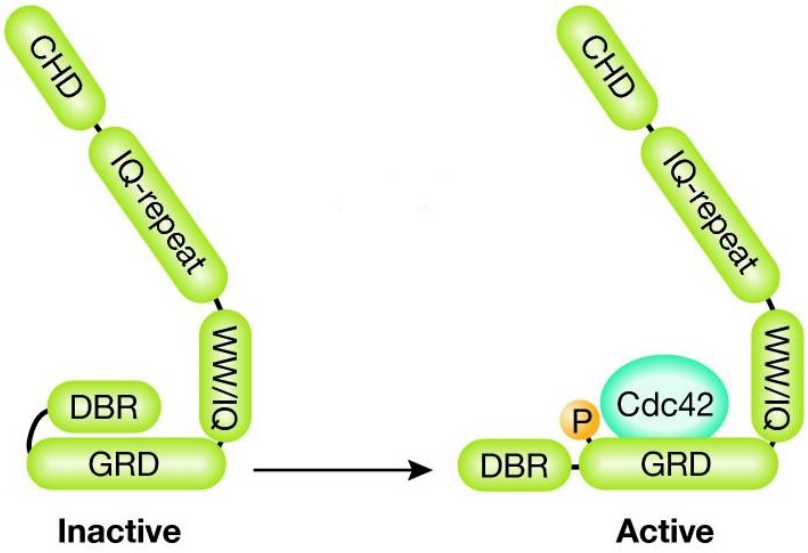

Figure 11. Conformational change of IQGAP1.

The DBR (RGCT domain) can fold on the GRD domain disabling Cdc42-binding and conferring to a closed conformation. Phosphorylation of IQGAP1 on S1443 or binding of Cdc42 can relieve this autoinhibition and open the structure. Figure from Brandt and Grosse, 2007.

Calmodulin (calcium-modulated protein) is an important multifunctional calcium-mediated signalling molecule in eukaryotic cells. IQGAP1 can associate with calmodulin through its IQ-motifs (Mateer *et al.*, 2002). As described previously, siRNA-mediated depletion of IQGAP1 reduces the amount of calmodulin at the actin-rich cortex. Hence, IQGAP1 targets calmodulin to the cortex (Psatha *et al.*, 2007). Accumulating evidence suggests that Cdc42/Rac1 and calmodulin can influence the

binding of IQGAP1 to other proteins. For example, binding of calmodulin to IQGAP1 inhibits the binding of Cdc42, E-cadherin and actin (Bashour *et al.*, 1997; Joyal *et al.*, 1997; Li *et al.*, 2005).

IQGAP1 is able to bind and to cross-link actin filaments in form of dimers or oligomers (Bashour *et al.*, 1997; Fukata *et al.*, 1997). Interestingly, GTP-Cdc42 was shown to enhance (Fukata *et al.*, 1997), while calmodulin was proven to decrease (Bashour *et al.*, 1997) the actin-cross-linking activity of IQGAP1. Recent data, resolving the structure of Cdc42-bound GRD domain of IQGAP1, suggests that Cdc42 (but not Rac1) induces the dimerization of IQGAP1 thereby enhancing F-actin crosslinking and contributing to strong adherens junction formation (LeCour *et al.*, 2016). In the model, two IQGAP molecules form a parallel complex that is stabilized by four Cdc42 proteins binding their GRD domains.

Through binding to E-cadherin and β-catenin, IQGAP1 also plays a role in adhesion. IQGAP1 induces the dissociation of α-catenin from the E-cadherin–β-catenin complex (competing with α-catenin for the same binding site on β-catenin) thereby uncoupling the adhesion machinery from the actin cytoskeleton (Figure 12) (Fukata *et al.*, 1999). Thus, overexpression of IQGAP1 leads to a decrease in E-cadherin–mediated cell-cell adhesive activity in mouse L-fibroblasts expressing E-cadherin (Kuroda *et al.*, 1998). Interestingly, binding of active Cdc42 to IQGAP1 abolishes the interaction with E-cadherin and β-catenin thus increasing cell adhesion (Kuroda *et al.*, 1998; Fukata *et al.*, 1999). Importantly, calmodulin binding can also influence the interaction between E-cadherin and IQGAP1, since a previous study revealed that calmodulin and E-cadherin compete for binding to IQGAP1. Disruption of the binding of calmodulin to IQGAP1 by the calmodulin antagonist CGS9343B increased IQGAP1 at areas of MCF-7 cell-cell contacts and enhanced the association of IQGAP1 with components of the cadherin-catenin complex, resulting in impaired E-cadherin function (Li *et al.*, 2005).

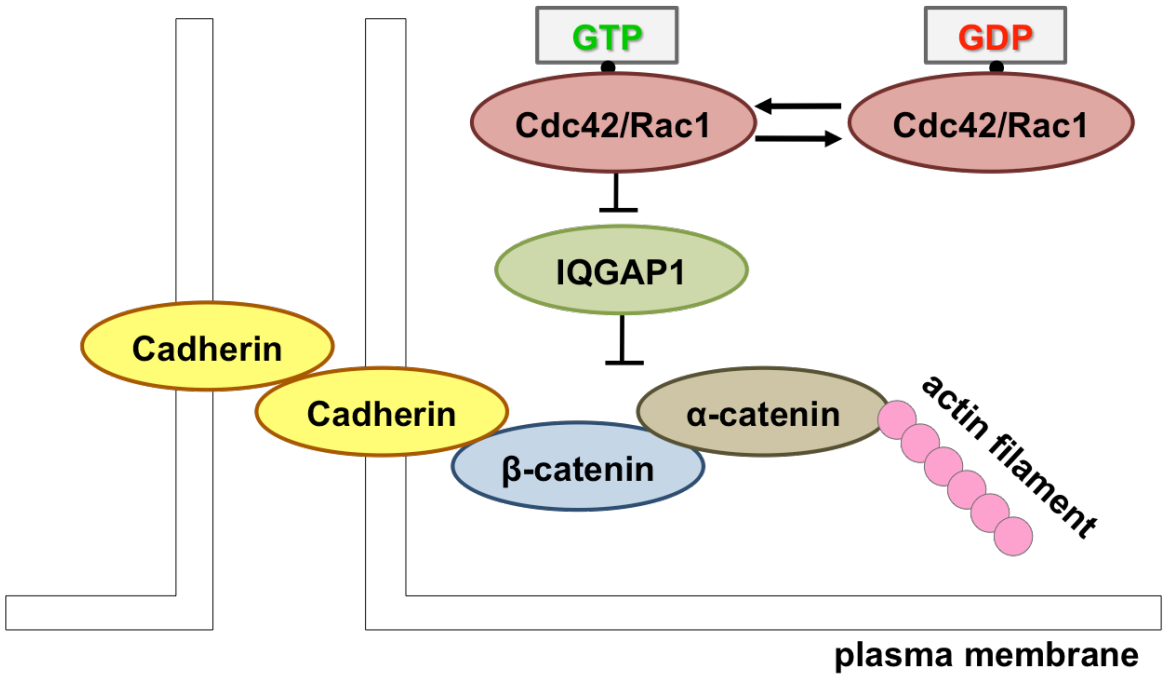

Figure 12. Model illustrating the effect of IQGAP1 and Cdc42/Rac1 on cell adhesion.

The inactive, GDP-bound Cdc42 and Rac1 cannot interact with IQGAP1, allowing IQGAP1 to interact with β-catenin. Binding of IQGAP1 dissociates α-catenin from the cadherin-catenin complex, leading to weak adhesion. Activated, GTP-bound Cdc42 and Rac1 interact with IQGAP1, impairing its interaction with β-catenin and thus resulting in the stabilization of the cadherin-catenin complex. Figure modified from Fukata *et al.*, 1999.

IQGAP1 was also shown to capture microtubule plus ends in complex with activated Cdc42 and Rac1 via the microtubule plus-end-associated protein CLIP-170 (Fukata *et al.*, 2002). IQGAP1 co-sediments with MTs in the presence - but not in the absence - of CLIP-170. This model was extended by Watanabe *et al.*, who found that the Adenomatous polyposis coli (APC) protein, an important tumor suppressor in the human colon, can also form a tripartite complex with IQGAP1 and Cdc42/Rac1, which interaction is necessary for the stabilization of the IQGAP1 – CLIP-170 interaction and thereby for correct MT tethering to the cortex (Watanabe *et al.*, 2004).

Menin seems to function upstream of IQGAP1, since its overexpression increases IQGAP1 accumulation at the plasma membrane, reduces the GTP-Rac1 but increases the E-cadherin/β-catenin interaction with IQGAP1. In turn, β-catenin and E-cadherin are reduced at cell-cell contacts in Men1-negative mice. Interestingly, Rac1 OE can prevent the membrane accumulation of IQGAP1 in menin OE cells (Yan *et al.*, 2009).

IQGAP1 was also identified as a PIPKIγ-interacting protein through its IQ-motifs (Choi *et al.*, 2013). Additionally, IQGAP1 interacts with the lipid product $PI(4,5)P_2$ via a polybasic motif in its RGCT domain. These interactions can recruit IQGAP1 to the plasma membrane. Moreover, $PI(4,5)P_2$ binding to IQGAP1 was shown to enhance actin polymerization and branching through the neuronal Wiskott–Aldrich syndrome protein (N-WASP) – actin-related protein 2/3 (Arp 2/3) complex in vitro (Choi *et al.*, 2013).

Another interaction partner and regulator of IQGAP1's localization is ezrin. Knock-down of ezrin reduces the cortical localization of IQGAP1 in interphase human epithelial ECV304 cells (Nammalwar *et al.*, 2014).

1.5.3 Function of IQGAP1 in mitosis and spindle orientation

IQGAP1 was also shown to play a role in spindle orientation. In a 3D-MDCK model system the epithelial growth factor receptor (EGFR) was found in a complex with IQGAP1, controlling the orientation of the mitotic spindle (Bañón-Rodríguez *et al.*, 2014). EGFR was shown to be responsible for maintaining the basolateral localization of IQGAP1, which is in turn required for the basolaterally restricted distribution of NuMA but not for that of LGN. If this polarized localization of IQGAP1 or EGFR is disturbed, NuMA cannot be recruited to the basolateral membrane, which results in mitotic spindle misorientation and defects in single lumen formation (Bañón-Rodríguez *et al.*, 2014).

1.5.4 IQGAP1 and cancer

Since IQGAP1 is preferentially localizing to the actin-rich cell cortex and cell-cell contacts, it is likely to be involved in processes influencing migration and cell-cell adhesion. Indeed, overexpression of IQGAP1 enhances, while its knock-down inhibits cell motility (Swart-Mataraza *et al.*, 2002). This function is most probably caused by the ability of IQGAP1 to increase active Cdc42 levels in mammalian cells, resulting in filopodia formation, and the promotion of cell migration and invasion (Swart-Mataraza *et al.*, 2002). It is therefore not surprising that IQGAP1 was found to be overexpressed in a number of human tumors. (For the latest list see: Johnson *et al.*, 2009.) Mouse xenograph experiments from 2008 even showed that IQGAP1

enhances mammary tumorigenesis. Namely, IQGAP1 overexpressing MCF-7 cells form more invasive tumors in immunocompromised mice then MCF-7 cells with stable knock-down of IQGAP1 (Jadeski *et al.*, 2008). Thereby IQGAP1 could be a potential therapeutic target in case of tumors with aberrant IQGAP1 accumulation. Blocking the formation of IQGAP1–Cdc42/Rac1 complexes would decrease the amount of active Cdc42/Rac1 in cancer cells, thereby reducing their potential to metastasize (Jadeski *et al.*, 2008).

In line with its pro-migratory effect, IQGAP1 has been reported to inhibit cell-cell adhesion through binding to E-cadherin and β-catenin, thereby displacing α-catenin and the actin cytoskeleton from the cortex (Kuroda *et al.*, 1998). Interestingly, immunohistochemical studies showed increased IQGAP1 staining at cell-cell contacts at the invasive front of certain tumor samples. At these sites of cortically accumulated IQGAP1 reduced expression of adherens junction molecules (like the tumor suppressor E-cadherin) was observed and this was thought to contribute to reduced adhesion of tumor cells (Takemoto *et al.*, 2001).

It is possible that interaction partners of IQGAP1 also contribute to IQGAP1-induced tumorigenesis. For example, overexpression of IQGAP1 was shown to enhance the nuclear localization of β-catenin in human cells, where the latter can transcriptionally activate several genes that encode oncoproteins and cell cycle regulators, including c-myc and cyclin D1 (Briggs *et al.*, 2002).

More importantly, IQGAP1 interacts with and contributes to the activation of several mitogen-activated protein kinase (MAPK) signalling cascade members, including B-Raf, MEK and ERK, thereby promoting proliferation (Roy *et al.*, 2005). As a scaffold, IQGAP1 brings these kinases in close proximity to facilitate their sequential phosphorylation (Jameson *et al.*, 2013). Since up-regulation of the MAPK cascade occurs in >30% of cancers (Downward, 2003), targeting the pathway could be a promising treatment strategy. Unlike most MAPKs (Scholl *et al.*, 2007), the MAPK scaffold IQGAP1 is not required for viability (Jameson *et al.*, 2013), which makes it a good candidate for alternative MAPK cascade inhibition. Treatment of mice with cell-permeable peptides (corresponding to the WW domain of IQGAP1) disrupts IQGAP1–ERK1/2 interactions and inhibits Ras-driven tumorigenesis (Jameson *et al.*, 2013).

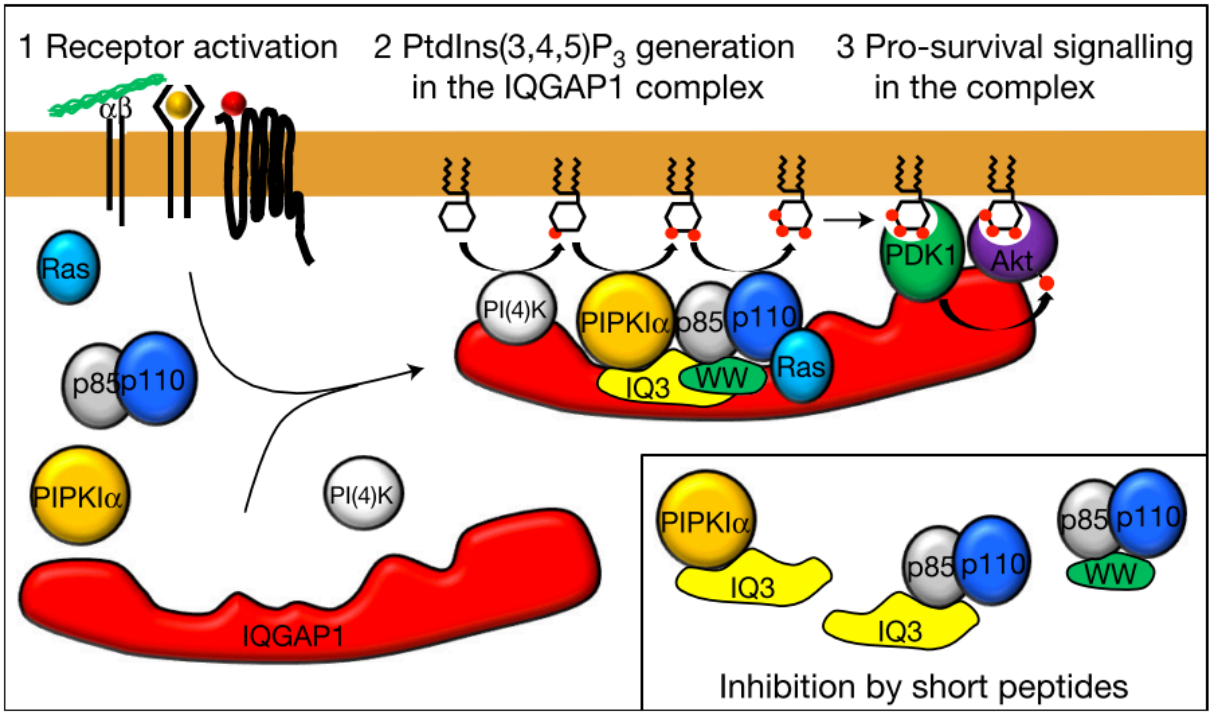

Figure 13. IQGAP1 acts as a scaffold for the PI(3)K-Akt pathway.

IQGAP1-mediated $PI(3,4,5)P_3$-generation and downstream signalling. PIPKIα and PI(3)K (p85 and p110 subunits) bind to the WW and IQ domains of IQGAP1. PIPKIα generates $PI(4,5)P_2$ that is channeled to PI(3)K, facilitating efficient $PI(3,4,5)P_3$ synthesis. The $PI(3,4,5)P_3$ in turn activates downstream effectors such as PDK1 and Akt. Figure from Choi et al., 2016.

Alteration of the phosphatidylinositol-3-kinase – Protein kinase B (PI(3)K–Akt) pathway is linked to many human diseases including cancer (Luo *et al.*, 2003). Akt activation was shown to be reduced upon PIPKIα inhibition in prostate cancers and led to selective elimination of cancer cells (Semenas *et al.*, 2014). Recently, Choi *et al.* showed that IQGAP1 scaffolds the PI(3)K pathway to regulate cell survival through PDK1 and Akt (Figure 13) (Choi *et al.*, 2016). In their study, inhibiting the interaction of IQGAP1 with PIPKIα or PI(3)K with cell-permeable peptides repressed phosphatidylinositol-3,4,5-trisphosphate ($PI(3,4,5)P_3$) synthesis and Akt activation and selectively diminished cancer cell survival. Although the IQGAP1 pathway is present in normal and transformed cells, some cancer cells appear to depend on this pathway for survival (Choi *et al.*, 2016), which opens a door for the IQGAP1 – Akt pathway interactions to be candidates for targeted cancer chemotherapy.

In addition, IQGAP1 seems to have a role in cell cycle progression and mitotic spindle orientation, which are also associated with cancer formation. Adachi and

colleagues found that siRNA-mediated silencing of IQGAP1 leads to cytokinesis defects and to the formation of multinucleated HeLa cells (Adachi *et al.*, 2014). Another recent study using the 3D-MDCK model system demonstrated a key role of IQGAP1 in controlling the orientation of the mitotic spindle (Bañón-Rodríguez *et al.*, 2014). Taken together, being an oncoprotein, IQGAP1 seems to play an important role in tumorigenesis and metastasis.

2 Objectives

MISP plays an important role in spindle orientation and metaphase-to-anaphase transition (Zhu *et al.*, 2013). So far there are only three studies published on MISP (Maier *et al.*, 2013; Zhu *et al.*, 2013; Kumeta *et al.*, 2014), leaving the molecular function of this protein obscure. Although MISP was shown to interact with and regulate the localization of the dynactin complex subunit $p150^{glued}$ (Zhu *et al.*, 2013), it is still not clear how MISP is linked to spindle orientation, in which pathways it is involved.

Therefore, the aim of the presented thesis is to better characterize the function of MISP in spindle orientation through identifying and characterizing novel interaction partners. This should be achieved with a mass-spectrometry screen after immunoprecipitation of MISP. Afterwards, the identified potential binding partners should be validated biochemically and might be confirmed with co-localization experiments. If a proven interaction partner is found, the nature of the interaction is to be uncovered, if it is a regulator, an effector or another type of binding partner. Finally, the functional significance of this interaction should be revealed. Hopefully, the finding will contribute to a better understanding of the mechanisms underlying the regulation of mitosis and spindle orientation by MISP.

3 Results

3.1 MISP interacts and co-localizes with IQGAP1

3.1.1 Mass spectrometry screen for MISP-interacting proteins

To better understand the mechanisms underlying the function of MISP in spindle orientation and mitotic progression I performed a screen to discover novel MISP interacting proteins. I immunoprecipitated FLAG-MISP or FLAG as a control from taxol-blocked HeLa cell lysates and detected co-precipitating proteins by mass spectrometry analysis together with the Protein Analysis unit of the Genomics and Proteomics Core Facility of the DKFZ (Figure 14).

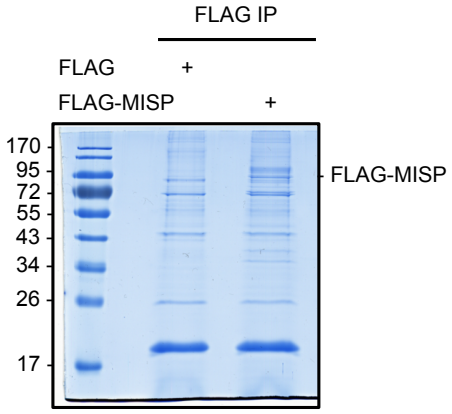

Accession	Description	Score	Mass	Matches	Seqs	Cover
CDK1_HUMAN	Cyclin-dependent kinase 1 OS=Homo sapiens GN=CDK1 PE=1 SV=3	593	34131	26	10	41.8
IQGA1_HUMAN	Ras GTPase-activating-like protein IQGAP1 OS=Homo sapiens GN=IQGAP1 PE=1 SV=1	109	189761	3	3	2.4
CDC42_HUMAN	Cell division control protein 42 homolog OS=Homo sapiens GN=CDC42 PE=1 SV=2	95	21587	5	3	25.1
MARE1_HUMAN	MT-associated protein RP/EB family member 1 OS=Homo sapiens GN=MAPRE1 PE=1 SV=3	68	30151	2	2	11.2

Figure 14. Selected results of mass spectrometry analysis.

HeLa cells were transfected with FLAG or FLAG-MISP and blocked overnight in mitosis with taxol treatment. Cell lysates were subjected to immunoprecipitation with FLAG M2 beads and co-precipitating proteins were analyzed using mass spectrometry. Efficient FLAG-MISP enrichment is shown on the Coomassie stained SDS polyacrylamide gel, which was directly sent for mass spectrometrical analysis. In the table, interacting proteins relevant for this study are shown. Mass – protein mass (Da), Seqs – number of sequences, Cover – coverage (%).

In this screen, I identified the scaffolding protein IQGAP1, which has already been indicated in a previous screen as a potential interaction partner of MISP (Hein *et al.*, 2015). Two other published interaction partners, the plus-tip-binding protein EB1 (Maier *et al.*, 2013) and Cyclin-dependent kinase 1 (Cdk1) (Zhu *et al.*, 2013) were also found in the screen, validating the results. Interestingly, the small signaling molecule Cdc42, a well-characterized binding partner of IQGAP1, was also identified in the analysis (Figure 14).

3.1.2 Validation of the MISP - IQGAP1 interaction in vivo and in vitro

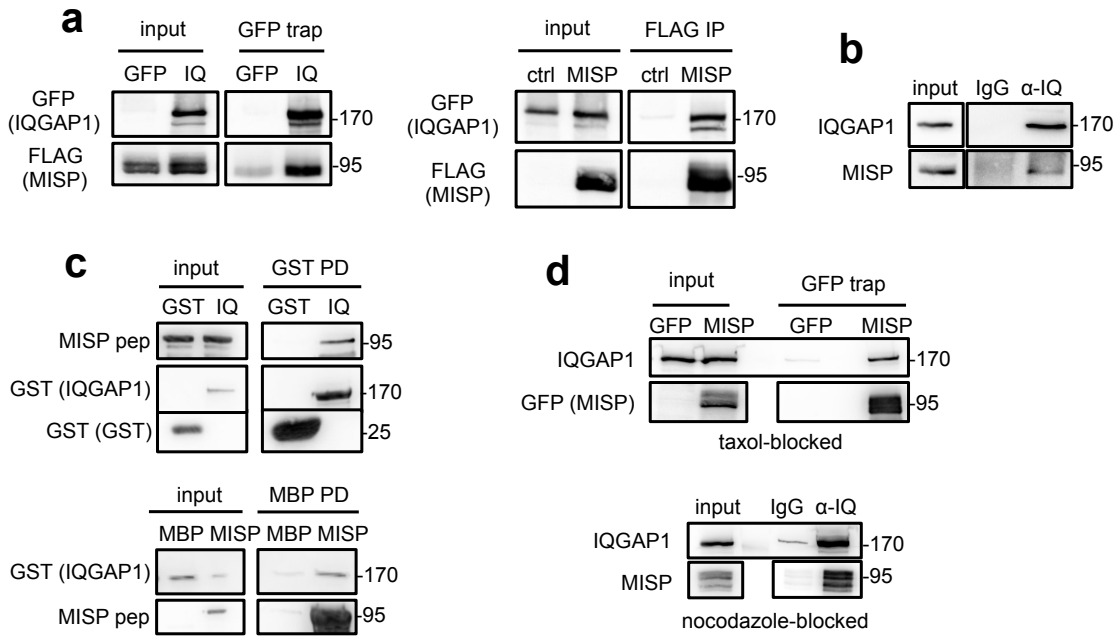

Figure 15. MISP interacts with IQGAP1 in asynchronous and mitotic cells and in vitro.

(a) HEK293T cells transiently overexpressing GFP-IQGAP1 and FLAG-MISP were used for co-immunoprecipitation experiments from both sides (GFP trap or FLAG M2 beads). (b) Endogenous immunoprecipitation using IQGAP1 antibody or control immunoglobulin (IgG) was carried out in HeLa cell lysates and MISP was detected in the eluate. (c) In vitro interaction between purified MBP-MISP and GST-IQGAP1 was detected by GST and MBP pull-down experiments. (d) Upper panel: co-immunoprecipitation of endogenous IQGAP1 with GFP-MISP from taxol-blocked HeLa cells, lower panel: co-immunoprecipitation of endogenous MISP and IQGAP1 from HeLa cells treated with nocodazole.

Next, I wanted to investigate whether this interaction could be corroborated with co-immunoprecipitation (co-IP) experiments coupled to immunoblot analysis. In fact, the interaction between the two proteins could be confirmed by co-IP experiments

with overexpressed proteins in HEK 293T cells (Figure 15a). In addition, using antibodies against the endogenous proteins, I could show in vivo complex formation between MISP and IQGAP1 in HeLa cell lysates (Figure 15b). Furthermore, I asked whether the interaction between IQGAP1 and MISP was direct. Therefore, I conducted in vitro pull-down assays using recombinant proteins (GST-tagged IQGAP1 and MBP-tagged MISP) and confirmed that IQGAP1 and MISP are also part of a complex in vitro (Figure 15c). Half-endogenous and endogenous IP experiments in HeLa cells showed that the IQGAP1-MISP interaction is also present in mitotically blocked cells (Figure 15d). Taken together, MISP seems to bind IQGAP1 directly.

3.1.3 MISP binds to the C-terminal domains of IQGAP1

After validating the interaction, I wanted to narrow down which domain of IQGAP1 interacts with MISP. Interaction studies with the N- (aa 1-863) and C-terminal (aa 764-1657) half of IQGAP1 revealed that MISP strongly binds to the C-terminal part of IQGAP1 (Figure 16a-c), which contains a part of the IQ motifs, the GRD domain, responsible for Cdc42 and Rac1 binding, and the RGCT domain. Interestingly, both the GRD and the RGCT domain showed an interaction with MISP (Figure 16b), suggesting that MISP might bind to IQGAP1 through multiple binding domains. Next, I checked if the phosphorylation status of MISP by Plk1 has an influence on the interaction with IQGAP1. Surprisingly, although the phosphorylation of MISP by Plk1 seems to play an important role in its mitotic function (Zhu *et al.*, 2013), no difference in binding of the phosphomutants (6DP – phospho-mimicking, 7AP - non-phosphorylatable) to IQGAP1 could be observed (Figure 16d).

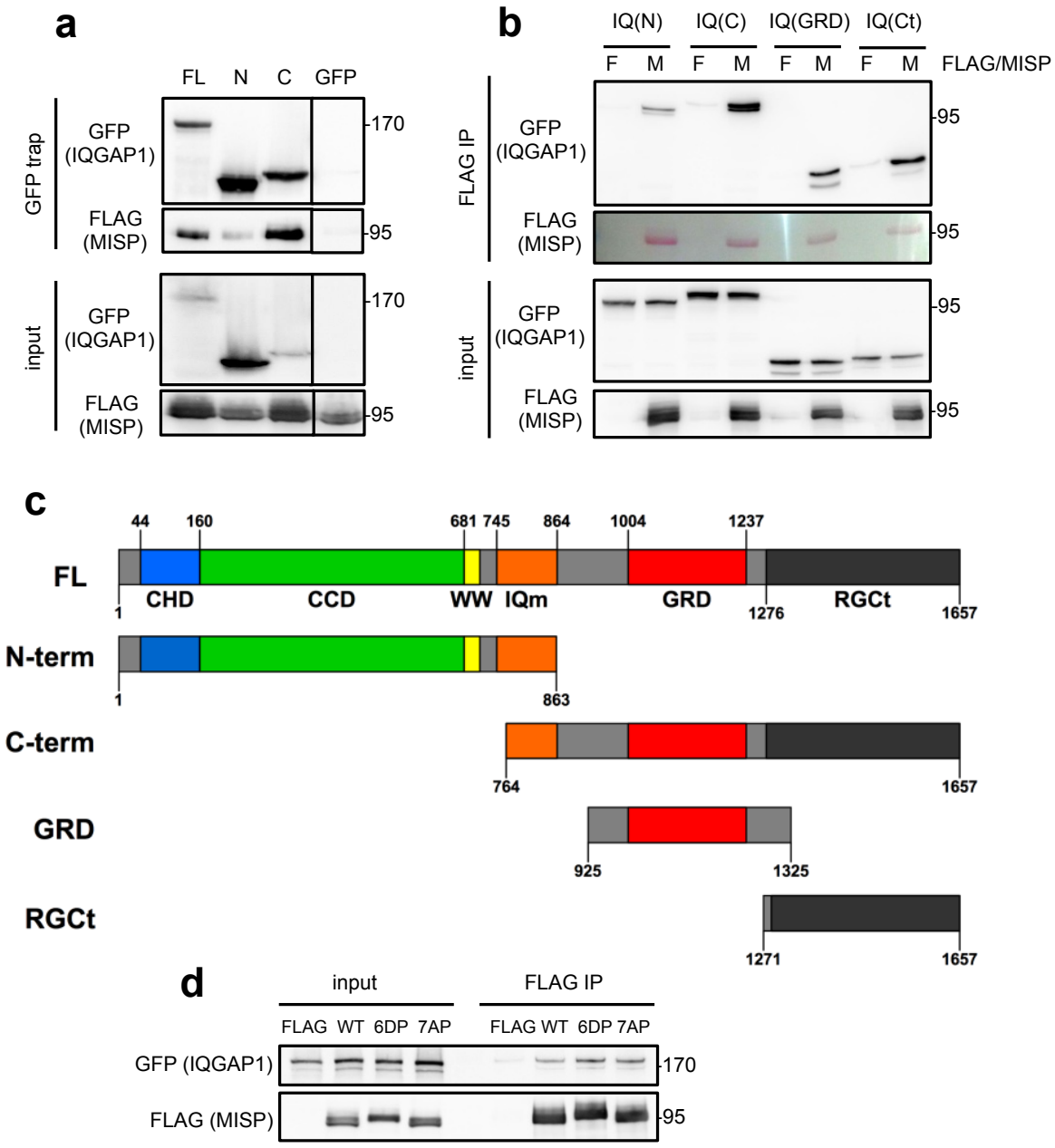

Figure 16. MISP interacts with the C-terminal half of IQGAP1.

(a) FLAG-MISP was co-expressed with full-length (FL), N-terminal (N) or C-terminal part (C) of GFP-tagged IQGAP1 or GFP alone in HEK293T cells. The GFP trap experiment shows co-precipitation of FLAG-MISP with the different IQGAP1 constructs. (b) FLAG-MISP was co-expressed with GFP-IQGAP1 truncation constructs: N-terminal (N), C-terminal (C), GRD or RGCT (Ct) domains in HEK293T cells. FLAG IP experiment shows co-precipitation of the different IQGAP1 constructs with FLAG-MISP. (c) Graphic illustrating the different IQGAP1 truncation constructs. (d) Interaction of MISP phosphomutants with IQGAP1. FLAG alone, MISP wild-type (WT), MISP phosphomimicking mutant for Plk1 (6DP) and MISP non-phosphorylatable mutant for Plk1 (7AP) together with GFP-IQGAP1 were overexpressed in HEK293T cells and the interaction was studied with FLAG IP.

3.1.4 MISP co-localizes with IQGAP1 in interphase and mitosis

In order to reveal where in the cell this interaction might take place, I visualized the co-localization of the two proteins by fluorescent microscopy after immunostaining for the endogenous proteins. MISP and IQGAP1 localize to actin structures both in interphase and mitosis. Their co-localization was most pronounced at actin-rich peripheral regions in interphase (Figure 17a) and near the plasma membrane in mitosis (Figure 17b). This co-localization would favor the interaction between the two proteins in interphase and mitotic HeLa cells.

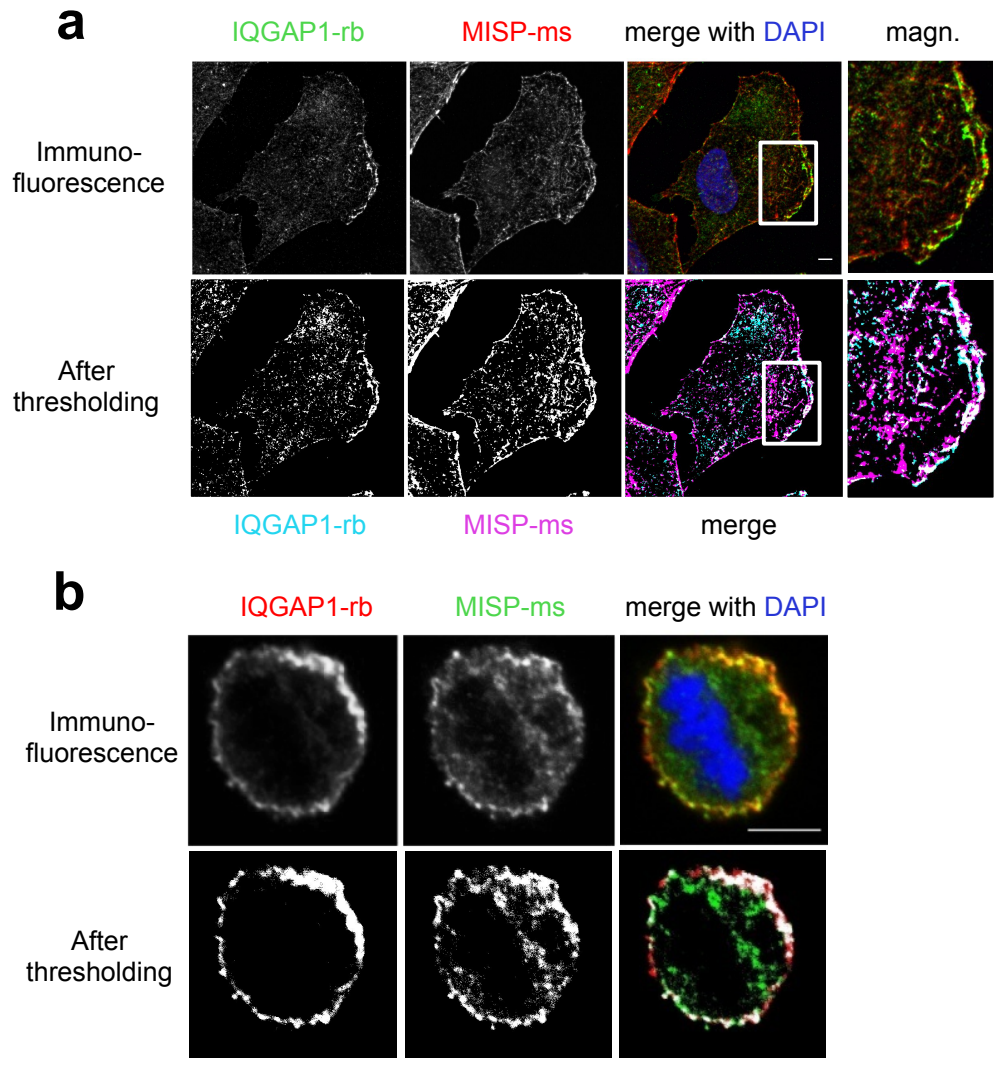

Figure 17. IQGAP1 co-localizes with MISP.

HeLa cells were immunostained for MISP and IQGAP1 and co-localization was visualized in interphase (a) and in mitosis (b) in single-plane confocal images; scale bar, 5 µm. Lower pictures: In the merge images white pixels mark the co-localizing areas of MISP and IQGAP1 staining after the different stainings have been thresholded manually. Rectangles mark magnified areas.

3.2 MISP regulates IQGAP1 distribution at the cell cortex in mitosis

3.2.1 MISP and IQGAP1 do not influence each other's cellular levels

The next step was to investigate the functional importance of the MISP-IQGAP1 interaction and to reveal the hierarchy between the two proteins. To gain insight into the functional consequences of this interaction, I first checked by immunoblotting if the down-regulation of either MISP or IQGAP1 changes the levels of the other protein. As shown in Figure 18, overexpression or siRNA-mediated depletion of either IQGAP1 or MISP had no effect on the overall cellular levels of the other protein.

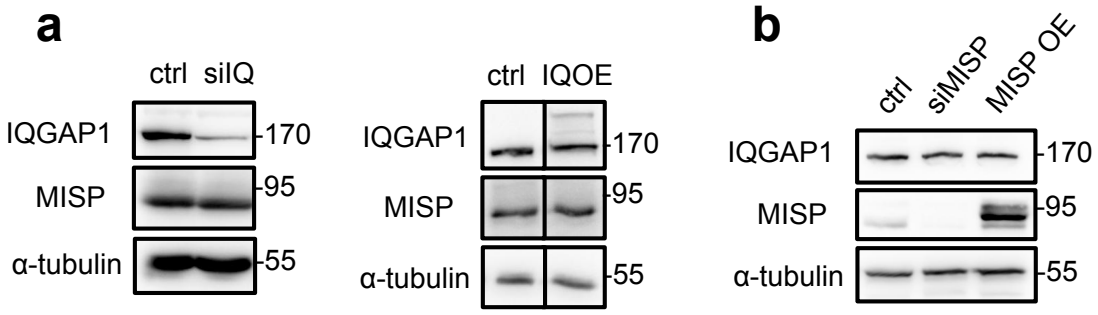

Figure 18. MISP and IQGAP1 have no effect on each other's cellular protein levels.

HeLa cells after siRNA-mediated depletion or overexpression of IQGAP1 (a) or MISP (b) were lysed and subjected to immunoblotting. α-tubulin was used as a loading control.

3.2.2 IQGAP1 accumulates at the cell cortex in mitosis upon siRNA-mediated depletion of MISP

To investigate whether MISP is involved in the regulation of IQGAP1 localization in mitosis, I analyzed the distribution of IQGAP1 at the cortex upon MISP down-regulation. IQGAP1 was localized both in the cytosol and at the cell cortex in mitotic cells (Figure 19a). Interestingly, depletion of MISP using two different siRNAs increased the cortical localization of IQGAP1 in HeLa Kyoto cells (Figure 19a,b). This cortical accumulation of IQGAP1 could also be observed in two additional human cell lines: in the alveolar epithelial adenocarcinoma cell line A549 and in the breast adenocarcinoma cell line MCF-7 (Figure 19c). Interestingly, ectopic expression of MISP (MISP OE) did not have an impact on IQGAP1 levels at the cell cortex (Figure 19a). The cortical elevation of IQGAP1 upon MISP knock-down could be rescued

upon expression of a siRNA-resistant (Zhu *et al.*, 2013) version of MISP (Figure 19a). In contrast, IQGAP1 depletion did not have an effect on the cortical localization of MISP in mitosis (Figure 19d), excluding the possibility that the two proteins mutually influence each other's localization.

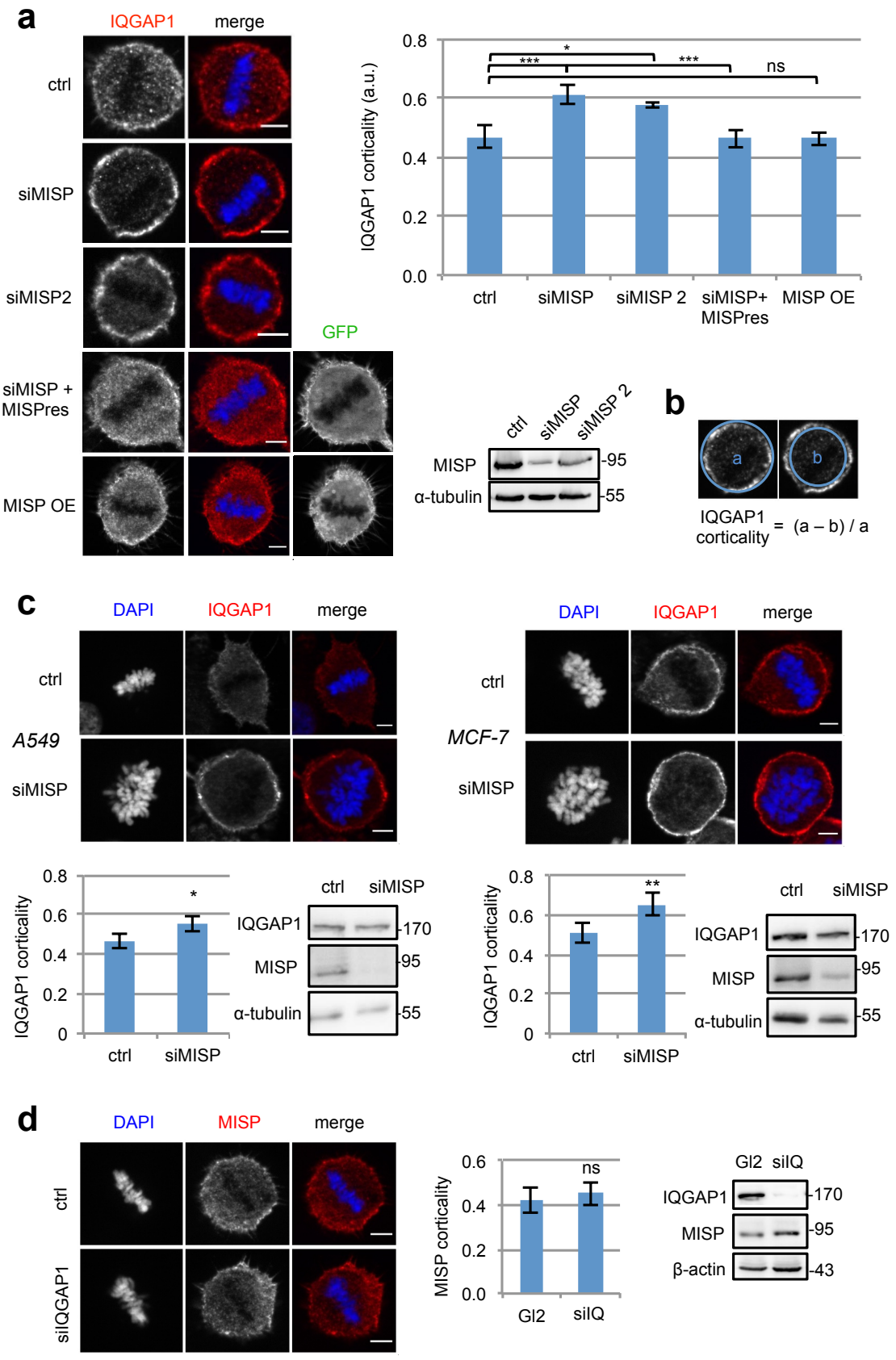

Figure 19. IQGAP1 gets recruited to the cell cortex upon MISP depletion in mitosis.

(a) HeLa Kyoto cells treated with control or MISP siRNA or a GFP-MISP construct were immunostained for IQGAP1 and mitotic cells were observed. MISPres, siRNA-resistant form of MISP. Single equatorial images; scale bar, 5 µm. Chart: Corresponding quantification of IQGAP1 signal at the cortex in control, MISP KD, rescue or MISP OE conditions. Values represent mean ± SD of 3 independent experiments, n=15, one-way ANOVA with Bonferroni's test. Immunoblot showing downregulation efficiency of MISP with two different siRNAs, α-tubulin is used as loading control. (b) Illustration of how cortical IQGAP1 signal was quantified. (c) Fluorescence images show the localization of endogenous IQGAP1 in mitotic control and MISP KD A549 (left) and MCF-7 (right) cells. Single equatorial images; scale bar, 5 µm. Charts: Cortical accumulation of endogenous IQGAP1 was quantified as shown in (b). Values represent mean ± SD of 3 independent experiments, n=15. Western blots show knock-down efficiency, α-tubulin is used as loading control. (d) Cortical localization of MISP in control and IQGAP1-depleted mitotic HeLa Kyoto cells was visualized and quantified as shown in (b). Single equatorial plane; scale bar, 5 µm. Values represent mean ± SD of 3 independent experiments, n=15. Western blots show knock-down efficiency, β-actin is used as loading control.

3.2.3 Depletion of MISP induces the recruitment of IQGAP1 from the cytosol to the cell cortex

Since the total cellular levels of IQGAP1 did not change after MISP down-regulation (Figure 18b and Figure 19c), it seemed plausible that a cytosolic pool of IQGAP1 gets recruited to the cell cortex upon MISP-depletion. Therefore I compared the cytosolic and cortical amounts of IQGAP1 in control and MISP KD cells using immunofluorescence microscopy. While cortical levels of IQGAP1 increased upon MISP down-regulation, cytosolic IQGAP1 levels decreased (Figure 20a) suggesting that IQGAP1 is recruited from the cytosol to the cell cortex in MISP-depleted cells.

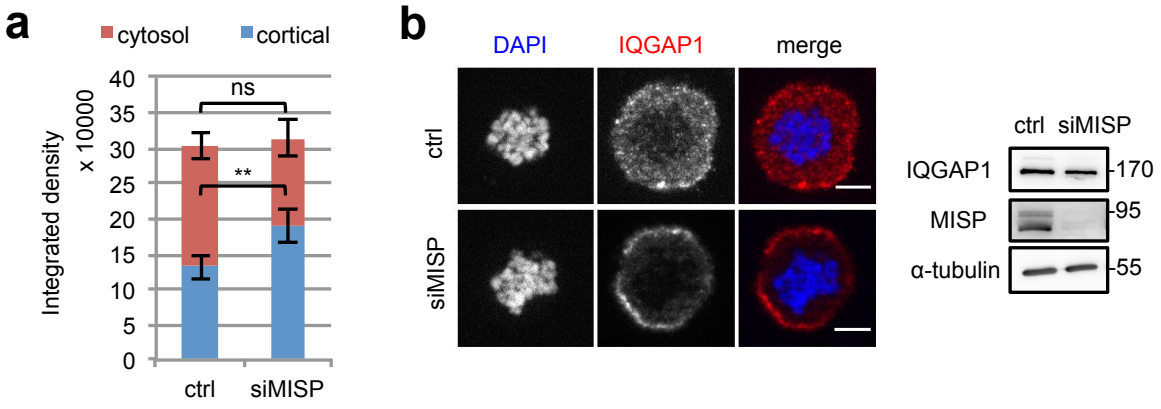

Figure 20. Upon MISP-depletion IQGAP1 gets recruited to the cell cortex from the cytosol in a MT-independent manner.

(a) Quantification of the distribution of IQGAP1 between cortex and cytosol in control and MISP-depleted mitotic HeLa Kyoto cells, n=15. (b) Nocodazole-blocked HeLa Kyoto cells treated with control or MISP siRNA were immunostained for IQGAP1. Single equatorial plane; scale bar, 5 µm. Immunoblot shows down-regulation efficiency of MISP, α-tubulin is used as loading control.

3.2.4 Cortical accumulation of IQGAP1 upon MISP knock-down is microtubule-independent

A possible mechanism for IQGAP1 to localize to the cell cortex in mitosis would be transportation via astral microtubules. In order to investigate if microtubules play a role in the cortical accumulation of IQGAP1 upon MISP knock-down, I treated the cells with a high dose of the microtubule-depolymerizing agent nocodazole overnight. IQGAP1 could be recruited to the cell cortex even in the absence of MTs upon MISP depletion (Figure 20b), suggesting that the cortical localization of IQGAP1 is not MT-dependent.

3.2.5 Cortically accumulated IQGAP1 recovers slower after photobleaching

I also wanted to study the dynamics of this cortical pool of IQGAP1 in control and MISP-depleted cells. For that, I used the fluorescence recovery after photobleaching (FRAP) method. Small, cortical regions of the same size in mitotic HeLa cells expressing GFP-IQGAP1 treated with control or MISP siRNA were bleached and fluorescence recovery was measured over time. While the immobile fraction did not change, I observed a slower recovery of GFP-IQGAP1 at the cortex after MISP depletion than after control siRNA treatment (Figure 21a-b). This result could arise from the decreased cytosolic fraction of IQGAP1 upon MISP-depletion and might suggest, that upon MISP-depletion IQGAP1 has a stronger interaction with cortical proteins.

3.2.6 Akt activation is impaired after MISP-depletion

Having identified a strong accumulation of IQGAP1 at the cortex upon MISP KD several questions emerge: What is the function of this pool of IQGAP1 at the cell cortex? What recruits IQGAP1 to the cell cortex? Does this pool correspond to an active or inactive state of IQGAP1? In order to find out if IQGAP1 is still able to fulfill its function I took advantage of a downstream protein, Akt (or Protein kinase B).

Since IQGAP1 was shown to be involved in the activation of Akt (Chen *et al.*, 2010; Sbroggio *et al.*, 2011; Choi *et al.*, 2016), the phosphorylation status of Akt (on S473) was analyzed and a decreased phospho-Akt signal was detected upon MISP depletion both in untreated and serum-induced HeLa Kyoto or MCF-7 cells (Figure 21c). This result is similar to IQGAP1-depleted cells, which also show reduced Akt activation (Choi *et al.*, 2016), and might suggest that cortical accumulation of IQGAP1 after MISP knock-down renders IQGAP1 nonfunctional and therefore it cannot activate downstream signaling pathways efficiently.

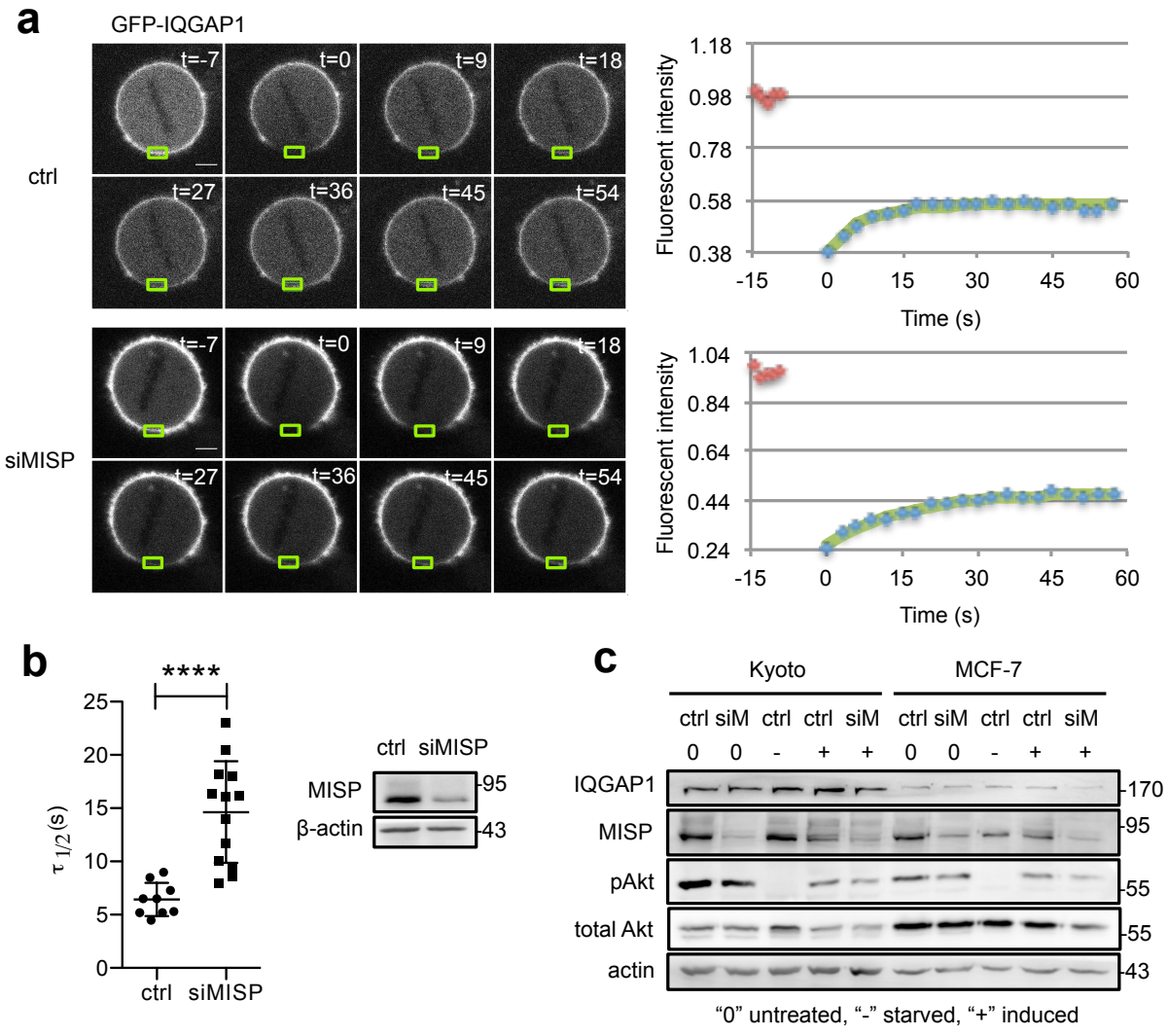

Figure 21. FRAP experiment and Akt activation after MISP KD.

(a) FRAP experiment of control and MISP siRNA-treated HeLa cells inducibly overexpressing GFP-IQGAP1. Green rectangles mark the bleached areas; scale bar, 5 µm. Red squares on the graphs indicate pre-bleaching data, blue squares show recovery after bleaching with a green single exponential trend line. (b) τ 1/2 of FRAP experiments shows recovery half-time

of control and MISP-depleted cells in one representative experiment, $p<0.0001$. Western blots show knock-down efficiency, β-actin is used as loading control. (c) Immunoblot of control and MISP KD samples for Akt activation in untreated, serum starved (20 h) and induced (30 min 20% FBS after 20 h starvation) conditions, β-actin is used as loading control.

3.3 MISP regulates IQGAP1 distribution at the cell cortex in mitosis in a Cdc42-dependent manner

3.3.1 Cdc42 WT and CA overexpression prevents IQGAP1 accumulation at the cell cortex in mitosis upon MISP knock-down

The small GTPase family members Cdc42 and Rac1 were shown to be regulators of IQGAP1 activity and its affinity towards interaction partners (Kuroda *et al.*, 1996). For example, Cdc42/Rac1 can inhibit the IQGAP1-β-catenin interaction and thereby regulate the subcellular localization of IQGAP1 (Fukata *et al.*, 1999). The tumor suppressor protein menin was shown to regulate IQGAP1's localization in a Rac1-dependent manner (Yan *et al.*, 2009). Menin overexpression increases IQGAP1 accumulation at the plasma membrane, reduces IQGAP1's affinity towards Rac1 and leads to an overall decrease in active Rac1 levels. Rac1 overexpression can prevent targeting of IQGAP1 to the cell cortex by increased amounts of menin (Yan *et al.*, 2009). Since I found Cdc42 (and not Rac1) in the mass spectrometry screen as a MISP-interacting protein (Figure 14) and Cdc42 was also shown to be involved in the regulation of spindle orientation (Mitsushima *et al.*, 2009), I investigated whether overexpression of Cdc42 could rescue the cortical accumulation of IQGAP1 upon MISP depletion.

It is difficult to study and influence the temporal and local activity status of Cdc42, therefore many studies utilize constitutively active or dominant negative mutants. Constitutively active (CA) mutants are GTPase-deficient, unable to hydrolyze GTP and therefore signal constitutively to their effector proteins. Common constitutively active mutations are Gly12Val (G12V) or Gln61Leu (Q61L). Dominant-negative (DN) Cdc42 contains a substitution mutation of Thr17Asn (T17N) or Asp118Ala (D118A), which allows binding of GEFs but inhibits downstream interactions (Davis *et al.*, 1998; Heasman and Ridley, 2008).

Surprisingly, expression of both Cdc42 wild-type (WT) and Cdc42 constitutively active (CA, Q61L) could diminish cortical accumulation of IQGAP1 in the absence of MISP, while expression of Cdc42 dominant negative (DN, T17N) did not alter the subcellular distribution of IQGAP1 upon MISP knock-down (Figure 22). From these results it seems that the activity status of Cdc42 plays an important role in its function of regulating IQGAP1 localization after MISP depletion. In contrast, overexpression of the DN form of Cdc42 alone did not trigger the cortical accumulation of IQGAP1 and the CA form did not reduce it (Figure 22), suggesting that the phenotype is specific to MISP and not only caused by the activation status of Cdc42.

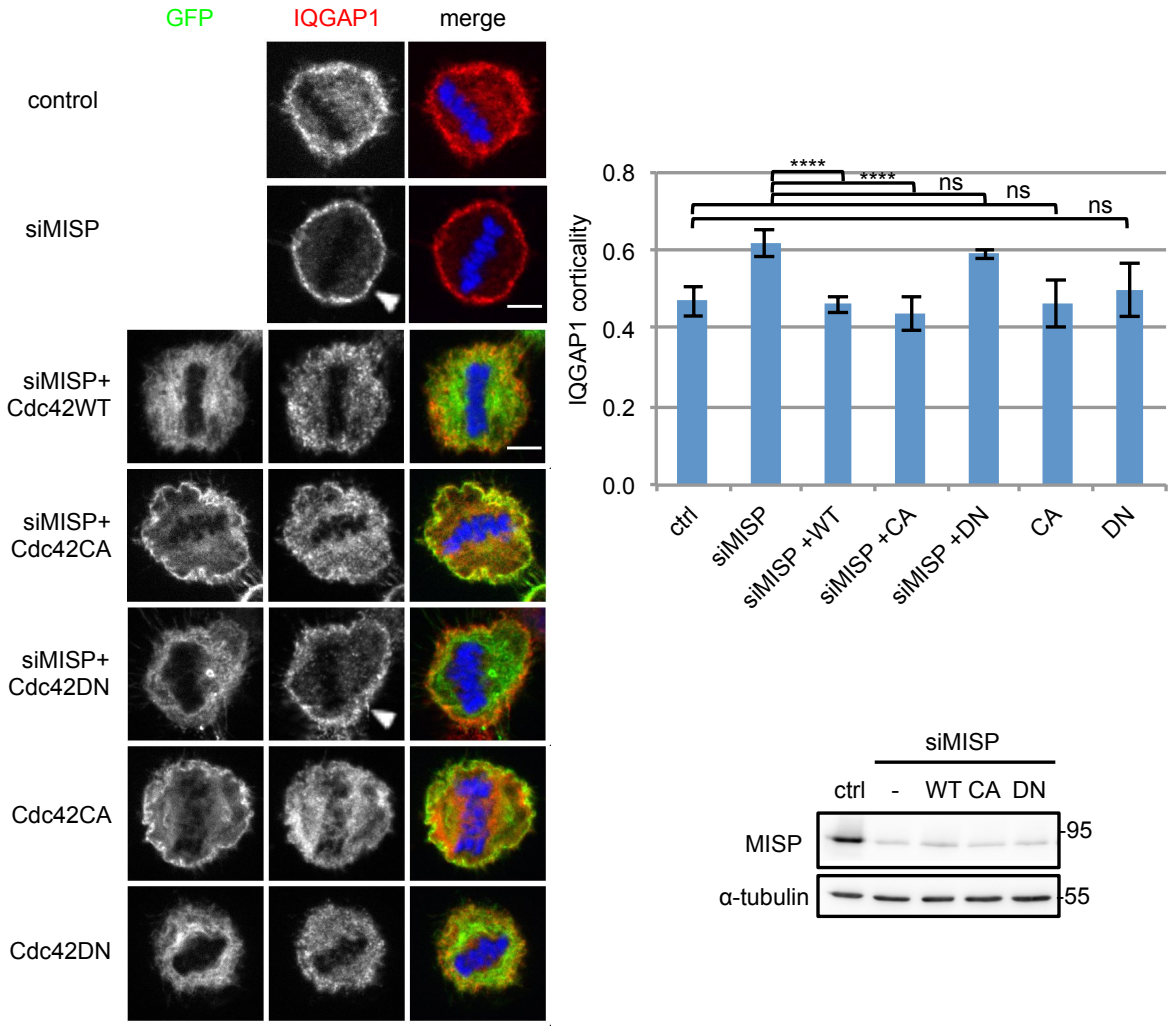

Figure 22. MISP controls the cortical accumulation of IQGAP1 in a Cdc42-dependent manner.

Immunostaining for IQGAP1 in control and MISP-depleted mitotic HeLa Kyoto cells overexpressing different Cdc42 constructs (WT – wild-type, CA – constitutively active, DN – dominant negative). Arrowheads show cortically accentuated IQGAP1. Single equatorial

images; scale bar, 5 µm. Chart: IQGAP1 corticality was quantified as in **Error! Reference source not found.**Figure 19b. Values represent mean ± SD of 3 independent experiments, n=15, one-way ANOVA with Bonferroni's test. WB: Immunoblotting showing MISP down-regulation in different conditions, α-tubulin is used as loading control.

3.3.2 Cdc42-binding deficient IQGAP1 does not accumulate at the cell cortex upon MISP-depletion

IQGAP1 binds to Cdc42 via a short amino acid motif (aa 1054-1077) within the GRD domain (Mataraza *et al.*, 2003). In order to show that the interaction between IQGAP1 and Cdc42 is required for the regulation of IQGAP1's localization at the cell cortex by MISP, I generated a deletion mutant of IQGAP1 that is unable to bind Cdc42 (IQGAP1ΔCdc42, Δ1054-77, (Mataraza *et al.*, 2003)). Unlike IQGAP1WT, IQGAP1ΔCdc42 did not accumulate at the cell cortex in mitosis upon MISP depletion (Figure 23a). I also confirmed that unlike IQGAP1WT, this mutant is unable to bind active Cdc42 but still capable of binding to MISP (Figure 23b). From these data, it can be concluded that MISP regulates IQGAP1 levels at the cell cortex and that accumulation of IQGAP1 at the cell cortex is dependent on Cdc42, although it cannot be excluded that this mutation affects other properties of IQGAP1.

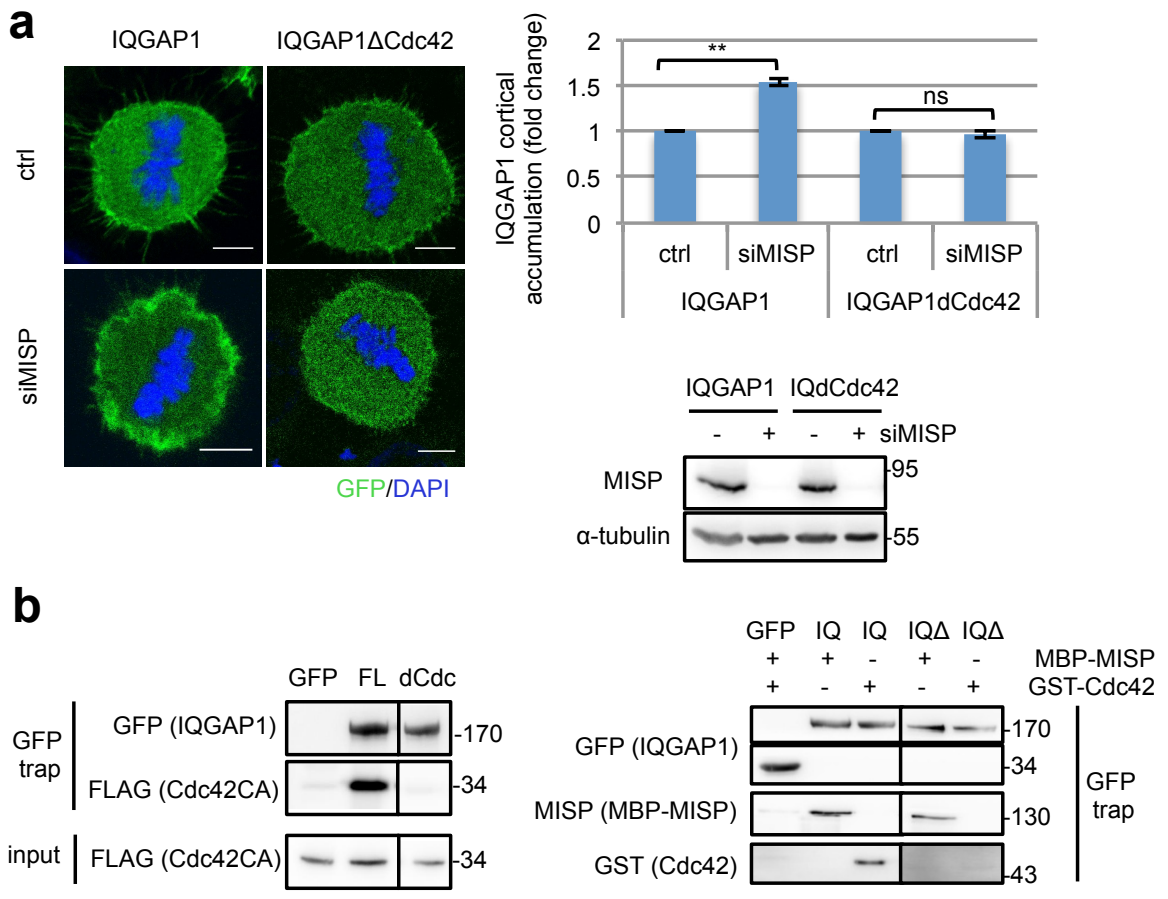

Figure 23. IQGAP1ΔCdc42 does not accumulate at the cell cortex upon MISP KD.

(a) Cortical accumulation of overexpressed WT or Cdc42-binding deficient IQGAP1 (IQdCdc, Δaa1054-77) was analyzed in control and MISP siRNA treated HeLa Kyoto cells in mitosis by fluorescence microscopy. Single equatorial plane; scale bar, 5 µm. Chart: Cortical accumulation of the constructs was measured in control and siMISP cells like in **Figure 19**b. Results were normalized to control and one-sample t-test was carried out on log2-transformed data. Values represent mean ± SD of 3 independent experiments, n=30, p=0.0025 and 0.1425 in interphase, and p=0.0017 and 0.4104 in mitosis. Western blot shows down-regulation efficiency, α-tubulin is used as loading control. (b) Left: GFP trap experiment in HEK293T cell lysates for the interaction of IQGAP1 (FL) and IQGAP1ΔCdc42 (dCdc) with Cdc42CA. Right: Half-in-vitro experiment showing the binding of MISP and Cdc42 to IQGAP1 (IQ) and IQGAP1ΔCdc42 (IQΔ). GFP/GFP-IQGAP1/GFP-IQGAP1ΔCdc42 was pulled down from HEK293T cell lysates, washed and incubated with recombinant MBP-MISP or GST-Cdc42.

3.4 MISP interacts with the active form of Cdc42 through IQGAP1

3.4.1 MISP interacts and co-localizes with Cdc42 WT and CA

Given that Cdc42 plays a role in the cortical accumulation of IQGAP1 provoked by MISP down-regulation, and Cdc42 was found in the mass spectrometry screen as a MISP-interacting protein, I aimed at characterizing the interaction between MISP and Cdc42 in more detail. Since in vivo it is not yet possible to study only the active or inactive pool of Cdc42, the mutant proteins Cdc42 CA (constitutive active, Q61L) and DN (dominant-negative, T17N) were used. Co-IP experiments revealed that MISP strongly interacts with the constitutively active form of Cdc42 and less strongly with the wild-type, while only a slight interaction with the dominant-negative form was detectable (Figure 24a). This strong interaction with the constitutively active mutant could also be observed in mitosis (Figure 24b).

Furthermore, I also analyzed the co-localization of Cdc42 mutants with endogenous MISP in mitotic HeLa Kyoto cells. I found that MISP predominantly co-localized with Cdc42CA, which shows a strong cortical enrichment. MISP also co-localized with Cdc42WT at some regions but not with Cdc42DN at the cell cortex (Figure 24c).

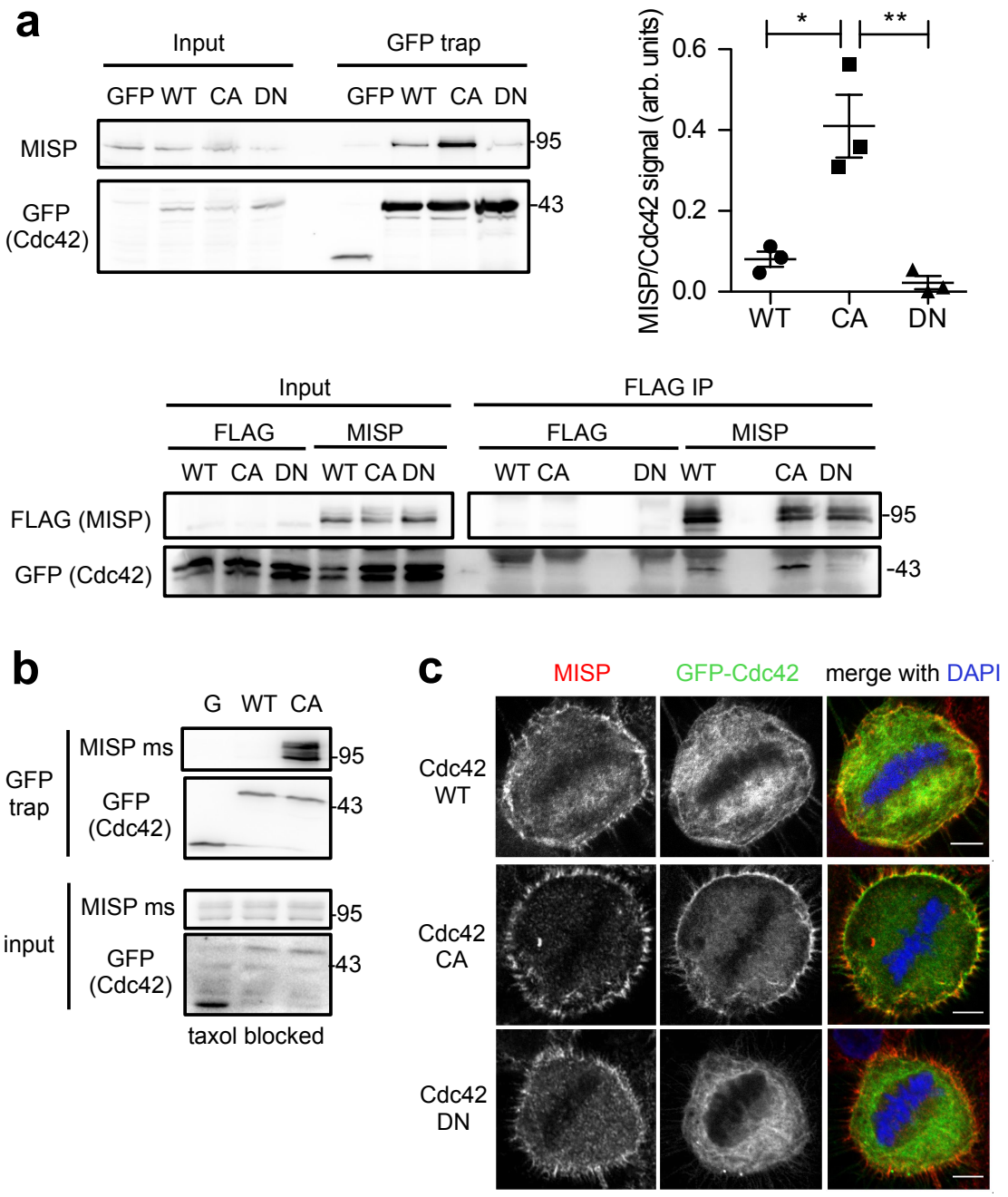

Figure 24. MISP interacts and co-localizes with Cdc42 WT and CA.

(a) Upper blot: Co-immunoprecipitation experiment of overexpressed Cdc42 mutants and endogenous MISP in HeLa Kyoto cells. Chart: quantification of MISP co-precipitation relative to the amount of Cdc42. Values represent mean ± SD of 3 independent experiments, p=0.0149, 0.0083. Lower blot: HEK293T cells were transfected with empty FLAG or FLAG-MISP plasmid and GFP-tagged Cdc42 mutants. Following FLAG IP, GFP-Cdc42 co-precipitation was detected by Western blotting. (b) Co-immunoprecipitation experiment of GFP as a control or GFP-Cdc42 WT/CA and endogenous MISP in mitotically blocked HeLa cells. (c) MISP immunostaining of HeLa Kyoto cells overexpressing GFP-Cdc42 mutants. Single equatorial plane; scale bar, 5 µm.

3.4.2 MISP regulates the activity of Cdc42 but it is not a GEF

Proteins specifically interacting with the active form of GTPases might influence their activation. To find out if MISP could affect the activity of Cdc42, I depleted or overexpressed MISP in HeLa cells and a collaboration partner, Berati Cerikan (Schiebel Lab, ZMBH, Heidelberg) analyzed the activity status of the three most abundant Rho GTPase family members: RhoA, Rac1 and Cdc42. Using a Rho G-LISA activation assay we identified a specific decrease in the level of GTP-bound Cdc42 in response to siRNA-mediated MISP depletion, while GTP-bound RhoA and Rac1 levels were not affected (Figure 25a).

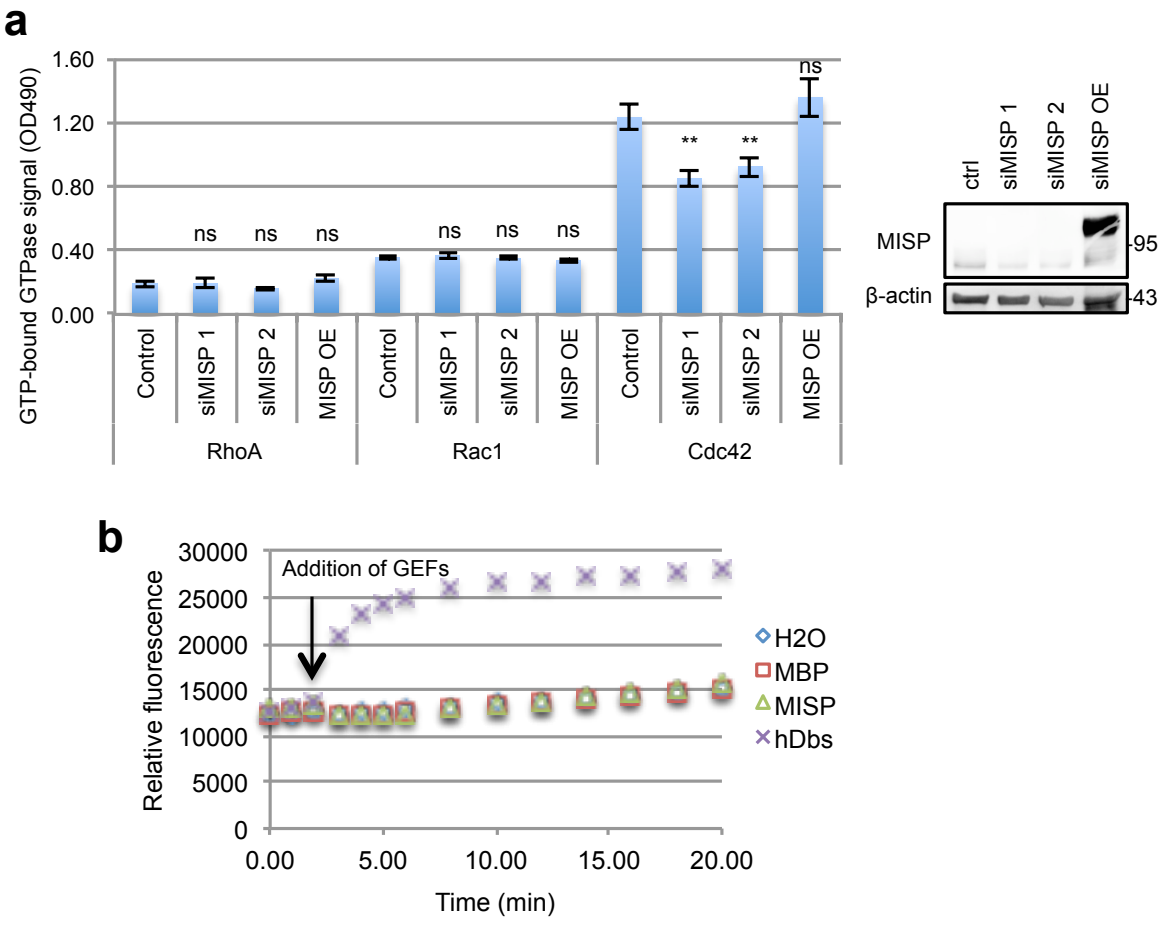

Figure 25. MISP-depletion leads to Cdc42 deactivation but MISP is not a Cdc42-GEF.

(a) HeLa Kyoto cells were transfected with control/MISP siRNAs or a GFP-MISP plasmid. Active Cdc42 levels were quantified using the Rho G-LISA activation assay (Cytoskeleton). Values represent mean ± SD of 3 independent experiments, one-way ANOVA with Bonferroni's. Western blot shows down-regulation or overexpression of MISP, β-actin is used as loading control. (b) In vitro Cdc42-GEF assay was performed with purified MBP-MISP, MBP alone, water as a negative and hDbs – a proven Cdc42 GEF – as a positive control.

Fluorescence intensity, which is proportional with the amount of produced GTP-Cdc42, was measured over time after the addition of the purified proteins. (RhoGEF exchange assay, Cytoskeleton).

Knowing that MISP knock-down induces Cdc42 deactivation, the question emerges if MISP is an activator protein for Cdc42, in other words if MISP is a Cdc42 a guanine nucleotide exchange factor (GEF). Therefore, I used a commercially available GEF assay to study if MISP can catalyze the GDP to GTP exchange of Cdc42. I could not show that purified MISP would activate Cdc42 (Figure 25b), which is in line with the observation that MISP OE does not lead to an increase in active Cdc42 in the cells (Figure 25a). These results suggest that MISP regulates the activity of Cdc42, although MISP itself does not act as an activator, a GEF for Cdc42.

3.4.3 Cdc42 OE cannot rescue MISP down-regulation phenotypes

It was previously shown that both MISP and Cdc42 have a role in mitotic spindle orientation (Jaffe *et al.*, 2008; Mitsushima *et al.*, 2009; Zhu *et al.*, 2013). Depletion of Cdc42 or overexpression of a dominant negative mutant (Cdc42T17N) leads to increased spindle angles (Mitsushima *et al.*, 2009). Since down-regulation of MISP leads to deactivation of Cdc42, I investigated whether co-expression of Cdc42CA could rescue the spindle misorientation effect induced by down-regulation of MISP. However, Cdc42CA overexpression did not normalize the spindle angles after MISP-depletion (Figure 26a). I also checked if Cdc42CA could compensate for the loss of MISP in terms of astral MTs. As shown in Figure 26b, Cdc42CA could not rescue the loss of astral MTs observed after MISP-depletion. Notably, Cdc42CA OE alone resulted in spindle misorientation and loss of astral MTs, implicating that similarly to deregulation, artificial over-stabilization of active Cdc42 can lead to defects in spindle orientation and astral MT anchoring at the cortex (Figure 26a,b).

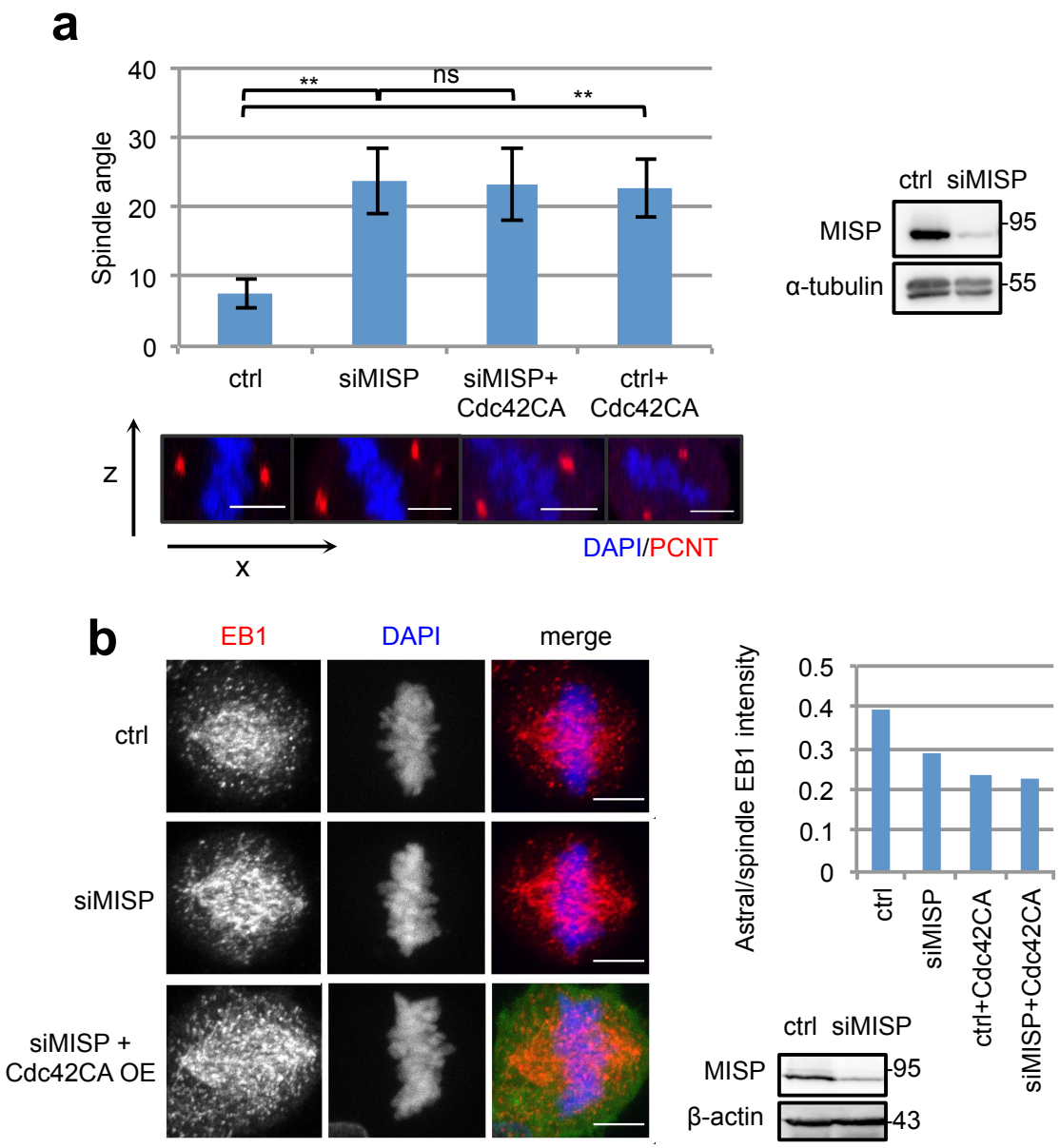

Figure 26. Cdc42CA OE does not rescue mitotic spindle misorientation and loss of astral MTs upon MISP KD.

(a) Spindle angle relative to the substratum was measured in mitotic HeLa cells inducibly expressing GFP-Cdc42CA treated with control or MISP siRNA in the presence or absence of doxycycline. Data represents mean ± SD of 3 independent experiments, n=15, one-way ANOVA with Bonferroni's. Lower panel: representative x-z side views. Centrosomes were visualized by pericentrin (PCNT) staining; scale bar, 5 μm. Immunoblot shows knock-down efficiency, α-tubulin is used as loading control. (b) HeLa cells inducibly overexpressing Cdc42CA were treated with control or MISP siRNA in the presence or absence of doxycycline and immunostained for the plus-tip binding protein EB1. Maximum projection of z-stack images were used for visualization; scale bar, 5 μm. Chart: astral/spindle EB1 intensity was quantified in sum projections by calculating the intensities of an ellipse drawn around the cell "a" and around the spindle "b" with the following formula: (a-b)/b (n=20). Immunoblot shows knock-down efficiency, β-actin is used as loading control.

3.4.4 MISP, IQGAP1 and Cdc42 form a complex

The preferential binding of MISP to active Cdc42 (Figure 24a) resembles that of IQGAP1 and Cdc42. IQGAP1 was shown to bind and stabilize Cdc42 in its active form (Hart *et al.*, 1996), hence it is possible that the three proteins interact in a complex. To this end, I conducted a double sequential immunoprecipitation experiment. FLAG or FLAG-MISP and GFP-Cdc42CA were co-expressed in HEK 293T cells and proteins were immunoprecipitated with FLAG-beads. The eluate was subjected to GFP trap to enrich for Cdc42CA. Western blot analysis of the bound proteins revealed that endogenous IQGAP1 specifically co-precipitated with MISP and Cdc42CA (Figure 27a) confirming the ternary complex formation.

3.4.5 IQGAP1 mediates the interaction between MISP and Cdc42

In this complex it would be conceivable that MISP interacts with and regulates the activity of Cdc42 through IQGAP1. Therefore, with an in vitro pull-down assay I checked if MISP could directly bind to Cdc42. While the interaction between IQGAP1 and MISP appeared to be direct (Figure 15c), no specific interaction could be detected between MISP and Cdc42 in vitro (Figure 27b), suggesting that MISP binds Cdc42 through IQGAP1.

I also tried to support this finding with an in vivo experiment. I made use of a HeLa cell line, in which IQGAP1 was knocked out using the CRISPR method (IQGAP1 KO) (Cerikan *et al.*, 2016), and checked if MISP can bind to active Cdc42 in these cells. Indeed, no interaction between MISP and Cdc42CA could be detected in the IQGAP1 KO HeLa cell line, although the interaction was clearly visible in the parental HeLa WT cells (Figure 27c).

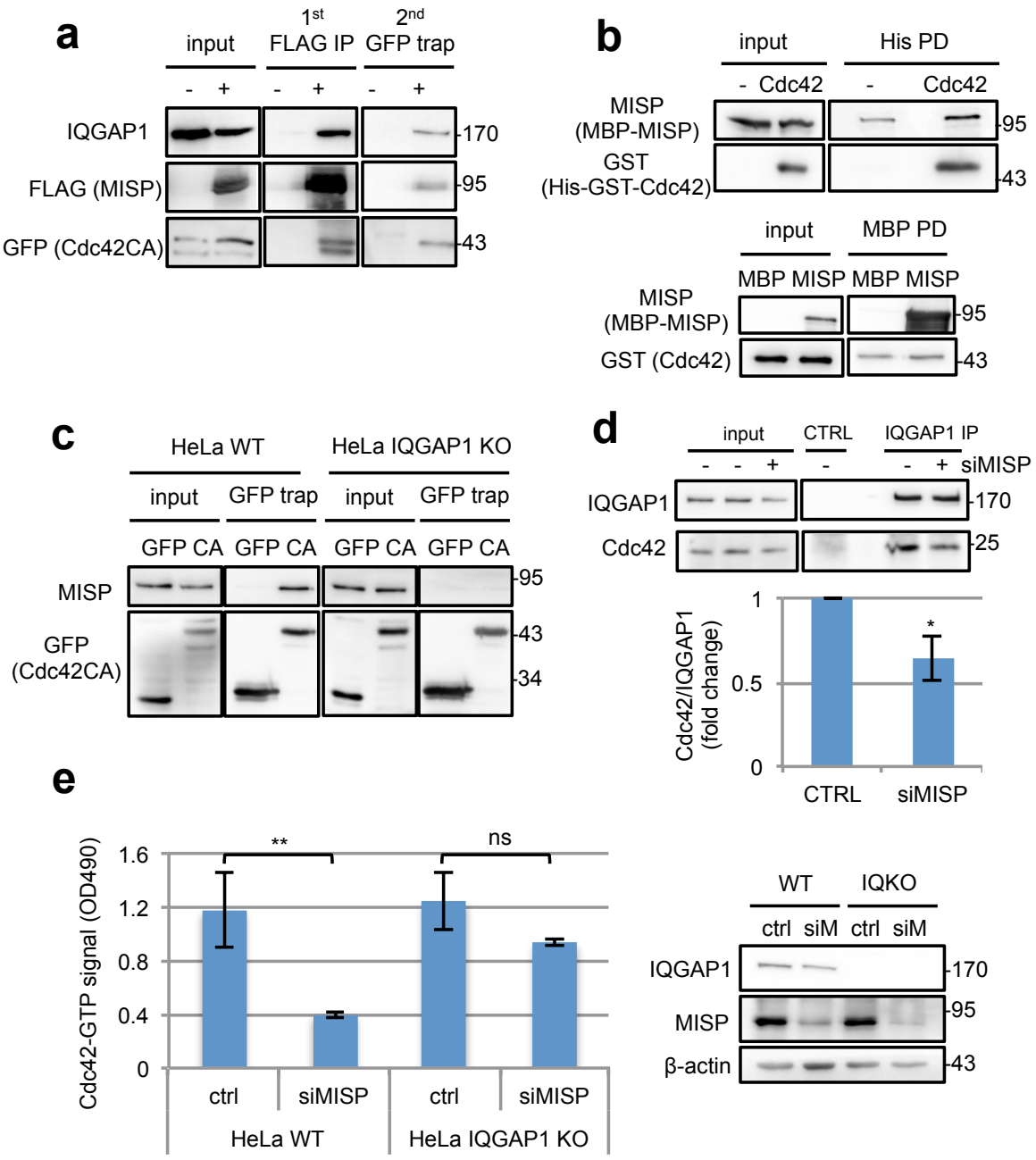

Figure 27. IQGAP1 mediates the interaction between MISP and Cdc42 and influences the activation status of Cdc42 in a MISP-dependent manner.

(a) Sequential immunoprecipitation of HEK293T cells transfected with FLAG-tag or FLAG-MISP and GFP-Cdc42CA to analyze complex formation. First, FLAG-MISP was enriched on beads and then bound proteins were eluted and subjected to a GFP trap to enrich for Cdc42CA. After the final elution IQGAP1 co-precipitation was detected with WB. (b) In vitro interaction between purified MBP-MISP and GST-His-Cdc42 was studied by His and MBP pull-down experiments. (c) Co-precipitation of endogenous MISP with GFP-Cdc42CA was analyzed in wild-type (WT) and IQGAP1 knock-out (IQGAP1 KO) HeLa cells. (d) Endogenous IQGAP1 was immunoprecipitated from control or MISP siRNA-treated HeLa cell

lysates. Co-precipitating Cdc42 was quantified relative to bound IQGAP1. Results were normalized to control and one-sample t-test was carried out on log2-transformed data. Values represent mean ± SD of 3 independent experiments, p=0.0471. (e) Cdc42 activation experiment of HeLa WT and IQGAP1 knock-out (KO) cells transfected with control or MISP siRNAs (Rho G-LISA activation assay, Cytoskeleton). Values represent mean ± SD of 3 independent experiments, p=0.0083 and 0.0741. Immunoblot shows downregulation efficiency of MISP, β-actin is used as loading control.

Previously, it was shown that IQGAP1 OE leads to an increase in active Cdc42 levels (Hart *et al.*, 1996; Swart-Mataraza *et al.*, 2002). Given that MISP does not directly interact with Cdc42, it might influence the activity of Cdc42 through IQGAP1. In order to prove that IQGAP1 is the mediator responsible for the decrease in active Cdc42 levels upon MISP KD, I performed endogenous immunoprecipitation experiments with an IQGAP1 antibody in control and MISP siRNA-treated HeLa cells and measured co-precipitating Cdc42 relative to IQGAP1. There was a clear reduction of Cdc42 bound to IQGAP1 in the absence of MISP, indicating a change in the Cdc42-binding affinity of IQGAP1 (Figure 27d). Since IQGAP1 binds predominantly to the active form of Cdc42 (Hart *et al.*, 1996), this could lead to a reduction in overall active Cdc42 levels upon MISP down-regulation. The fact that upon MISP-depletion, IQGAP1 looses its affinity for Cdc42, and could contribute to decreased GTP-Cdc42 levels, supports the hypothesis that IQGAP1 becomes nonfunctional upon cortical recruitment in terms of downstream pathway components like phosphorylated Akt (Figure 21c) or active Cdc42.

I tried to strengthen this finding by checking the activation of Cdc42 in wild-type (WT) and IQGAP1 KO HeLa cells. If the deactivation of Cdc42 upon MISP KD is dependent on IQGAP1, no change in Cdc42 activation should be detected in the IQGAP1 KO cells upon MISP knock-down. I found that MISP depletion had no effect on Cdc42 activation in IQGAP1 KO cells (Figure 27e), confirming the mediator role of IQGAP1 in this process. Collectively, these data indicate that MISP interacts with and regulates the activity of Cdc42 through IQGAP1.

3.5 IQGAP1 OE rescues several MISP KD phenotypes and restores active Cdc42 levels

3.5.1 IQGAP1 OE restores the correct spindle angle after MISP KD

Loss of MISP induces mitotic defects including spindle misorientation accompanied by shortened astral MTs and prolonged mitosis (Maier *et al.*, 2013; Zhu *et al.*, 2013). First, since MISP depletion leads to cortical accumulation of IQGAP1, I tried to rescue the spindle orientation defects caused by the loss of MISP by eliminating the aberrant cortical accumulation of IQGAP1. Therefore, I co-depleted MISP and IQGAP1 but it did not rescue the spindle misorientation phenotype (Figure 28a,b). This result would also be in line with the hypothesis that the cortically accumulated pool of IQGAP1 is nonfunctional (Figure 21c, Figure 27d) and it is not causing the phenotypes per se. Overexpression of IQGAP1 (and thereby presumably stabilization of active Cdc42), however, normalized the spindle angles after MISP knock-down (Figure 28), suggesting that IQGAP1 acts on the same pathway, downstream of MISP in spindle orientation. Overexpression of the Cdc42-binding mutant of IQGAP1 failed to normalize spindle angles (Figure 28), emphasizing the function of the Cdc42-binding capacity of IQGAP1 in spindle orientation downstream of MISP.

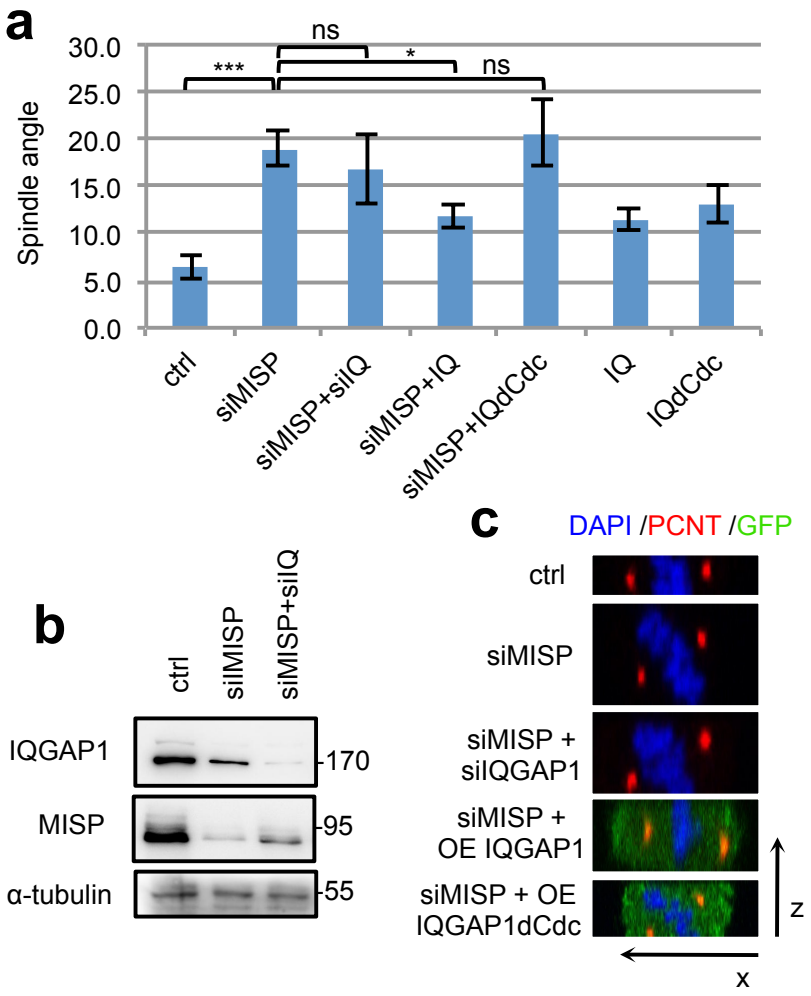

Figure 28. IQGAP1 OE rescues mitotic spindle misorientation caused by MISP KD.

(a) Spindle angles were measured relative to the substratum in mitotic HeLa Kyoto cells treated with control/MISP/IQGAP1 siRNA and GFP-IQGAP1/GFP-IQGAP1dCdc42 constructs. Values represent mean ± SD of 3 independent experiments, n=15, p=0.0007 compared to controls, one-way ANOVA with Bonferroni's test. (b) Immunoblot shows down-regulation efficiency, α-tubulin is used as loading control. (c) Spindle angles are depicted by representative x-z side views, centrosomes were visualized by pericentrin (PCNT) staining.

3.5.2 IQGAP1 OE rescues centrosome reorientation defects after MISP depletion

Spindle orientation defects often imply failure in directional cell migration (Buttrick *et al.*, 2008; Cabello *et al.*, 2010; Negishi *et al.*, 2016). Cell migration is linked to MT-organizing centers (MTOCs) and an intact MT network (Gotlieb *et al.*, 1981). Therefore, I investigated the orientation of centrosomes in MCF-7 cells grown in monolayer two hours after wounding. During directional cell migration the

centrosome orients towards the leading edge, in this case towards the wound (Figure 29a) (Albrecht-Buehler and Bushnell, 1979; Gotlieb *et al.*, 1981; Kupfer *et al.*, 1982). As expected, MISP down-regulation led to a decrease in cells with oriented centrosomes, but upon expression of IQGAP1, centrosome reorientation defects could be rescued in MISP-depleted cells (Figure 29). Similarly to spindle misorientation, centrosome reorientation could also not be rescued when the Cdc42-binding mutant of IQGAP1 was overexpressed (Figure 29).

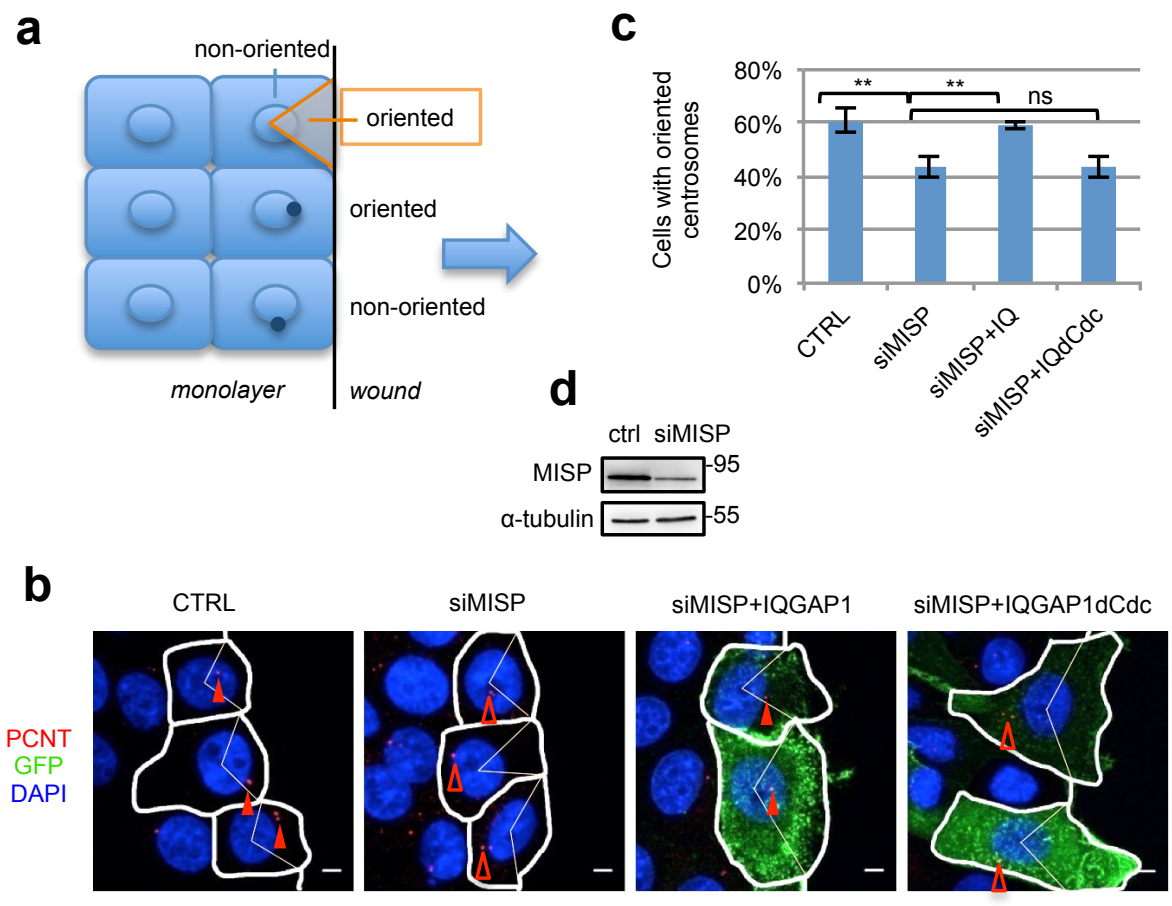

Figure 29. IQGAP1 OE rescues centrosome reorientation defects provoked by MISP KD.

(a-d) MCF-7 cells treated with control/MISP siRNA and GFP-IQGAP1/GFP-IQGAP1dCdc42 constructs were grown to confluence, wounded and centrosome position was analyzed by microscopy 2 hours after wounding. (a) Graphic showing how oriented centrosomes were categorized. Blue dots represent centrosome(s), the black line shows the position of the wound, arrow indicates the direction of movement. If the centrosome positioned within the area of a triangle connecting cell contacts at the leading edge with the center of the nucleus (orange), it was considered as oriented. (b) Representative images of cells bordering the wound are shown in a centrosome reorientation experiment (maximum projections of z-stack

images). Closed red arrowheads indicate oriented, open red arrowheads indicate non-oriented centrosomes visualized by pericentrin (PCNT) antibody, cell borders are marked with thick white lines, thin white lines mark the area where oriented centrosomes should be positioned, Scale bar, 5 µm. (c) Corresponding quantification showing percentage of cells with oriented centrosomes. Values represent mean ± SD of 3 independent experiments, n=100, one-way ANOVA with Bonferroni's test. (d) Immunoblot showing MISP KD, α-tubulin is used as loading control.

3.5.3 IQGAP1 OE normalizes mitotic duration in MISP-depleted cells

Another phenotype of MISP depletion is the impairment of the metaphase-to-anaphase transition (Zhu *et al.*, 2013). To find out whether IQGAP1 overexpression could also rescue the metaphase arrest upon loss of MISP, I performed time-lapse video microscopy in HeLa cells inducibly overexpressing IQGAP1 after control or MISP siRNA treatment. As described previously (Zhu *et al.*, 2013), MISP depletion increased the time from nuclear envelope breakdown (NEB) to anaphase onset from around 30 minutes in control siRNA-treated cells to 45 minutes in MISP-depleted cells, while overexpression of IQGAP1 could reduce this time to 35 minutes in the absence of MISP (Figure 30). This suggests that IQGAP1 has a role not only in spindle orientation but also in mitotic progression downstream of MISP.

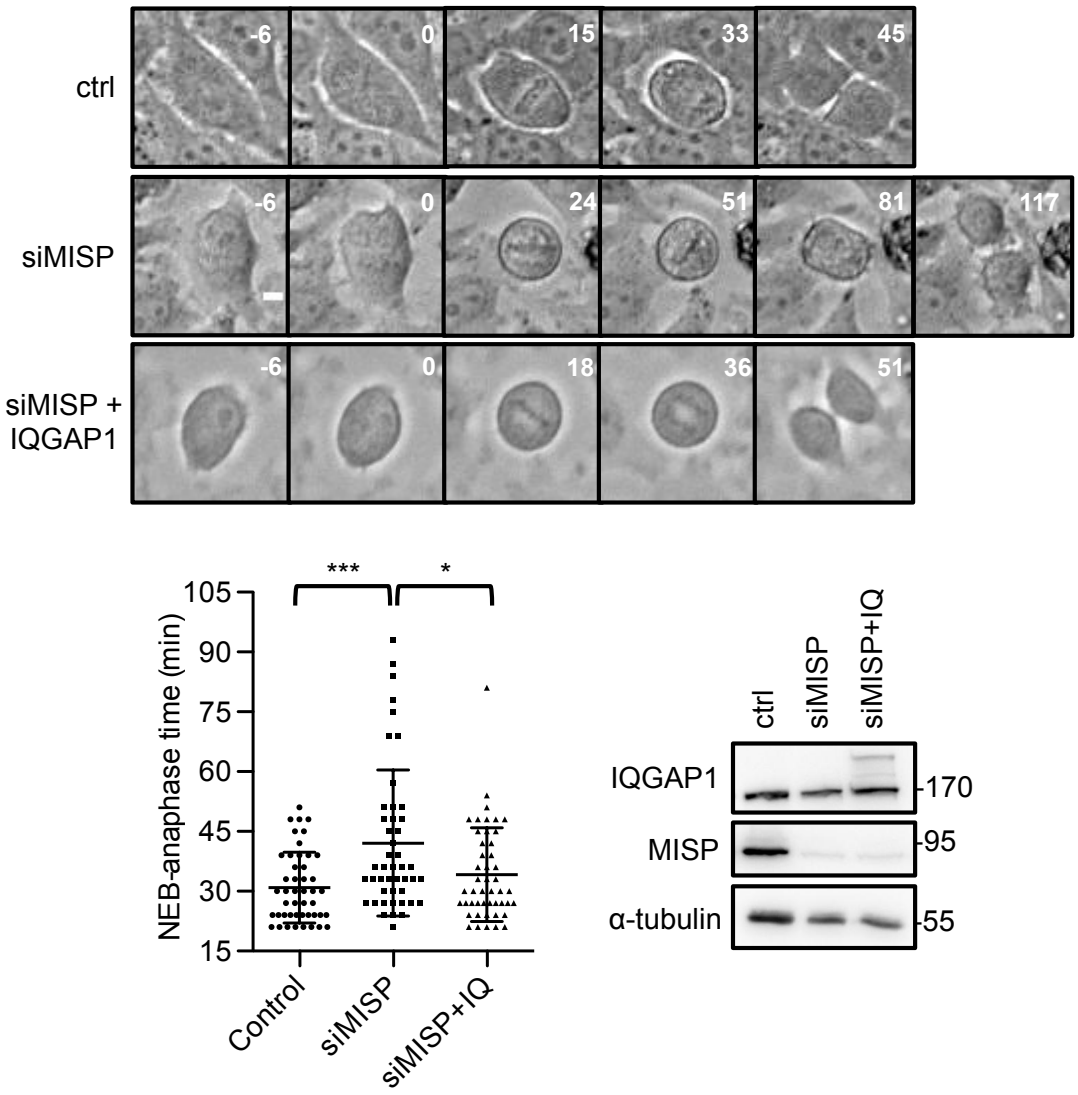

Figure 30. IQGAP1 OE normalizes mitotic duration altered after MISP KD.

NEB-anaphase time of HeLa cells inducibly overexpressing GFP-IQGAP1 was measured by live-cell imaging in control and MISP KD cells. Brightfield images show mitotic progression. Numbers indicate minutes, time point zero is set to NEB (second image). The next image shows the first congressed metaphase plate (for siMISP also a second metaphase plate was imaged), followed by the onset of mitosis and the settled daughter cells. Scale bar, 10 µm. Chart: Dot plot showing time spent in mitosis. Values represent mean ± SD, n=46, Mann-Whitney test, p=0.0007 and 0.0226. Immunoblot shows MISP KD and IQGAP1 OE, α-tubulin is used as loading control.

3.5.4 IQGAP1 OE restores active Cdc42 levels after MISP knock-down

Given that MISP depletion causes a decrease in Cdc42 activation (Figure 25a), I asked the question whether the rescue effect of IQGAP1 OE upon MISP knock-down could be attributable to its active Cdc42-stabilizing ability. Indeed, overexpression of

IQGAP1 in MISP-depleted cells could restore the Cdc42-GTP signal to nearly control levels (Figure 31), which might contribute to its rescue effects upon MISP down-regulation.

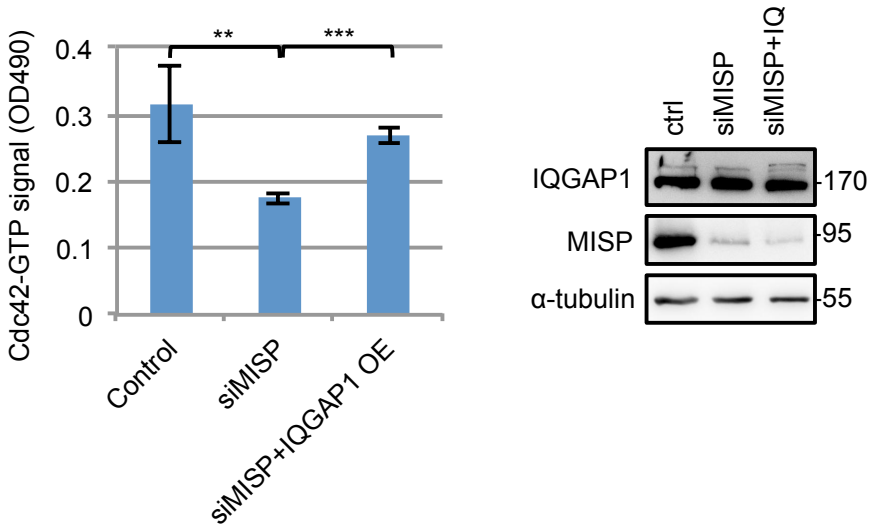

Figure 31. IQGAP1 OE restores active Cdc42 levels after MISP KD.

Active Cdc42 levels were measured in HeLa cell lysates upon IQGAP1 OE after MISP KD (RhoA/Rac1/Cdc42 GLISA, Cytoskeleton). Values represent mean ± SD of 3 independent experiments, p=0.0072 and 0.0003. Western blot shows down-regulation efficiency, α-tubulin is used as loading control.

3.5.5 IQGAP1ΔCdc42 OE is not able to rescue MISP KD phenotypes

Importantly, as shown above, expression of IQGAP1ΔCdc42 did not rescue either the spindle misorientation (Figure 28) or the centrosome reorientation phenotype (Figure 29) after MISP KD pointing to the importance of Cdc42-binding of IQGAP1 in its ability to rescue the phenotype. Taken together, these results suggest that IQGAP1 overexpression can rescue MISP depletion phenotypes most probably by restoring the levels of active Cdc42 in the cells.

3.6 IQGAP1 compensates for the loss of MISP in astral MT stabilization

3.6.1 IQGAP1 OE counteracts loss of astral MTs upon MISP KD

Since astral MTs are key factors for regulating spindle orientation parallel to the substratum in HeLa cells, defects in astral MTs can affect spindle orientation

(Toyoshima and Nishida, 2007; Toyoshima *et al.*, 2007). MISP seems to play a role in spindle orientation via capturing astral MTs at the cell cortex in mitosis (Zhu *et al.*, 2013). To assess whether IQGAP1 is involved in MISP-induced stabilization of astral MTs, I checked if IQGAP1 OE could also rescue the loss of astral MTs observed upon MISP down-regulation. To visualize the MT plus ends, EB1, a MT+TIP binding protein was stained. While MISP depletion led to a reduction of astral EB1 intensity, IQGAP1 OE could compensate for the loss of MISP and restored normal astral/spindle EB1 distribution (Figure 32a). I corroborated this finding by visualizing MTs with another staining, α-tubulin. Loss of astral MTs upon MISP knock-down could also be rescued by IQGAP1 OE in cells where MTs were stained with α-tubulin (Figure 32b). Interestingly, IQGAP1 OE per se did not have an effect on astral MT intensity, emphasizing its function in astral MT stabilization after MISP knock-down.

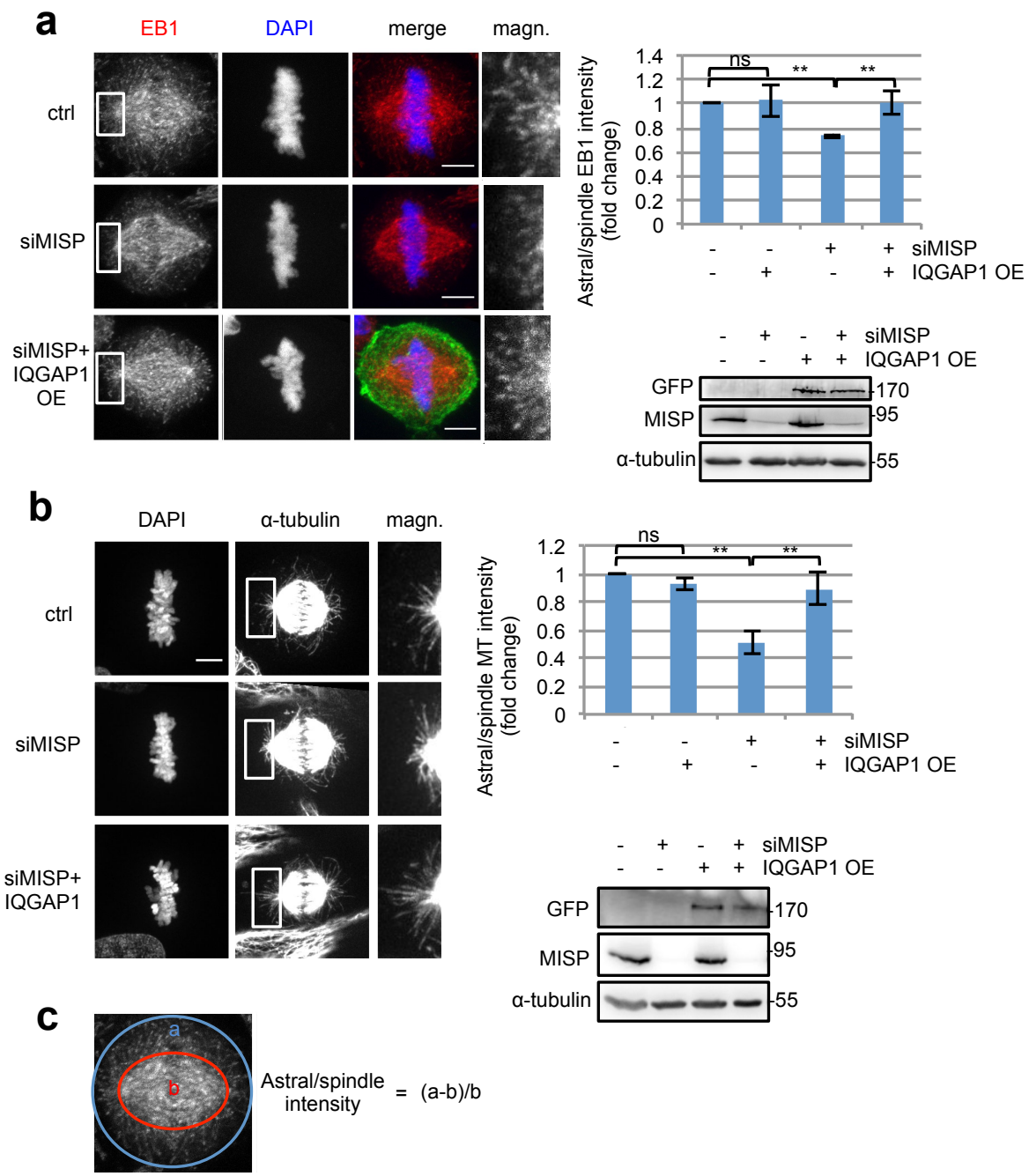

Figure 32. IQGAP1 abrogates the destabilizing effect of MISP KD on astral MTs.

(a) Maximum projections of confocal images showing MT plus ends stained by EB1 in mitotic HeLa cells inducibly overexpressing GFP-IQGAP1 treated with control or MISP siRNA. Maximum projection images; scale bar, 5 μm. Rectangles mark magnified areas. Chart: Quantification was carried out in sum projections using ImageJ. Results were normalized to control and one-sample t-test was carried out on log2-transformed data. Values represent mean ± SD of 3 independent experiments, n=15, p-values: 0.7824, 0.0014, 0.0044. Western blot shows down-regulation efficiency, α-tubulin is used as loading control. (b) Maximum projections of confocal images showing astral MTs stained by α-tubulin in mitotic HeLa cells inducibly overexpressing GFP-IQGAP1 treated with control or MISP siRNA. Images were deconvolved with the ZEN software built-in deconvolution software, strength was manually

set to 1. Maximum projection images; scale bar, 5 µm. Chart: Quantification was carried out in sum projections using ImageJ. Results were normalized to controls and one-sample t-test was carried out on log2-transformed data. Values represent mean ± SD of 3 independent experiments, n=15, p-values: 0.1421, 0.0099, 0.0042. Western blot shows down-regulation efficiency, α-tubulin is used as loading control. (c) Graphic showing how astral/spindle EB1 or α-tubulin signal was quantified.

3.6.2 IQGAP1 OE restores astral MT dynamics upon MISP KD

MISP depletion leads to a reduction and shortening of astral MTs (Zhu *et al.*, 2013) but how exactly this reduction arises is still unclear. To get insight into how MISP regulates the dynamics of astral MTs, short-term live-cell imaging was applied to mitotic HeLa cells stably expressing GFP-EB3 (Sironi *et al.*, 2011), and the movements of single astral MTs were followed. The 30-second movies were converted to kymographs, where the length and angle correspond to the stability and speed of the MTs, respectively (Figure 33a). Timely tracking of EB3 comets in control/MISP siRNA treated cells revealed that astral MTs in MISP-depleted cells grew slower, were reduced in length and most of them did not reach the cell cortex, while the total number of astral MT comets emanating from a spindle pole did not change (Figure 33b-d). These results suggest that MISP knock-down leads to a decreased stability of astral MTs. Strikingly, IQGAP1 OE in MISP-depleted cells restored the speed and track-length of these plus-tip comets demonstrating a joint role of MISP and IQGAP1 in stabilization of astral MTs at the cell cortex. Together these data imply that the stabilization of astral MTs by MISP is dependent on IQGAP1.

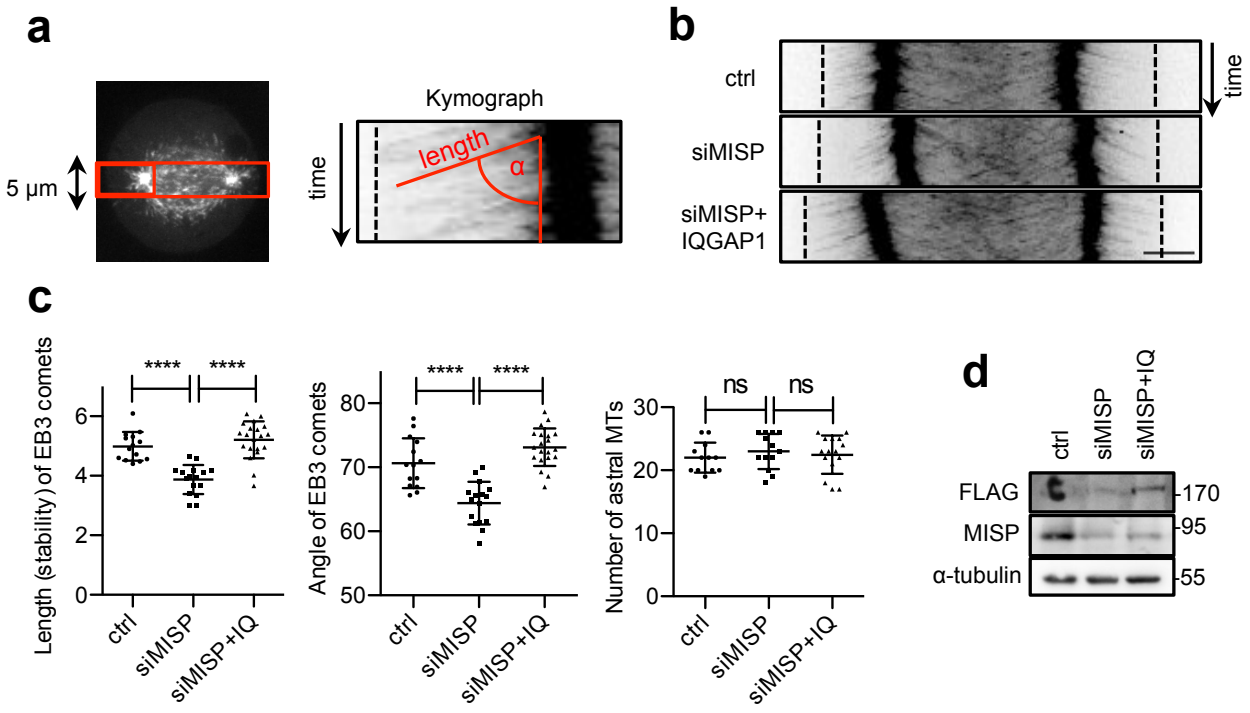

Figure 33. IQGAP1 OE restores altered astral MT dynamics upon MISP KD.

(a) Metaphase HeLa Kyoto cells stably expressing GFP-EB3 transfected with control/MISP siRNA and FLAG-IQGAP1 were imaged with a spinning disc microscope every 2 seconds over one minute. Kymographs from 5-µm-thick sections around the spindle poles (red rectangle) show the dynamics of EB3 comets. Length, zenith angle and number of EB3 comets were measured as illustrated. (b-c) Representative kymographs (b) and quantifications (c) of astral MT dynamics. Length (stability) and angle (speed) of 5 EB3 comets per centrosome were averaged and compared with one-way ANOVA with Bonferroni's tests, n=16, ****: p<0.0001. (d) Immunoblot shows MISP down-regulation efficiency, α-tubulin is used as loading control.

3.6.3 IQGAP1 OE restores p150^{glued} localization upon MISP KD

Finally, I was interested which motor protein could be involved in capturing astral microtubules in this pathway. MISP was shown to regulate the cortical distribution of the dynactin subunit p150^{glued} (Zhu *et al.*, 2013). Upon MISP depletion, the signal of p150^{glued} increases in a crescent-like structure at the cell cortex near one of the spindle poles (Zhu *et al.*, 2013). Interestingly, Cdc42 depletion leads to a similar effect on the localization of p150^{glued} as MISP (Mitsushima *et al.*, 2009). Therefore I checked if IQGAP1 overexpression could rescue this aberrant cortical accumulation of p150^{glued} upon MISP depletion. Indeed I found, that IQGAP1 OE after MISP KD normalized the cellular distribution of p150^{glued} (Figure 34). p150^{glued} could therefore act as an effector in regulating astral MT stability downstream of MISP and IQGAP1.

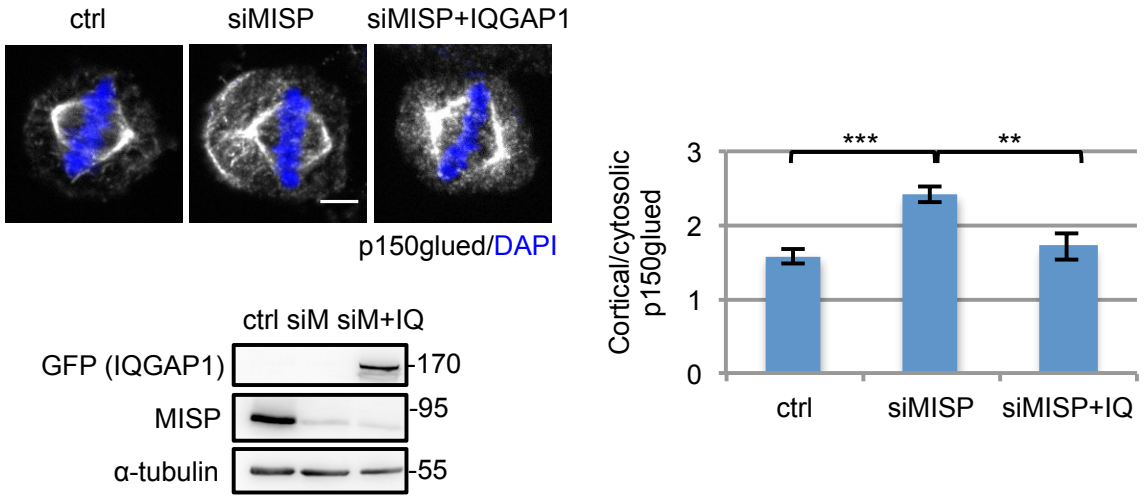

Figure 34. IQGAP1 OE compensates for the loss of MISP in regulating p150^{glued} localization.

Single plane confocal images showing p150^{glued} localization in mitotic HeLa cells transfected with control or MISP siRNA or MISP siRNA and GFP-IQGAP1. Equatorial planes with the strongest cortical accumulation of p150^{glued} are shown. Single, equatorial images; scale bar, 5 μm. Chart: Quantification was carried out using ImageJ by dividing the strongest line intensity of p150^{glued} at the cortex by the intensity of the same line in the cytosol right below the cortex. Values represent mean ± SD of 3 independent experiments, n=12, p-values: 9,99x10^{-4} and 0.0058. WB shows MISP downregulation, α-tubulin is used as loading control.

4 Discussion

Orientation of the cell division axis within multicellular organisms has been a major research focus for many decades. So far, little is known about how the proteins regulating this process collaborate to ensure accurate cell division orientation. Previous data have shown that the actin-binding protein MISP also regulates spindle orientation and affects cortical anchoring of astral microtubules (Zhu *et al.*, 2013). The aim of the thesis was to identify downstream effectors of MISP involved in spindle orientation and to determine how they are regulated by MISP in this process.

In addition to its known functions in mitosis and migration, I revealed that MISP is also involved in centrosome reorientation in interphase cells (Figure 29). Furthermore, my results show how MISP controls the dynamics of astral MTs. MISP influences the length and stability but not the number of astral MTs (Figure 33).

In this thesis I identified MISP as a regulator of IQGAP1 and Cdc42. Previously both IQGAP1 and Cdc42 were reported to have a role in spindle orientation (Jaffe *et al.*, 2008; Mitsushima *et al.*, 2009; Rodriguez-Fraticelli *et al.*, 2010; Bañón-Rodríguez *et al.*, 2014; Tuncay *et al.*, 2015). MISP depletion leads to deactivation of Cdc42 (Figure 25a), which can in turn induce mitotic aberrations. Knock-down of Cdc42 was shown to suppress mitotic PI(3)K activity, disrupt cortical actin structures and induce spindle misorientation (Mitsushima *et al.*, 2009). Moreover, I revealed that IQGAP1 binds MISP to regulate the activity of Cdc42 (Figure 27). Stabilization of active Cdc42 by IQGAP1 overexpression can rescue mitotic defects observed upon MISP-depletion (Figure 28-34).

But how does MISP regulate IQGAP1's affinity for Cdc42? Activity of IQGAP1 was supposed to be regulated by a conformational change (Grohmanova *et al.*, 2004; Rittmeyer *et al.*, 2008). In the open conformation IQGAP1 is able to bind Cdc42, while in its closed conformation, when the C-terminus folds on the Cdc42-binding region, interaction with Cdc42 is repressed. Therefore I hypothesize that MISP-binding is required to maintain IQGAP1 in its open, active form by binding to its C-terminus (Figure 16). So, it enables IQGAP1 to bind and stabilize active Cdc42 (see Figure 35 for a model).

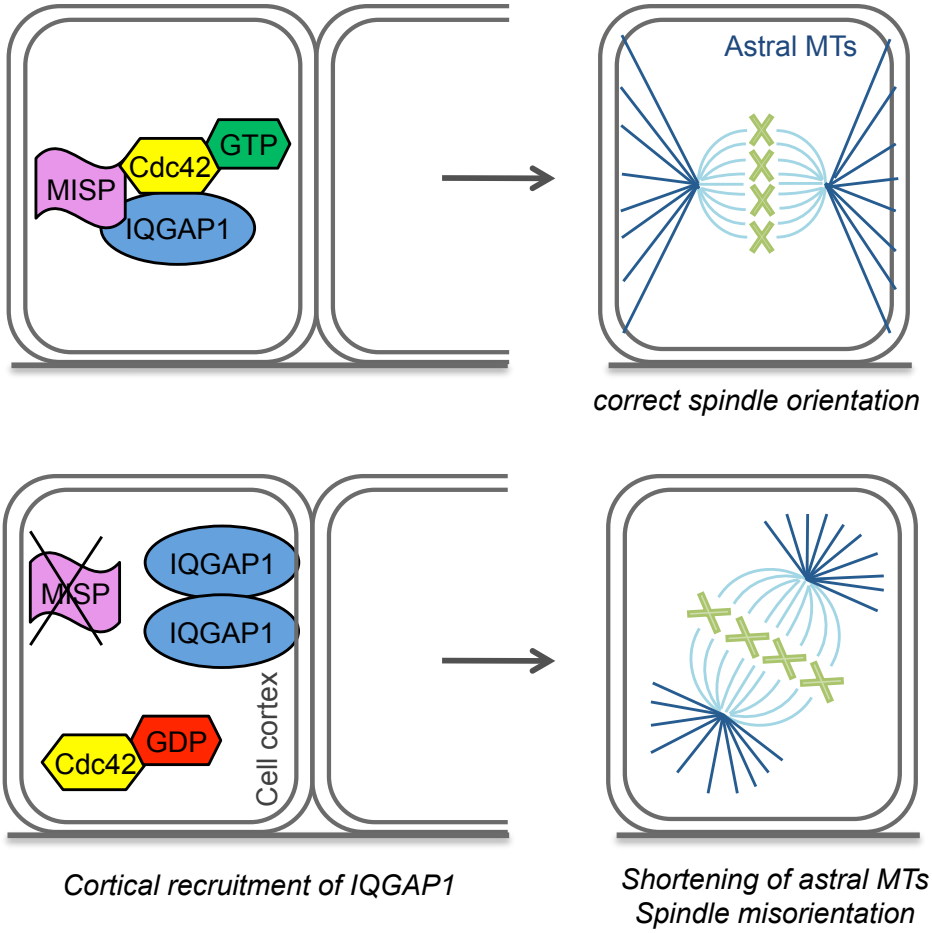

Figure 35. Proposed model for the regulation of IQGAP1 localization at the cell cortex and of its function by MISP in spindle orientation.

Model summarizing the effects of MISP KD on IQGAP1 and Cdc42 and thereby astral MTs and mitotic spindle orientation. In control cells (upper part) MISP contributes to the stabilization of active Cdc42 by IQGAP1 ensuring proper spindle orientation. Upon MISP depletion (lower part), IQGAP1 is recruited to the cell cortex thereby losing its affinity towards active Cdc42 leading to decreased active Cdc42 levels. This in turn induces shortening of astral MTs and spindle misorientation.

In contrast, upon loss of MISP conformation of IQGAP1 might shift to the closed form and as a result decreasing its ability to bind active Cdc42 (Figure 27d) and leading to reduced Cdc42 activity (Figure 25a). This closed form of IQGAP1 might accumulate at the cell cortex (Figure 19), probably by binding to the E-cadherin / β-catenin complex (Fukata *et al.*, 1999; Noritake *et al.*, 2005). Overexpression of active Cdc42 after MISP knock-down may lead to an open conformation of IQGAP1 followed by its dissociation from the cortex (Figure 22). Therefore, the balance might be shifted and cause spindle misorientation (Figure 26). Alternatively, the strong

binding of IQGAP1 to Cdc42CA might make IQGAP1 unable to release it, which is required for the downstream functions of IQGAP1. Overexpression of IQGAP1 after MISP depletion, however, might only moderately increase the proportion of the open conformation due to saturation at the cortex. This can lead to the stabilization of the right amount of active Cdc42 (Figure 31) that ensures proper anchoring of astral MTs (Figure 32 and Figure 33) and thereby orderly mitotic progression and spindle orientation (Figure 30 and Figure 28).

The identified pathway of MISP→IQGAP1→Cdc42 seems to be hierarchical, since MISP has no effect on Cdc42 activity itself in IQGAP1 KO cells (Figure 27e). However, Cdc42 can influence cortical accumulation of IQGAP1 in the absence of MISP (Figure 22), which might work as a feedback loop. Former studies also showed that IQGAP1 might act both as a regulator and an effector of Cdc42 (Hart *et al.*, 1996; Kuroda *et al.*, 1996; Fukata *et al.*, 1999; Swart-Mataraza *et al.*, 2002) – rendering the regulatory pathway more complex.

The importance of the Cdc42-binding capacity of IQGAP1 in its functions downstream of MISP was not only demonstrated by the change in IQGAP1 localization after MISP depletion and Cdc42 overexpression (Figure 22) but also with the altered localization and nonfunctionality of the mutant IQGAP1 that fails to bind Cdc42. More precisely, IQGAP1ΔCdc42 is not recruited to the cell cortex upon MISP depletion (Figure 23) and is unable to rescue MISP-depletion phenotypes like spindle misorientation (Figure 28) or centrosome reorientation (Figure 29). However, it cannot be excluded that the deletion of the Cdc42-binding region changes the conformation of IQGAP1 in a way that interactions with other binding partners are disturbed.

The finding that MISP regulates the function of IQGAP1 appears to be similar to the regulation of IQGAP1 by menin but they have opposite effects (Yan *et al.*, 2009). While MISP down-regulation increases IQGAP1 accumulation at the plasma membrane (Figure 19), menin overexpression causes a similar effect. The two proteins seem to affect the affinity of IQGAP1 for different partners from the Rho GTPase family: menin OE reduces the Rac1 interaction and overall GTP-Rac1 levels, while MISP knock-down affects Cdc42 in a similar manner (Figure 27d and Figure 25a). In both cases Rac1 or Cdc42 OE can prevent the membrane

accumulation of IQGAP1 (Figure 22). Since menin OE increases the E-cadherin/β-catenin interaction with IQGAP1 and therefore affects cell-cell adhesion, it would be interesting to investigate if MISP depletion also has an effect on cell-cell adhesion.

Although upon MISP depletion I could show an increased, MT-independent accumulation of IQGAP1 at the cell cortex (Figure 19 and Figure 20b) and slower dynamics of this cortical pool as shown by FRAP experiments (Figure 21a-b), it is still an open question what recruits IQGAP1 to the cortex and what is its function there. Despite the fact that IQGAP1ΔCdc42 is not recruited to the cell cortex upon MISP depletion (Figure 23), it seems that it is not Cdc42 that anchors IQGAP1 near the plasma membrane, since overexpression of Cdc42 rather prevents this cortical localization (Figure 22). A possible scenario could be that phosphatidylinositol kinases exert this function. It has been shown that in response to receptor activation, PIPKIγ (or phosphatidylinositol-4-phosphate-5-kinase-1-gamma), which phosphorylates phosphatidylinositol-4-phosphate to form PIP2, plays an important role in the leading edge recruitment of IQGAP1 (Choi *et al.*, 2013). There, PIP_2 (generated by PIPKIγ) is supposed to activate IQGAP1 by relieving its auto-inhibitory conformation and so facilitates actin polymerization by IQGAP1. Moreover, IQGAP1 was also shown to scaffold the mitogen-activated protein kinase (MAPK) pathway components PI(4)K, PIPKIa, PI(3)K, Ras, PDK1 and Akt at the plasma membrane by bringing them in close proximity to facilitate their sequential phosphorylation and PIP_3 generation (Choi *et al.*, 2016). However, the most promising candidate seems to be the cadherin/catenin complex, which was also shown to interact with IQGAP1 (Kuroda *et al.*, 1998; Fukata *et al.*, 1999). It is believed that IQGAP1 regulates the interaction of β-catenin with α-catenin in a way that it can dissociate α-catenin and the actin network from β-catenin at the cell-cell contacts thereby uncoupling the actin meshwork from the cell cortex. Moreover, Cdc42 and Rac1 can inhibit the binding of IQGAP1 to β-catenin, negatively regulating its function (Kuroda *et al.*, 1998; Fukata *et al.*, 1999). Taken together, IQGAP1 seems to have numerous binding partners at the cell cortex therefore further experiments are necessary to assess which of them is responsible for the cortical accumulation of IQGAP1 upon MISP knock-down.

Whether Cdc42 or IQGAP1 has a direct role in spindle orientation downstream of MISP, remains to be elucidated. On the one hand, Cdc42 was shown to regulate spindle orientation through maintaining the midcortical localization of the dynactin

complex subunit p150^{glued} (Mitsushima *et al.*, 2009). Interestingly, MISP is also supposed to regulate spindle orientation via p150^{glued} (Zhu *et al.*, 2013). p150^{glued} gets more widely dispersed at the cortex of Cdc42-depleted cells, which is similar to the effect of MISP-depletion, increasing the cortical accentuation of p150^{glued}. In this work I show that IQGAP1 can compensate for the loss of MISP in regulating the localization of p150^{glued} (Figure 34), pointing to the fact that IQGAP1 acts in the same pathway as but downstream of MISP.

On the other hand, both MISP and IQGAP1 are thought to link the microtubules with cortical actin (Fukata *et al.*, 2002; Zhu *et al.*, 2013). As overexpression of IQGAP1 can rescue destabilization of astral MTs caused by lack of MISP (Figure 32 and Figure 33), it could be possible that that MISP regulates the stability of astral MTs through IQGAP1. How IQGAP1 is involved in spindle orientation is still not fully understood but it regulates for example the localization of NuMA in polarized cells (Bañón-Rodríguez *et al.*, 2014). MISP could therefore affect the cortical localization of NuMA through IQGAP1 and so influence astral MT capturing at the cortex. Alternatively, IQGAP1 could exert its function on astral MTs via its interaction partners: the cytoplasmic linker protein 170 (CLIP-170) (Fukata *et al.*, 2002) or the tumor suppressor adenomatous polyposis coli (APC) (Watanabe *et al.*, 2004). Further work is required to decipher how MISP – together with IQGAP1 and Cdc42 – regulates the anchoring of astral MTs at the cell cortex.

Another important question is how MISP stabilizes the IQGAP1-Cdc42 complex. In the hypothetical mechanism I postulate that it is the conformation of IQGAP1, which influences its affinity for Cdc42 and MISP might stabilize IQGAP1 in a conformation that favors Cdc42 binding. Binding of IQGAP1 to all its interaction partners does not happen at the same time and can be influenced by other proteins. It was hypothesized that binding of Cdc42 leads to a conformational change in IQGAP1, since it enhances F-actin crosslinking and affects interactions with β-catenin and CLIP-170 (Fukata et al., 1997, 2002). But the function of IQGAP1 can also be affected by self-association: dimerization or oligomerization (Fukata et al., 1997; Ren et al., 2005; LeCour et al., 2016). LeCour *et al*. showed that four Cdc42 (not Rac1) molecules stabilize one IQGAP dimer through the GRD domains and promote its scaffolding function (LeCour *et al.*, 2016). Therefore it is also possible that MISP is

involved in the dimerization of IQGAP1 or stabilizes the IQGAP1-dimer – Cdc42 complexes. That might be the reason why an increase in active Cdc42 levels upon MISP overexpression could not be revealed (Figure 25a). Future work might reveal if MISP has a role in the self-association of IQGAP1.

Although MISP has not been linked to any specific disease yet, spindle misorientation is implicated in a number of diseases including cancer (Neumüller and Knoblich, 2009; Castanon and González-Gaitán, 2011). Moreover, through regulating IQGAP1 and Cdc42, it might also be involved in other processes. IQGAP1 was shown to be up-regulated and accumulated at the plasma membrane in a variety of human cancers (Johnson et al., 2009; White et al., 2009). Increased IQGAP1 levels, which lead to a rise in active Cdc42 pools, are associated with enhanced tumor proliferation, invasion and angiogenesis. Hypothetically, since MISP can regulate the localization and the Cdc42-stabilizing activity of IQGAP1, MISP might help us combat these aggressive tumor types. Similar to results obtained by overexpression of a dominant-negative mutant of IQGAP1 in human breast cancer epithelial cells (Jadeski et al., 2008), MISP down-regulation could reduce GTP-bound Cdc42 and neoplastic transformation.

The presented data suggest that the rescue function of IQGAP1 after MISP depletion is dependent on its Cdc42-stabilizing activity (Figure 28 and Figure 29), creating a pathway of MISP-IQGAP1-Cdc42 in spindle orientation. It is known that the activity of Cdc42 has to be finely tuned in order to ensure proper mitotic progression and spindle orientation. Both deactivation (Jaffe *et al.*, 2008; Mitsushima *et al.*, 2009) and overactivation (Figure 26) of Cdc42 leads to spindle misorientation. We know that MISP depletion leads to Cdc42 deactivation through IQGAP1 (Figure 27) and this could lead to spindle misorientation, however, the exact mechanism still needs to be clarified. Future work is needed to shed light on how the MISP-IQGAP1-Cdc42 pathway coordinates the ternary complex components to ensure proper spindle orientation.

In summary, this thesis identifies MISP, as novel regulator of IQGAP1 and Cdc42. MISP-depletion leads to cortical accumulation of IQGAP1, which is accompanied by a decreased affinity for Cdc42 and a drop in active Cdc42 levels. Acting downstream of MISP, IQGAP1 excess, and thereby normalization of active Cdc42 levels, can

compensate for the loss of MISP in mitotic progression, p150^{glued} localization, astral MT stabilization and spindle orientation. These findings contribute to our understanding of the regulation mechanisms for the oncoprotein IQGAP1. As IQGAP1 is a known regulator of Cdc42 and has been correlated with tumor progression, its regulation has the potential to impact strategies for specific cancer type treatment. Targeting either the MISP/IQGAP1 or the Cdc42/IQGAP1 interaction may decrease the amount of active Cdc42 in cancer cells and thereby prevent tumor progression. Future studies on the exact mechanism of IQGAP1 and Cdc42 regulation by MISP, and on their relevance in specific diseases will be required in order to reveal potential clinical applications.

5 Materials and methods

5.1 Plasmids and clonings

The identity of all constructs was verified by sequencing (LGC Genomics).

Construct	Vector backbone/source
FLAG	pCMV-3Tag-1A
GFP	pEGFP-C1
GST	pGEX-4T-3
MBP	pMal
GFP-MISP	Zhu et al, 2013
FLAG-MISP	Zhu et al, 2013
FLAG-MISP(6DP)	Zhu et al, 2013
FLAG-MISP(7AP)	Zhu et al, 2013
MBP-MISP	pMal, cloned by colleague
GST-Hisx6-Cdc42	pFAT2 / Elmar Schiebel, ZMBH
GFP-IQGAP1	Addgene #30112
GFP-IQGAP1-N (1-863)	pEGFP-N1 / Fernando Martín-Belmonte, SNRC
GFP-IQGAP1-C (763-1657)	pEGFP-N1 / Fernando Martín-Belmonte, SNRC
GFP-Cdc42 (WT)	Addgene #12975
GFP-Cdc42CA (Q61L)	Addgene #12986
GFP-Cdc42DN (T17N)	Addgene #12976

Construct	Vector backbone/source	Method	Primers	Restriction enzymes
FLAG-Cdc42CA (Q61L)	pCMV-3Tag-1A + GFP-Cdc42(CA)	PCR + ligation	1+2	EcoRI + XhoI
GFP-IQGAP1-GRD (1001-1240)	pEGFP-C1 + IQGAP1	PCR + ligation	3+4	XhoI + BamHI
GFP-IQGAP1-RGCT (1271-1657)	pEGFP-C1 + IQGAP1	PCR + ligation	5+6	XhoI + BamHI
GFP-IQGAP1-ΔCdc (Δ1054-77)	pEGFP-C1 + IQGAP1	PCR + ligation	7+8 9+10	BsmBI-(XhoI)-BsmBI
GST-IQGAP1	pGEX-4T-3	PCR + ligation	11+12	XmaI + XhoI
tetON_GFP-IQGAP1	pcDNA5_FRT-TO + IQGAP1	PCR+ INFUSION	13+14	HindIII + XhoI

Primers used for the clonings:

Primer number	Sequence (5'-3')
1	aaaaagaattcatgcagacaattaagtgtg
2	aaaaactcgagtcatagcagcacac
3	aaaaactcgagagttcatggactctgtaatc
4	aaaaaggatccttacatcttattggaagcagcatg
5	aaaaactcgaggtgatgtcccagagcttc
6	aaaaaggatccaattacttcccgtagaac
7	gatggatgaaaggagacgtc
8	gatggatgaaaggagacgtc
9	aaaaactcgaggaaattatggatgacaaatc
10	tagcacgtctctgcatgg
11	aaaaacccgggaatccgccgcagacgagg
12	aaaaactcgagatcaattacttcccgtagaac
13	gtttaaacttaagctgagctgtacctagcgc
14	gccctctagactcgatcaattacttcccgtagaac

5.2 siRNAs

Protein	sequence (sense, 5'-3')	Source	final cc
MISP 1 (Ol2)	GUGUCCAAGUUGUGGAUGAdTdT	Eurofins	40 uM
MISP 2 (Ol4)	ACUCGGUGUCUGAGUCUCCCUUCUU	Eurofins	40 uM
IQGAP1	TGCCATGGATGAGATTGGAdTdT	Eurofins	40 uM
Control (firefly luciferase, GL2)	AACGUACGCGGAAUACUUCGAdTdT	Eurofins	40 uM

5.3 Cell lines

Name	Cell type	Source
HEK293T	Human embryonic kidney 293 cells with the SV40 T-antigen	ATCC® CRL-3216™
HeLa	Human cervical adenocarcinoma cells	ATCC® CCL-2™
HeLa Kyoto	Human cervical adenocarcinoma cells	CVCL_1922
A549	Human alveolar basal epithelial adenocarcinoma cells	ATCC® CCL-185™
MCF-7	Human breast adenocarcinoma cells	ATCC® HTB-22™
HeLa Cdc42CA	HeLa cells inducibly expressing GFP-Cdc42CA	Cerikan *et al*, 2016
HeLa IQGAP1 KO	IQGAP1 knock-out HeLa cells	Cerikan *et al*, 2016
HeLa Kyoto EB3	HeLa Kyoto stably expressing GFP-EB3	Sironi *et al*, 2011
HeLa IQGAP1	HeLa cells inducibly expressing GFP-IQGAP1	Self-generated

5.4 Generation of HeLa cells inducibly expressing GFP-IQGAP1

GFP-IQGAP1 was PCR amplified from pEGFP-IQGAP1 (Addgene #30112) and cloned into a pcDNA5/FRT/TO vector (Invitrogen). The cloned plasmid was then transfected into Flp-In TRex tetracycline transactivator HeLa cells together with the Flp recombinase encoding plasmid pOG44 (Invitrogen). Hygromycin-resistant colonies were pooled and expanded. Transgene expression was induced with 1 µg/ml doxycycline (SigmaD9891) overnight (16 h).

5.5 Mammalian cell culture

Cells were cultured in Dulbecco's Modified Eagle's Medium (DMEM, Sigma) with 1 g/l glucose for A549, HeLa and HeLa Kyoto cells or 4.5 g/l glucose for HEK293T and MCF-7 cells (ATCC) supplemented with 10% FBS (Lonza) and 1% penicillin-streptomycin (Sigma, 100 U/ml penicillin and 0.1 mg/ml streptomycin). Cells were split at 80-90% confluence. Cell line authentication (based on SNP-profiling) was performed by Multiplexion, Heidelberg. Mycoplasma tests were conducted on a monthly basis (LookOut Mycoplasma PCR Detection Kit, MP0035-1KT, Sigma).

5.6 Transfections and treatment

Cells were transfected with the plasmid constructs using polyethylenimine (PEI, Polysciences) the day after seeding. PEI was added to the serum-free medium – DNA mixture to a final concentration of 5 µg/ml (1 mg/ml stock solution in ddH_2O, pH 7.4, sterile filtered), the mixture was vortexed and incubated at room temperature (RT) for 5 minutes. Finally, the transfection mix was added to the cells' medium dropwise. In case of HeLa cells, medium was replaced with DMEM after 4 hours. Cells were harvested 20 hours post-transfection.

Transfection of cells with siRNA was performed using the reverse transfection method and the transfection reagent Lipofectamine® 2000 (according to the manufacturer's instructions). Briefly, cells were plated right before transfection, and the reaction mixture (siRNA – to a final concentration of 40 nM, serum-free DMEM and Lipofectamine 2000, incubated for 5 min at RT) was added dropwise to the wells. Medium was replaced with DMEM after 4-20 hours. Cells were harvested 48 h after siRNA transfection.

To arrest cells in mitosis by interfering with microtubule stability, cells were treated either with 100 ng/ml nocodazole (AppliChem) or 100 nM taxol (Sigma) overnight (for 16h).

5.7 Antibodies

Primary antibodies						
Protein	**species**	**clonality**	**Source and catalog nr**	**WB**	**IF**	**IP**
MISP	rabbit	poly	home-made (Zhu *et al.*, 2013)	1:5000	1:1000	-
MISP	mouse	mono	from Alwin Krämer, supernatant from hybridoma (Maier *et al.*, 2013)	undiluted	undiluted	-
IQGAP1	rabbit	poly	Abcam 86064	1:1000	1:300	2-5 µg
IQGAP1	mouse	mono	Santa Cruz (sc-376021)	1:500	-	-
Cdc42	mouse	mono	Cytoskeleton, ACD03	1:1000	-	-
FLAG M2	mouse	mono	Sigma (F1804)	1:5000	1:1000	-
GFP	rabbit	poly	home-made, against FL, unpublished	1 µg/ml	-	-
EB1	mouse	mono	BD Biosciences 610535	1:1000	1:500	-
pAkt	mouse	mono	S473, CST #587F11	1:1000	-	-
Akt	rabbit	poly	CST #9272	1:1000	-	-
p150glued	mouse	mono	BD Biosciences 612709	-	1:500	-
α-tubulin	mouse	mono	Sigma (B-5-1-2, T5168)	1:10000	1:1000	-
actin	mouse	mono	Calbiochem (JLA20)	1:5000	-	-
GST (Z5)	rabbit	poly	Santa Cruz (sc-459)	1:1000	-	-
Pericentrin	rabbit	poly	Abcam (ab4448)	-	1:3000	-
normal mouse IgG	mouse	poly	Santa Cruz (sc-2025)	-	-	-
normal rabbit IgG	rabbit	poly	Santa Cruz (sc-2027)	-	-	-

Secondary antibodies					
Name	**species**	**clonality**	**Source and catalog nr**	**WB**	**IF**
Anti-mouse IgG HRP	goat	poly	Novus Biologicals (NB7160)	1:5000	-
Anti-rabbit IgG HRP	donkey	poly	Jackson Lab. (115-035-003)	1:5000	-
Anti-mouse IgG Alexa 488	goat	poly	Molecular Probes (A-11001)	-	1:300
Anti-mouse IgG Alexa 594	goat	poly	Molecular Probes (A-11032)	-	1:300
Anti-rabbit IgG Alexa 488	goat	poly	Molecular Probes (A-11034)	-	1:300
Anti-rabbit IgG Alexa 568	goat	poly	Molecular Probes (A-11011)	-	1:300

5.8 Preparation of cell lysates

Cells were harvested either with on-dish lysis or by centrifugation. For on-dish lysis, cells were washed twice with PBS and after the second wash, PBS was thoroughly aspirated and cells were collected by scraping in 800 µl ice-cold lysis buffer (150 mM Tris-HCl, pH 8.5, 200 mM NaCl, 0.1% Triton X-100, 0.1% NP-40,

10 mM ß-glycerophosphate, 5 mM NaF, 2 mg/ml aprotonin, 2 mg/ml leupeptin, 20 mg/ml trypsin inhibitor, 20 µg/ml TPCK, 10 µg/ml TLCK, 1 mM Na_3VO_4). Mitotic cells were harvested by centrifugation after either a mitotic shake-off or scraping off the cells with a cell scraper. Cells were pelleted by centrifugation at 300 g for 2 min, washed with cold PBS, pelleted again and lysed in lysis buffer (or snap-frozen and stored at -80°C until needed). After 30 min incubation on ice, lysates were cleared by centrifugation at 16 000 g for 7 min. The supernatant was used for further experiments. Protein concentration was determined based on the Bradford method (Bio-Rad Protein Assay). For direct Western blot analysis lysate was boiled in Laemmli buffer at 95°C for 5 min and 25-50 µg of protein was loaded on an SDS-polyacrylamide gel.

5.9 Immunoprecipitations (IPs)

For IPs with overexpressed proteins, cells from one 15-cm dish were used.

- **FLAG IPs** were performed using FLAG M2 affinity beads (Sigma). Beads were prepared as follows: 10-30 µl of FLAG bead suspension per reaction was washed once with TBS (50 mM Tris-HCl, 150 mM NaCl, pH 7.4), once with 0.1 M glycine-HCl, pH 3.5 to remove unbound FLAG antibody, once with TBS and once with lysis buffer.
- For **GFP IPs**, home-made GFP trap beads were used. Briefly, GFP-binding protein (#49172, Addgene) was purified from *E.coli,* and after size-exclusion chromatography, covalently coupled to NHS-activated sepharose beads (GE Healthcare, 17090601), as described in Kubala *et al.*, 2010.
- For **endogenous IPs**, lysates were precleared with sepharose CL-4B beads (Pharmacia Biotech) on a rotating wheel at 4°C for 30 min. Then, 2-10 mg of cell lysates were incubated with 2-5 µg antibodies against the protein of interest (or normal mouse or rabbit IgG as control) on a rotating wheel at 4°C. After one hour, 20 µl protein G- (for mouse antibodies) or protein A- (for rabbit antibodies) coupled sepharose beads were added to the reactions.

After a 1- or 2-hour incubation period with the beads at 4°C, protein complexes were collected by centrifugation and washed three times with lysis buffer

supplemented with 200 mM NaCl (final concentration: 400 mM). Immunoprecipitated proteins were eluted from the beads by a 5-min boiling in 20-30 µl 2x Laemmli buffer.

5.10 Complex Immunoprecipitation

For analysis of ternary protein complexes, sequential IPs were performed. First, the FLAG-tagged protein was immunoprecipitated from the cell lysates with FLAG M2 beads for 2 hours, then washed and eluted for 30 min on ice with 500 ng/µl 3xFLAG peptide in 100 µl lysis buffer. 10µl of the eluate was spared for later analysis. 400 µl lysis buffer and 20 µl GFP trap beads were added to the eluate and incubated for 2 h at 4°C. After a triple wash, bound proteins were eluted by 5 min boiling in 2x Laemmli buffer.

5.11 Protein purification and pull-down assays

100 ml of LB medium (+ 1% glucose for MBP-tagged constructs) with the appropriate antibiotic was inoculated with colonies of BL21-Rosetta competent cells transformed with the bacterial expression plasmid of interest. Culture was grown on a shaking incubator at 37°C until an OD600 value of 1 was reached. The medium was diluted to 1 l and grown again at 37°C until OD600 value 0.6. The culture was cooled down to 18°C and protein expression was induced by the addition of 0.5 mM isopropyl-β-D-thiogalactopyranoside (IPTG) overnight. Bacteria were harvested by centrifugation. Pellets were resupended in 30 ml *E. coli* lysis buffer (50 mM Tris-HCl, pH 7.5, 250 mM NaCl, 1 mM $MgCl_2$, 5% glycerol, 1 mM DTT, 10 µg/ml TPCK, 5 µg/ml TLCK, 2 mg/ml aprotonin, 2 mg/ml leupeptin, 20 mg/ml trypsin inhibitor) and proteins were extracted by sonication for 4 x 30 sec. Lysate was cleared by centrifugation for 30 min at 15000 g at 4°C (SA-600 rotor, Sorvall). Next, the protein containing supernatant was incubated for 2 h with 500 µl

- glutathione agarose CL-4B beads (Sigma-Aldrich) for GST-tagged constructs
- His-binding Ni-NTA agarose beads (Qiagen) for His-tagged constructs
- amylose beads (NEB) for MBP-tagged constructs.

After a triple wash with the lysis buffer, bound proteins were eluted with 1 ml lysis buffer containing

- 100 mM glutathione (pH 8.5) for GST-tagged constructs
- 300 mM imidazole (pH 7.5) for His-tagged constructs
- 10 mM maltose (pH 7.5) for MBP-tagged constructs.

The GST-tagged proteins were dialysed against PBS overnight at 4°C. The concentration of the protein solution was calculated from its absorbance at 280 nm (SPECTROstar Nano, BMG Labtech) using the molar extinction coefficient. The protein solution was concentrated to 1 mg/ml (if below) with Vivaspin columns (GE Healthcare), snap-frozen in liquid nitrogen and stored at -80°C.

To analyze direct interactions, GST/MBP pulldown assays were performed. 15 µg MBP-MISP was incubated with 15 µg GST-tagged protein or equimolar amount of GST/MBP alone as control in 500 µl lysis buffer for 30 min at 4°C. Thereafter, 10-10 µl settled glutathione agarose / amylose beads were added and the mixtures were incubated for 1-2 h rotating at 4°C. After a triple washing step with lysis buffer, bound proteins were eluted by boiling in 2x Laemmli buffer for 5 min. Samples and 2% inputs were analysed by SDS-PAGE and western blotting.

5.12 GTPase activation assay

To measure the activation status of the Rho family of GTPases, the RhoA / Rac1 / Cdc42 G-LISA Activation Assay (BK135) from Cytoskeleton was used according to the kit manual. The principle behind the measurement is, that a RhoA-, Rac1-, or Cdc42-GTP-binding protein is linked to the wells of a 96 well plate. The specific active, GTP-bound GTPases in cell lysates will bind to the wells while the inactive, GDP-bound GTPases are removed during washing steps. The bound active Cdc42 is detected with a Cdc42 specific antibody. These experiments were conducted by our collaborator, Berati Cerikan (ZMBH, Heidelberg, Elmar Schiebel's Lab).

5.13 GEF assay

To find out if MISP is a guanine-nucleotide exchange factor for Cdc42, the RhoGEF exchange assay (BK100) from Cytoskeleton was used according to the

manufacurer's instructions. Briefly, purified Cdc42 was incubated with mant-(N-methylanthraniloyl)-GTP, a fluorophore-labeled GTP analog, whose intensity increases dramatically when bound to the GTPase. Fluorescence intensity is measured over time after the addition of the purified potential GEF (MISP) in different concentrations or the positive control Dbs (a proven Cdc42 GEF) with a plate reader at 440 nm (excitation 360 nm).

5.14 Immunofluorescence staining

Cells grown on coverslips were fixed in 4% paraformaldehyde (PFA) for 5-10 min at room temperature (or in methanol for 5 min at -20°C for α-tubulin and EB1 staining). After washing with PBS, cells were permeabilized and blocked with IF solution (3% BSA, 0.5% Triton X-100 and 0.02% sodium azide in PBS) for 30 min at RT. Samples were incubated for 1-2 hours with primary antibodies diluted in IF solution. After a triple wash with IF solution, coverslips were incubated for 30-60 min with the appropriate Alexa 488/568/647-coupled secondary antibodies (Molecular Probes) diluted in IF solution. Then, for staining nuclei, coverslips were kept in 1 µg/ml Hoechst 33258 solution (in PBS) for 5 min followed by a 5-min PBS wash. Coverslips were dried and mounted onto glass slides with Mowiol mounting medium.

5.15 Microscopy

Samples were analyzed either with Zeiss ObserverZ1 inverted microscope or with a Zeiss LSM-700 confocal microscope with the following settings. Zeiss motorized inverted Observer.Z1 equipped with a mercury arc burner HXP 120 C and a live-cell chamber for temperature, CO_2 and humidity control. Illumination: 365/470/555/590, detection: gray scale CCD camera AxioCamMRm system and a 63×/1.4 Oil Pln Apo DICII objective. A Zeiss Apotome optical sectioning device with structured illumination was used during z-stack imaging for near-confocal images. Zeiss LSM-700: Upright motorized Zeiss Imager.Z2 with a 63×/1.4 Oil DIC III objective. Laser lines: 405/488/555/639 nm.

Z-stacks were taken at an interval of 0.5 µm and with a 0.05 µm resolution. Stainings for samples to be compared were done in parallel and images were captured under the same exposure conditions. Images were processed and analyzed

with ImageJ software (Schneider *et al.*, 2012) single planes or sum projections were used for quantifications, maximum z-stack projections for visualization purposes.

5.15.1 Quantification of cortical signals

For quantification of cortical IQGAP1 intensity, cells were fixed with PFA and stained with the rabbit IQGAP1 antibody (Abcam). In case of mitotic cells, the equatorial z-section was used to calculate the relative intensity of the cortical and overall IQGAP1 signal. A circle was drawn just around the mitotic cell (a) and another one right below the cortex (b). Results were obtained with the integrated densities of the circles using the following formula: (a-b)/a. For interphase cells, the z-section with the strongest signal at the cell contacts was used. Integrated density of a straight line drawn at the strongest site of the cell-cell contact was divided by the integrated density of the same line measured in the cytoplasm right below this cortical region.

5.15.2 Quantification of astral microtubule intensity

Quantification of astral MT intensities was done on methanol fixed samples stained with α-tubulin or EB1. In sum projection of z-stack images, integrated densities were measured using the oval function of ImageJ of the whole mitotic cell (a) and the mitotic spindle itself (b). Astral/spindle MT intensity was calculated with the following formula: (a-b)/b.

5.15.3 Spindle orientation experiments

Cells were seeded onto fibronectin-coated coverslips. After treatment and staining with pericentrin antibody, z-stack confocal images (0.5 µm/stack) were acquired of metaphase cells with the Zeiss LSM700 or LSM710 system. After Z-projection of a line going through the two centrosomes in x-y dimension, the angle of the line connecting the two centrosomes in x-z dimension was measured with the ImageJ software (NIH).

5.15.4 Live cell imaging

The length of mitosis was studied in HeLa cells with a Zeiss Observer Z1 inverted microscope equipped with a living cell chamber. HeLa cells inducibly expressing

GFP-IQGAP1 were seeded on a 6-well plate and transfected with control or MISP siRNA. Expression of IQGAP1 was induced with 1 µg/ml doxycycline (SigmaD9891) 8 h before imaging. Cells were imaged 32 h post-transfection for 16 h. During imaging cells were kept at 37°C with 5% CO_2 in a humidified atmosphere. Brightfield images were taken with the 10x objective (0.3 EC PlnN Ph1 DICI) every 3 minutes. The length of mitosis was measured with ImageJ from NEB to anaphase onset on at least 100 cells.

5.15.5 Live imaging of microtubule dynamics

HeLa cells stably expressing EGFP-EB3 (Sironi *et al.*, 2011) were seeded in the wells of a 6-well plate and reverse transfected with control or MISP siRNA using Lipofectamine 2000. The next day cells were transfected with mock or FLAG-IQGAP1 constructs and transferred into 4-well glass-bottom ibidi chambers (ibidi GmbH, Germany). 48 h post-transfection and 1 h after addition of SiR-DNA (SC007, Spirochrome) at 1 µM final concentration for DNA staining, mitotic cells were imaged with a PerkinElmer ERS-6 spinning disc confocal microscope equipped with a Nikon Plan Apo λ 100x NA 1.45 oil immersion objective (working distance 0.13 mm) and a Yokagawa CSU-22 confocal scanning unit. An environmental box built around the microscope allowed for temperature-, and CO_2 control. For excitation, 488 and 640 nm laser lines were used, emission was detected with a Hamamatsu C9100-02 EMCCD camera (1000 x 1000 pixel, 8 µm pixel size) with the following filter sets: (center wavelength [nm]/bandwidth [nm]): "Green": 527/55, "Far Red": dual pass filter 705/90. Image acquisition of z-stacks of 5 planes 0.2 µm apart was performed with the PerkinElmer Volocity software every 2 seconds for 1 minute of cells with a nicely aligned metaphase plate (judged by SiR-DNA staining). Sum projected z-stacks of the spindles were aligned with the spindle axis parallel to the x-axis. Kymographs were created in ImageJ (Schneider *et al.*, 2012) by selecting a region of 5 µm in height (y-axis) between the centrosomes with the function “reslice” and subsequent maximum projection along the y-axis of the original stack. In this kymograph the slope of traces represent the speed along the x-axis.

5.15.6 Fluorescence Recovery After Photobleaching (FRAP)

HeLa cells inducibly expressing EGFP-IQGAP1 were seeded in the wells of a 6-well plate and reverse transfected with control or MISP siRNA using Lipofectamine 2000. The next day cells were transferred into 4-well glass-bottom ibidi chambers (ibidi GmbH, Germany) and IQGAP1 expression was induced with doxycycline. 48 h post-transfection and 1 h after addition of SiR-DNA (SC007, Spirochrome) at 1 µM final concentration for DNA staining, mitotic cells were imaged on a Leica TCS SP5II confocal microscope with a Leica PL APO 63x/1.4 oil objective. Cells were kept at 37°C with 5% CO_2. For GFP excitation the 488 nm Argon laser line was used and fluorescence emission was collected between 500 to 560 nm. Mitotic cells with a nicely aligned metaphase plate were imaged, judged by SiR-DNA staining.

For acquiring pre-bleach intensities, five consecutive images were taken at 10% laser power. Then a 4 x 2 µm rectangle at the cell cortex was bleached with 5 laser pulses of 4 lasers (405/458/476/488) at 100% power, each lasting for 1.3 seconds. For recovery measurements 20 single section images were collected at 3 s intervals with 10% laser power. Intensities were normalized to pre-bleach data and plots were generated with the FRAP wizard of the Leica LAS AF software. Data points were exported to excel for better visualization.

5.16 Mass spectrometry analysis

Mass spectrometry (MS) analysis was performed at the DKFZ MS Core Facility. For identification of MISP-interacting proteins, Flag-MISP immunoprecipitates were prepared and resolved by SDS-PAGE. After colloidal blue staining, gel lanes were cut into slices, digested with trypsin after reduction and alkylation of cystines. Tryptic peptides were analyzed by nano LC-ESI-MS/MS using a nano Acquity UPLC system (Waters GmbH, Eschborn, Germany) coupled online to an LTQ Orbitrap XL mass spectrometer (Thermo Scientific). Data were acquired by scan cycles of one FTMS scan with a resolution of 60000 at m/z 400 and a range from 300 to 2000 m/z in parallel with six MS/MS scans in the ion trap of the most abundant precursor ions. Instrument control, data acquisition and peak integration were performed using the Xcalibur software 2.1 (Thermo Scientific, Bremen, Germany).

Database searches were performed against the SwissProt database with taxonomy “human” using the MASCOT search engine (Matrix Science, London, UK;

version 2.2.2). MS/MS files from the individual gel slices of each lane were merged into a single search. Peptide mass tolerance for database searches was set to 5 ppm and fragment mass tolerance was set to 0.4 Da. Significance threshold was $p<0.01$. Carbamidomethylation of cysteine was set as fixed modification. Variable modifications included oxidation of methionine and deamidation of asparagine and glutamine. One missed cleavage site in case of incomplete trypsin hydrolysis was allowed.

5.17 Statistics

Experiments were repeated at least three times. Unless indicated otherwise, statistics were performed from the mean values using unpaired, two-tailed t-tests with 95% confidence interval in the Prism Software (Graphpad). Multiple comparisons were conducted with one-way ANOVA analysis using Bonferroni's multiple comparisons test. No data point was excluded. Most of the graphs were generated with Microsoft Excel for illustration purposes; data analysis was done with Prism. Data are presented as mean ± SD. On the graphs, p-values are marked as follows: **** $p<0.0001$, *** $p<0.001$, ** $p<0.01$, * $p<0.05$, ns – not significant ($p>0.05$).

6 Acknowledgements

This thesis would not have been possible without the help, support and guidance of many people.

To start, I would like to express my appreciation to my supervisor Prof. Dr. Ingrid Hoffmann, whose advice and comments have been a great help during my PhD years. I also would like to thank my TAC members: Prof. Dr. Elmar Schiebel and Dr. Gislene Pereira for all their time, suggestions and constructive criticism.

I owe special thanks to our collaborators, Dr. Berati Cerikan for conducting the Rho GTPase activation assays and giving technical support, and to Prof. Dr. Elmar Schiebel for providing reagents and contributing to my work with discussions. I am indebted to many of my colleagues for their comments and help including Anne Kratz, Anna Haffner, Yvonne Kschonsak, Miriam Post, Kathrin Brunk, Petra Hubbe, Annalena Meyer, Joachim Butzer, Kai Richter, Felix Bärenz and Shota Suzuki. The members of the Rösl and Hoppe-Seyler labs have been great neighbors and I appreciate their technical support.

I would like to thank Fernando Martin-Belmonte, Jan Ellenberg, Alwin Krämer, David Sacks, Gary Bokoch and Brett Collins for providing reagents. Members of the DKFZ Microscopy and Mass Spectrometry Core Facility and the Nikon Center Heidelberg are acknowledged for providing excellent technical assistance.

Additionally, I would like to thank my family for their incredible support, encouragement and understanding. I wish to especially thank my husband - who never stopped pushing me towards success and believed in me even when I was doubtful - for his support and encouragement throughout my years in Germany. I would also like to thank my mother, who had to suffer the absence of her daughter, for supporting my career plans.

This work was subsidized by the grant from the Deutsche Krebshilfe (no.110243) and the DKFZ PhD program.

7 References

Abel, A. M., Schuldt, K. M., Rajasekaran, K., Hwang, D., Riese, M. J., Rao, S., Thakar, M. S., and Malarkannan, S. (2015). IQGAP1: Insights into the function of a molecular puppeteer. Mol. Immunol. *65*, 336–349.

Adachi, M., Kawasaki, A., Nojima, H., Nishida, E., and Tsukita, S. (2014). Involvement of IQGAP family proteins in the regulation of mammalian cell cytokinesis. Genes to Cells *19*, 803–820.

Albrecht-Buehler, G., and Bushnell, A. (1979). The orientation of centrioles in migrating 3T3 cells. Exp. Cell Res. *120*, 111–118.

Baena-López, L. A., Baonza, A., and García-Bellido, A. (2005). The Orientation of Cell Divisions Determines the Shape of Drosophila Organs. Curr. Biol. *15*, 1640–1644.

Ban, R., Irino, Y., Fukami, K., and Tanaka, H. (2004). Human Mitotic Spindle-associated Protein PRC1 Inhibits MgcRacGAP Activity toward Cdc42 during the Metaphase. J. Biol. Chem. *279*, 16394–16402.

Bañón-Rodríguez, I., Gálvez-Santisteban, M., Vergarajauregui, S., Bosch, M., Borreguero-Pascual, A., and Martín-Belmonte, F. (2014). EGFR controls IQGAP basolateral membrane localization and mitotic spindle orientation during epithelial morphogenesis. EMBO J. *33*, 129–145.

Bashour, A. M., Fullerton, A. T., Hart, M. J., and Bloom, G. S. (1997). IQGAP1, a Rac- and Cdc42-binding protein, directly binds and cross-links microfilaments. J. Cell Biol. *137*, 1555–1566.

Bielak-Zmijewska, A., Kolano, A., Szczepanska, K., Maleszewski, M., and Borsuk, E. (2008). Cdc42 protein acts upstream of IQGAP1 and regulates cytokinesis in mouse oocytes and embryos. Dev. Biol. *322*, 21–32.

Brandt, D. T., and Grosse, R. (2007). Get to grips: steering local actin dynamics with IQGAPs. EMBO Rep. *8*, 1019–1023.

Briggs, M. W., Li, Z., and Sacks, D. B. (2002). IQGAP1-mediated stimulation of transcriptional co-activation by beta-catenin is modulated by calmodulin. J. Biol. Chem. *277*, 7453–7465.

Bruce, A., Alexander, J., Julian, L., Martin, R., Keith, R., and Peter, W. (2008). Molecular Biology of the Cell, Garland Science.

Buttrick, G. J., Beaumont, L. M. A., Leitch, J., Yau, C., Hughes, J. R., and Wakefield, J. G. (2008). Akt regulates centrosome migration and spindle orientation in the early Drosophila melanogaster embryo. J. Cell Biol. *180*, 537–548.

Cabello, J., Neukomm, L. J., Günesdogan, U., Burkart, K., Charette, S. J., Lochnit, G., Hengartner, M. O., and Schnabel, R. (2010). The Wnt pathway controls cell death engulfment, spindle orientation, and migration through CED-10/Rac. PLoS Biol. *8*.

Carlier, M. F., Ducruix, A., and Pantaloni, D. (1999). Signalling to actin: The Cdc42-N-WASP-Arp2/3 connection. Chem. Biol. *6*.

Castanon, I., and González-Gaitán, M. (2011). Oriented cell division in vertebrate embryogenesis. Curr. Opin. Cell Biol. *23*, 697–704.

Cerikan, B., Shaheen, R., Colo, G. P., Gläßer, C., Hata, S., Knobeloch, K.-P., Alkuraya, F. S., Fässler, R., and Schiebel, E. (2016). Cell-Intrinsic Adaptation Arising from Chronic Ablation of a Key Rho GTPase Regulator. Dev. Cell *39*, 28–43.

Chen, F., Zhu, H. H., Zhou, L. F., Wu, S. S., Wang, J., and Chen, Z. (2010). IQGAP1 is

overexpressed in hepatocellular carcinoma and promotes cell proliferation by Akt activation. Exp. Mol. Med. *42*, 477–483.

Cherfils, J., and Zeghouf, M. (2013). Regulation of small GTPases by GEFs, GAPs, and GDIs. Physiol. Rev. *93*, 269–309.

Chircop, M. (2014). Rho GTPases as regulators of mitosis and cytokinesis in mammalian cells. LANDES Biosci., 37–41.

Choi, S., Hedman, A. C., Sayedyahossein, S., Thapa, N., Sacks, D. B., and Anderson, R. A. (2016). Agonist-stimulated phosphatidylinositol-3,4,5-trisphosphate generation by scaffolded phosphoinositide kinases. Nat. Cell Biol. *1*, 1–45.

Choi, S., Thapa, N., Hedman, A. C., Li, Z., Sacks, D. B., and Anderson, R. a (2013). IQGAP1 is a novel phosphatidylinositol 4,5 bisphosphate effector in regulation of directional cell migration. EMBO J. *32*, 2617–2630.

Coleman, M. L., Marshall, C. J., and Olson, M. F. (2004). RAS and RHO GTPases in G1-phase cell-cycle regulation. Nat. Rev. Mol. Cell Biol. *5*, 355–366.

Davis, C. R., Richman, T. J., Deliduka, S. B., Blaisdell, J. O., Collins, C. C., and Johnson, D. I. (1998). Analysis of the Mechanisms of Action of the Saccharomyces cerevisiae Dominant Lethal cdc42 G12V and Dominant Negative cdc42 D118A Mutations *. Biochemistry *273*, 849–858.

Downward, J. (2003). Targeting RAS signalling pathways in cancer therapy. Nat Rev Cancer *3*, 11–22.

Du, Q., and Macara, I. G. (2004). Mammalian Pins is a conformational switch that links NuMA to heterotrimeric G proteins. Cell *119*, 503–516.

Erickson, J. W., and Cerione, R. A. (2001). Multiple roles for Cdc42 in cell regulation. Curr. Opin. Cell Biol. *13*, 153–157.

Fink, J. *et al.* (2011). External forces control mitotic spindle positioning. Nat. Cell Biol. *13*, 771–778.

Fukata, M. *et al.* (1999). Cdc42 and Rac1 regulate the interaction of IQGAP1 with beta-catenin. J. Biol. Chem. *274*, 26044–26050.

Fukata, M., Kuroda, S., Fujii, K., Nakamura, T., Shoji, I., Matsuura, Y., Okawa, K., Iwamatsu, A., Kikuchi, A., and Kaibuchi, K. (1997). Regulation of Cross-linking of Actin Filament by IQGAP1, a Target for Cdc42. J. Biol. Chem. *272*, 29579–29583.

Fukata, M., Watanabe, T., Noritake, J., Nakagawa, M., Yamaga, M., Kuroda, S., Matsuura, Y., Iwamatsu, A., Perez, F., and Kaibuchi, K. (2002). Rac1 and Cdc42 capture microtubules through IQGAP1 and CLIP-170. Cell *109*, 873–885.

Gillies, T. E., and Cabernard, C. (2011). Cell division orientation in animals. Curr. Biol. *21*, R599–R609.

Gloerich, M., Bianchini, J. M., Siemers, K. A., Cohen, D. J., and Nelson, W. J. (2017). Cell division orientation is coupled to cell–cell adhesion by the E-cadherin/LGN complex. Nat. Commun. *8*, 13996.

Gotlieb, A. I., May, L. M., Subrahmanyan, L., and Kalnins, V. I. (1981). in Migrating Sheets of Endothelial Cells Distribution of Microtubule Organizing Centers Recording of the MTOC Position Cinemicrophotography. J. Cell Biol. *91*, 589–594.

Grohmanova, K., Schlaepfer, D., Hess, D., Gutierrez, P., Beck, M., and Kroschewski, R. (2004). Phosphorylation of IQGAP1 modulates its binding to Cdc42, revealing a new type of Rho-GTPase regulator. J. Biol. Chem. *279*, 48495–48504.

Hart, M. J., Callow, M. G., Souza, B., and Polakis, P. (1996). IQGAP1, a calmodulin-

binding protein with a rasGAP-related domain, is a potential effector for cdc42Hs. EMBO J. *15*, 2997–3005.

Heasman, S. J., and Ridley, A. J. (2008). Mammalian Rho GTPases: new insights into their functions from in vivo studies. Nat. Rev. Mol. Cell Biol. *9*, 690–701.

Hedman, A. C., Smith, J. M., and Sacks, D. B. (2015). The biology of IQGAP proteins: beyond the cytoskeleton. EMBO Rep. *16*, 427–446.

Hein, M. Y. *et al.* (2015). A Human Interactome in Three Quantitative Dimensions Organized by Stoichiometries and Abundances. Cell *163*, 712–723.

Iden, S., and Collard, J. G. (2008). Crosstalk between small GTPases and polarity proteins in cell polarization. Nat. Rev. Mol. Cell Biol. *9*, 846–859.

Jadeski, L., Mataraza, J. M., Jeong, H.-W., Li, Z., and Sacks, D. B. (2008). IQGAP1 stimulates proliferation and enhances tumorigenesis of human breast epithelial cells. J. Biol. Chem. *283*, 1008–1017.

Jaffe, A. B., Kaji, N., Durgan, J., and Hall, A. (2008). Cdc42 controls spindle orientation to position the apical surface during epithelial morphogenesis. J. Cell Biol. *183*, 625–633.

Jameson, K. L., Mazur, P. K., Zehnder, A. M., Zhang, J., Zarnegar, B., Sage, J., and Khavari, P. A. (2013). IQGAP1 scaffold-kinase interaction blockade selectively targets RAS-MAP kinase-driven tumors. Nat Med *19*, 626–630.

Johnson, M., Sharma, M., and Henderson, B. R. (2009). IQGAP1 regulation and roles in cancer. Cell. Signal. *21*, 1471–1478.

Joyal, J. L., Annan, R. S., Ho, Y.-D., Huddleston, M. E., Carr, S. A., Hart, M. J., and Sacks, D. B. (1997). Calmodulin Modulates the Interaction between IQGAP1 and Cdc42: IDENTIFICATION OF IQGAP1 BY NANOELECTROSPRAY TANDEM MASS SPECTROMETRY. J. Biol. Chem. *272*, 15419–15425.

Kiyomitsu, T., and Cheeseman, I. M. (2012). Chromosome- and spindle-pole-derived signals generate an intrinsic code for spindle position and orientation. Nat. Cell Biol. *14*, 311–317.

Kiyomitsu, T., and Cheeseman, I. M. (2013). Cortical dynein and asymmetric membrane elongation coordinately position the spindle in anaphase. Cell *154*, 391–402.

Kotak, S., Busso, C., and Gönczy, P. (2013). NuMA phosphorylation by CDK1 couples mitotic progression with cortical dynein function. EMBO J. *32*, 2517–2529.

Kotak, S., Busso, C., and Gönczy, P. (2014). NuMA interacts with phosphoinositides and links the mitotic spindle with the plasma membrane. EMBO J. *33*, 1815–1830.

Kubala, M. H., Kovtun, O., Alexandrov, K., and Collins, B. M. (2010). Structural and thermodynamic analysis of the GFP:GFP-nanobody complex. Protein Sci. *19*, 2389–2401.

Kumeta, M., Gilmore, J. L., Umeshima, H., Ishikawa, M., Kitajiri, S., Horigome, T., Kengaku, M., and Takeyasu, K. (2014). Caprice/MISP is a novel F-actin bundling protein critical for actin-based cytoskeletal reorganizations. Genes Cells *19*, 338–349.

Kupfer, a, Louvard, D., and Singer, S. J. (1982). Polarization of the Golgi apparatus and the microtubule-organizing center in cultured fibroblasts at the edge of an experimental wound. Proc. Natl. Acad. Sci. U. S. A. *79*, 2603–2607.

Kuroda, S. *et al.* (1998). Role of IQGAP1, a target of the small GTPases Cdc42 and Rac1, in regulation of E-cadherin- mediated cell-cell adhesion. Science *281*, 832–835.

Kuroda, S., Fukata, M., Kobayashi, K., Nakafuku, M., Nomura, N., Iwamatsu, A., and Kaibuchi, K. (1996). Identification of IQGAP as a putative target for the small GTPases, Cdc42 and Rac1. J. Biol. Chem. *271*, 23363–23367.

Laan, L., Pavin, N., Husson, J., Romet-Lemonne, G., Van Duijn, M., López, M. P., Vale, R. D., Jülicher, F., Reck-Peterson, S. L., and Dogterom, M. (2012). Cortical dynein controls microtubule dynamics to generate pulling forces that position microtubule asters. Cell *148*, 502–514.

LeCour, L., Boyapati, V. K., Liu, J., Li, Z., Sacks, D. B., and Worthylake, D. K. (2016). The Structural Basis for Cdc42-Induced Dimerization of IQGAPs. Structure *24*, 1499–1508.

Li, Z., McNulty, D. E., Marler, K. J. M., Lim, L., Hall, C., Annan, R. S., and Sacks, D. B. (2005). IQGAP1 promotes neurite outgrowth in a phosphorylation-dependent manner. J. Biol. Chem. *280*, 13871–13878.

Luo, J., Manning, B. D., and Cantley, L. C. (2003). Targeting the PI3K-Akt pathway in human cancer: Rationale and promise. Cancer Cell *4*, 257–262.

Machicoane, M., de Frutos, C. A., Fink, J., Rocancourt, M., Lombardi, Y., Gare, S., Piel, M., and Echard, A. (2014). SLK-dependent activation of ERMs controls LGN-NuMA localization and spindle orientation. J. Cell Biol. *205*, 791–799.

Maier, B., Kirsch, M., Anderhub, S., Zentgraf, H., and Krämer, A. (2013). The novel actin/focal adhesion-associated protein MISP is involved in mitotic spindle positioning in human cells. Cell Cycle *12*, 1457–1471.

Mataraza, J. M., Briggs, M. W., Li, Z., Frank, R., and Sacks, D. B. (2003). Identification and characterization of the Cdc42-binding site of IQGAP1. Biochem. Biophys. Res. Commun. *305*, 315–321.

Mateer, S. C., McDaniel, A. E., Nicolas, V., Habermacher, G. M., Lin, M.-J. S., Cromer, D. A., King, M. E., and Bloom, G. S. (2002). The mechanism for regulation of the F-actin binding activity of IQGAP1 by calcium/calmodulin. J. Biol. Chem. *277*, 12324–12333.

Minc, N., Burgess, D., and Chang, F. (2011). Influence of cell geometry on division-plane positioning. Cell *144*, 414–426.

Mitsushima, M., Toyoshima, F., and Nishida, E. (2009). Dual role of Cdc42 in spindle orientation control of adherent cells. Mol. Cell. Biol. *29*, 2816–2827.

Morin, X., and Bellaïche, Y. (2011). Mitotic Spindle Orientation in Asymmetric and Symmetric Cell Divisions during Animal Development. Dev. Cell *21*, 102–119.

Nammalwar, R., Heil, A., and Gerke, V. (2014). Ezrin interacts with the scaffold protein IQGAP1 and affects its cortical localisation. Biochem. Biophys. Acta *In Press*, 2086–2094.

Negishi, T., Miyazaki, N., Murata, K., Yasuo, H., and Ueno, N. (2016). Physical association between a novel plasma-membrane structure and centrosome orients cell division. Elife *5*, 1–29.

Nestor-Bergmann, A., Goddard, G., and Woolner, S. (2014). Force and the spindle: mechanical cues in mitotic spindle orientation. Semin. Cell Dev. Biol. *34*, 133–139.

Neumüller, R., and Knoblich, J. (2009). implications for stem cells and cancer Dividing cellular asymmetry: asymmetric cell division and its. Genes Dev. *23*, 2675–2699.

Noritake, J., Watanabe, T., Sato, K., Wang, S., and Kaibuchi, K. (2005). IQGAP1: a key regulator of adhesion and migration. J. Cell Sci. *118*, 2085–2092.

Nousiainen, M., Silljé, H. H. W., Sauer, G., Nigg, E. A., and Körner, R. (2006). Phosphoproteome analysis of the human mitotic spindle. Proc. Natl. Acad. Sci. USA *103*, 5391–5396.

Oceguera-Yanez, F., Kimura, K., Yasuda, S., Higashida, C., Kitamura, T., Hiraoka, Y., Haraguchi, T., and Narumiya, S. (2005). Ect2 and MgcRacGAP regulate the activation and function of Cdc42 in mitosis. J. Cell Biol. *168*, 221–232.

di Pietro, F., Echard, A., and Morin, X. (2016). Regulation of mitotic spindle orientation: an integrated view. EMBO Rep. *17*, 1106–1130.

Psatha, M. I., Razi, M., Koffer, A., Moss, S. E., Sacks, D. B., and Bolsover, S. R. (2007). Targeting of calcium:calmodulin signals to the cytoskeleton by IQGAP1. Cell Calcium *41*, 593–605.

Quesada-Hernández, E., Caneparo, L., Schneider, S., Winkler, S., Liebling, M., Fraser, S. E., and Heisenberg, C. P. (2010). Stereotypical cell division orientation controls neural rod midline formation in zebrafish. Curr. Biol. *20*, 1966–1972.

Ren, J. G., Li, Z., Crimmins, D. L., and Sacks, D. B. (2005). Self-association of IQGAP1: Characterization and functional sequelae. J. Biol. Chem. *280*, 34548–34557.

Rittmeyer, E. N., Daniel, S., Hsu, S.-C., and Osman, M. a (2008). A dual role for IQGAP1 in regulating exocytosis. J. Cell Sci. *121*, 391–403.

Roberts, P. J., Mitin, N., Keller, P. J., Chenette, E. J., Madigan, J. P., Currin, R. O., Cox, A. D., Wilson, O., Kirschmeier, P., and Der, C. J. (2008). Rho family GTPase modification and dependence on CAAX motif-signaled posttranslational modification. J. Biol. Chem. *283*, 25150–25163.

Rodriguez-Fraticelli, A. E., Vergarajauregui, S., Eastburn, D. J., Datta, A., Alonso, M. A., Mostov, K., and Martín-Belmonte, F. (2010). The Cdc42 GEF Intersectin 2 controls mitotic spindle orientation to form the lumen during epithelial morphogenesis. J. Cell Biol. *189*, 725–738.

Roy, M., Li, Z., and Sacks, D. B. (2005). IQGAP1 is a scaffold for mitogen-activated protein kinase signaling. Mol. Cell. Biol. *25*, 7940–7952.

Santamaria, A., Wang, B., Elowe, S., Malik, R., Zhang, F., Bauer, M., Schmidt, A., Silljé, H. H. W., Körner, R., and Nigg, E. A. (2011). The Plk1-dependent Phosphoproteome of the Early Mitotic Spindle. Mol. Cell. Proteomics *10*, M110.004457.

Sbroggio, M. *et al.* (2011). IQGAP1 regulates ERK1/2 and AKT signalling in the heart and sustains functional remodelling upon pressure overload. Cardiovasc. Res. *91*, 456–464.

Schneider, C. A., Rasband, W. S., and Eliceiri, K. W. (2012). NIH Image to ImageJ: 25 years of image analysis. Nat. Methods *9*, 671–675.

Scholl, F. A., Dumesic, P. A., Barragan, D. I., Harada, K., Bissonauth, V., Charron, J., and Khavari, P. A. (2007). Mek1/2 MAPK Kinases Are Essential for Mammalian Development, Homeostasis, and Raf-Induced Hyperplasia. Dev. Cell *12*, 615–629.

Seldin, L., Muroyama, A., and Lechler, T. (2016). NuMA-microtubule interactions are critical for spindle orientation and the morphogenesis of diverse epidermal structures. Elife *5*, 1–18.

Semenas, J., Hedblom, A., Miftakhova, R. R., Sarwar, M., Larsson, R., Shcherbina, L., Johansson, M. E., Härkönen, P., Sterner, O., and Persson, J. L. (2014). The role of PI3K/AKT-related PIP5K1α and the discovery of its selective inhibitor for treatment of advanced prostate cancer. Proc. Natl. Acad. Sci. U. S. A. *111*, E3689-98.

Sironi, L., Solon, J., Conrad, C., Mayer, T. U., Brunner, D., and Ellenberg, J. (2011). Automatic quantification of microtubule dynamics enables RNAi-screening of new mitotic spindle regulators. Cytoskeleton *68*, 266–278.

Smith, J. M., Hedman, A. C., and Sacks, D. B. (2015). IQGAPs choreograph cellular signaling from the membrane to the nucleus. Trends Cell Biol. *25*, 171–184.

Stengel, K., and Zheng, Y. (2011). Cdc42 in oncogenic transformation, invasion, and tumorigenesis. Cell. Signal. *23*, 1415–1423.

Swart-Mataraza, J. M., Li, Z., and Sacks, D. B. (2002). IQGAP1 is a component of Cdc42

signaling to the cytoskeleton. J. Biol. Chem. *277*, 24753–24763.

Takemoto, H., Doki, Y., Shiozaki, H., Imamura, H., Utsunomiya, T., Miyata, H., Yano, M., Inoue, M., Fujiwara, Y., and Monden, M. (2001). Localization of IQGAP1 is inversely correlated with intercellular adhesion mediated by e-cadherin in gastric cancers. Int. J. Cancer *91*, 783–788.

Tame, M. a, Raaijmakers, J. a, van den Broek, B., Lindqvist, A., Jalink, K., and Medema, R. H. (2014). Astral microtubules control redistribution of dynein at the cell cortex to facilitate spindle positioning. Cell Cycle *13*, 1162–1170.

Tanaka, T. U. (2010). Kinetochore–microtubule interactions: steps towards bi-orientation. EMBO J. *29*, 4070–4082.

Théry, M., and Bornens, M. (2006). Cell shape and cell division. Curr. Opin. Cell Biol. *18*, 648–657.

Théry, M., Jimenez-Dalmaroni, A., Racine, V., Bornens, M., and Julicher, F. (2007). Experimental and theoretical study of mitotic spindle orientation. Nature *447*, 493–496.

Théry, M., Racine, V., Pépin, A., Piel, M., Chen, Y., Sibarita, J.-B., and Bornens, M. (2005). The extracellular matrix guides the orientation of the cell division axis. Nat. Cell Biol. *7*, 947–953.

Thompson, S. L., Bakhoum, S. F., and Compton, D. A. (2010). Mechanisms of Chromosomal Instability. Curr Biol *20*.

Toyoshima, F., Matsumura, S., Morimoto, H., Mitsushima, M., and Nishida, E. (2007). PtdIns(3,4,5)P3 Regulates Spindle Orientation in Adherent Cells. Dev. Cell *13*, 796–811.

Toyoshima, F., and Nishida, E. (2007). Integrin-mediated adhesion orients the spindle parallel to the substratum in an EB1- and myosin X-dependent manner. EMBO J. *26*, 1487–1498.

Tuncay, H., Brinkmann, B. F., Steinbacher, T., Schürmann, A., Gerke, V., Iden, S., and Ebnet, K. (2015). JAM-A regulates cortical dynein localization through Cdc42 to control planar spindle orientation during mitosis. Nat. Commun. *6*, 8128.

Watanabe, T., Wang, S., Noritake, J., Sato, K., Fukata, M., Takefuji, M., Nakagawa, M., Izumi, N., Akiyama, T., and Kaibuchi, K. (2004). Interaction with IQGAP1 links APC to Rac1, Cdc42, and actin filaments during cell polarization and migration. Dev. Cell *7*, 871–883.

White, C. D., Brown, M. D., and Sacks, D. B. (2009). IQGAPs in cancer: a family of scaffold proteins underlying tumorigenesis. FEBS Lett. *583*, 1817–1824.

Wu, J., and Mlodzik, M. (2008). The frizzled extracellular domain is a ligand for Van Gogh/Stbm during nonautonomous planar cell polarity signaling. Dev. Cell *15*, 462–469.

Yan, J., Yuan, X., Bloom, G. S., and Hua, X. (2009). Menin Interacts with IQGAP1 to Enhance Intercellular Adhesion of β Cells. Oncogene *28*, 973–982.

Yasuda, S., Oceguera-Yanez, F., Kato, T., Okamoto, M., Yonemura, S., Terada, Y., Ishizaki, T., and Narumiya, S. (2004). Cdc42 and mDia3 regulate microtubule attachment to kinetochores. Nature *428*, 767–771.

Zheng, Z., Zhu, H., Wan, Q., Liu, J., Xiao, Z., Siderovski, D. P., and Du, Q. (2010). LGN regulates mitotic spindle orientation during epithelial morphogenesis. J. Cell Biol. *189*, 275–288.

Zhu, M., Settele, F., Kotak, S., Sanchez-Pulido, L., Ehret, L., Ponting, C. P., Gönczy, P., and Hoffmann, I. (2013). MISP is a novel Plk1 substrate required for proper spindle orientation and mitotic progression. J. Cell Biol. *200*, 773–787.

8 Appendix

8.1 List of figures